9 Far infrared spectroscopy

C. J. Reid and M. W. Evans

9.1 Introduction

This chapter deals with the investigation of molecular interactions and dynamics using spectroscopy in the range of frequencies from static to tetrahertz (THz). This implies that the averaged dynamical fluctuations of many interacting potentials are followed in detail over a span of time from ps to ks and longer.

It is important to realize from the beginning that the range zero–THz must be regarded in molecular dynamical terms as an entity. A major weakness of dielectric spectroscopy prior to the opening up of the far infra-red (THz) region in the sixties was the failure to realize that the dielectric loss and the optical power absorption coefficient are related manifestations of the same molecular process, the dipole reorientation. Thus while the loss for liquids peaks in the microwave (GHz) region and becomes apparently insignificant towards THz, the power absorption peaks in the latter region and reflects the short-time details of reorientation. As a result, dielectric measurements confined to lower frequencies by technical difficulties and considered only as loss, appeared to be explicable with mathematical models (such as rotational diffusion) developed primarily for the Brownian motion of colloidal particles moving in a bath of *much less massive* solvent molecules. Even after some twenty years of intense activity (Chantry, 1971; Muller and Rothschild 1971; Rowlinson and Evans, 1975; Evans, 1977a,b; Brot, 1975; Evans 1980; Evans, 1982) in the far infrared spectral range (of about 2–250 cm^{-1} or upwards of 60 GHz) the dielectric literature is still largely composed of papers whose authors seem unaware of its existence. These advocates of Debye's theory of rotational diffusion (Debye, 1929) or its empirical modifications attempt to photograph with a Daguerrotype the rapidity of short time (or far infrared) details and obtain only a blurred image, represented model-wise by the unrealistic Debye plateau of absorption at THz frequencies.

The analogy with the camera is, however, misleading in the sense that the conventional far infrared interferometer may take upwards of half an hour

to build up the spectrum which is therefore an *equilibrium* time (or ensemble) average of the molecular motions responsible for modulating the electromagnetic radiation. It is almost always assumed (Nelson, 1967) that a time average and ensemble average produce the same result when building mathematically the quantity of interest in interpreting a spectrum—i.e. a two-point time-correlation function, or its Fourier transform.

The correlation function has been available in the statistical literature since the early twenties, and it is used more frequently now than ever before in interpreting and interrelating spectral data from many different techniques. The natural method of calculating a model spectrum is to take the governing equation of motion (quantum mechanical—Heisenberg—or classical—Liouville) and solve it approximately using statistical methods from the start. This was the method used by Debye in his original paper of 1913 on rotational diffusion. However, at that time the concept of a correlation function was not available, and probability density functions were used through the medium (Wax, 1954) of Markov's ideas and Smoluchowski's equation of 1907. It is known now that the correlation functions of interest are integrals of the probability density functions over the relevant phase space.

If we confine ourselves to classical mechanics the correlation function of interest in zero–THz spectroscopy is that of the *macroscopic* dipole moment $\mathbf{M}$ of the sample under investigation. This is the vector sum of the individual molecular dipole moments $\boldsymbol{\mu}$. The correlation function of $\mathbf{M}$ is written at time t as:

$$C_{\mathbf{M}}(t) = \langle \mathbf{M}(0) \cdot \mathbf{M}(t) \rangle \tag{9.1}$$

and is a scalar. It is a difficult problem to relate this to

$$C_{\boldsymbol{\mu}}(t) = \langle \boldsymbol{\mu}(0) \cdot \boldsymbol{\mu}(t) \rangle, \tag{9.2}$$

the microscopic dipole moment *auto*-correlation function, because this requires the knowledge we are seeking. In current jargon it is essential to solve the internal field problem before $C_{\boldsymbol{\mu}}(t)$ can be calculated from $C_{\mathbf{M}}(t)$ or vice-versa. It is possible, however, to relate them approximately using, for example, micro–maco theorems (Kivelson and Madden, 1975) or, alternatively, ideas about the reaction field of a dipole elaborated from those of Onsager (1936). In jargon, these theories are concerned with the problem of the *dynamic* internal field. This has been the subject of much controversy during the seventies, which seems to have subsided with the appearance of a paper by Titulaer and Deutch (1975). To a newcomer, the basic ideas of the dipole moment cavity seem strange because the immediate environment of a fluctuating dipole moment is usually assumed to be a spherical region of fixed permittivity. This is a shibboleth of Onsager's which is rapidly being outmoded through the use of very powerful computers which attack directly

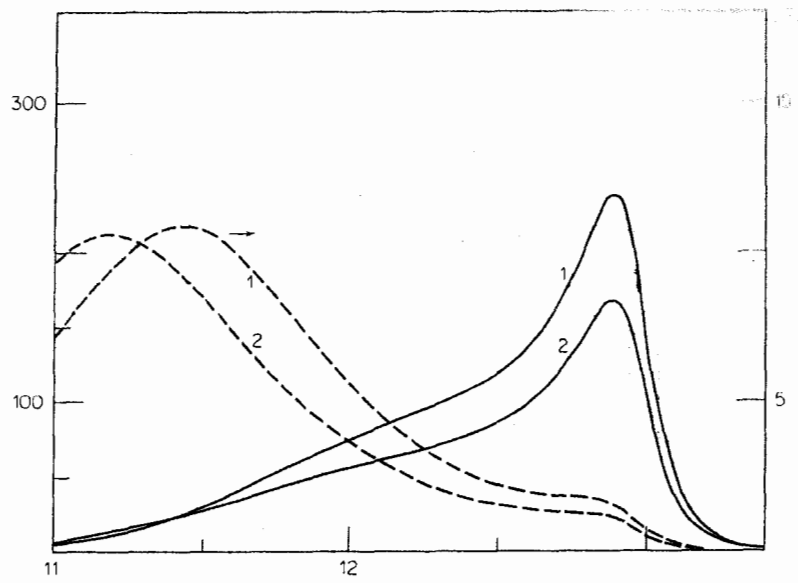

Figure 9.1 Analytic Nee–Zwanzig spectral profiles with and without an internal field factor: absorption representation, $\alpha(\omega)$; loss representation $\epsilon''(\omega)$. Curves 1, basic model (Nee and Zwanzig, 1970). Curves 2 include the Fatuzzo–Mason (1967) field factor. RHS ordinate: $\epsilon''(\omega) \times 10^2$; LHS ordinate: neper cm^{-1}; abscissa: log ω/s^{-1}. (Reproduced by permission from Evans, *J. Chem. Soc. Faraday Trans. II*, 1980)

the intricacies of molecular kinematics and, increasingly, electrodynamics. In another decade the dielectric cavity concept will be obsolete, and deservedly so. However, the internal field continues to cause confusion and continues to be given unnecessary prominence in the dielectric literature. In simple terms the field experienced by the molecular dipole moment is not the same as the field entering the bulk sample because of the shielding effect of other molecular potentials. The reference (or tagged) dipole also 'polarizes' its surroundings (or more accurately it interacts electrodynamically with the potentials of its nearest neighbours). This affects its own motion in a way that can be understood only by solving the complete N-body problem ($N = 6.0 \times 10^{23}$). By making drastic simplifications (e.g. using spherical dielectric cavities) these phenomena can be analytically reproduced. The results of one such theory, due to Fatuzzo and Mason (1967) are illustrated in Figure 9.1 for the dielectric loss $\epsilon''(\omega)$ and the optical power absorption coefficient $\alpha(\omega)$. Using Maxwell's equations these are related by:

$$\alpha(\omega) \quad \frac{\omega \epsilon''(\omega)}{cn(\omega)} \tag{9.3}$$

where c is the velocity of light and $n(\omega)$ the refractive index. We have the further useful relation

$$n(\omega)=\frac{1}{\sqrt{2}}((\epsilon'(\omega)^2+\epsilon''(\omega)^2)^{1/2}+\epsilon'(\omega))^{1/2} \tag{9.4}$$

where $\epsilon'(\omega)$ is the frequency-dependent dielectric permittivity.

It is important to understand the implications of equation (9.3), illustrated in Figure 9.1.

The frequency at which the loss, ϵ'', peaks is much lower than that (in the far infrared) at which $\alpha(\omega)$ is a maximum, although both measure the extent to which electromagnetic radiation is attenuated by the motions of many molecular dipoles. In fact $\alpha(\omega)$ peaks invariably in the far infrared while $\epsilon''(\omega)$ may sometimes be found at very much lower frequencies than shown in Figure 9.1.

Because of the existence of the far infrared peak in $\alpha(\omega)$ and because of the fundamental relations (9.3) and (9.4), the dielectric loss $\epsilon''(\omega)$ cannot be a symmetrical function of log frequency as envisaged by Debye. This can be illustrated vividly by converting Debye's equation for $\epsilon''(\omega)$ and $\epsilon'(\omega)$ into $\alpha(\omega)$, using equations (9.3) and (9.4). The result is illustrated in Figure 9.2. There is no peak in $\alpha(\omega)$, only a plateau, extending to infinite frequencies. The unadorned theory of rotational diffusion implies therefore that every dipolar liquid should be opaque in the visible, and must for this reason be discarded.

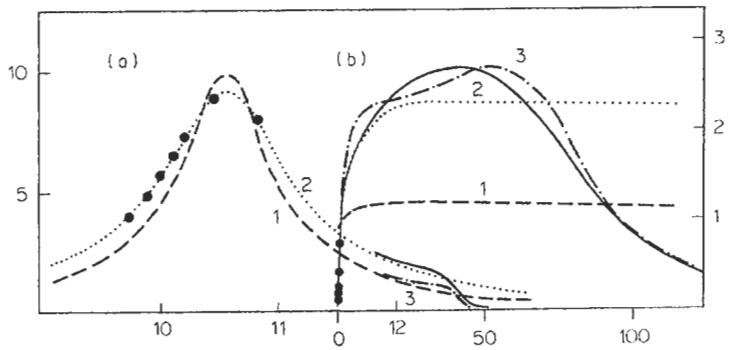

Figure 9.2 Spectral profiles for rotational diffusion models with reference to fluorobenzene-decalin data (293 K). ——— interferometric data; ● ● microwave points. (a) Attenuation per frequency (proportional to $\epsilon''(\omega)/\epsilon'(\omega)$); (b) absorption. (1) Debye model (matched to experimental loss peak); (2) Fuoss Kirkwood equation (representing a distribution of relaxation times); (3) itinerant oscillator fit (Section 9.4). (a) Ordinate: 10^{13} s cm^{-1}; abscissa: log f/(Hz). (b) Ordinate: neper cm^{-1}; abscissa: wavenumber (cm^{-1})

Our aim in this chapter is to develop the use of both $\epsilon''(\omega)$ and $\alpha(\omega)$ as sources of information about the details of molecular dynamics and interactions. These functions of ω provide us with information, presented in different ways. It is almost superfluous to say, therefore, that any attempt to reproduce $\epsilon''(\omega)$ mathematically (using $C_\mu(t)$) should be extended also to $\alpha(\omega)$.

The fundamental weakness in the isolated interpretation of $\varepsilon''(\omega)$ data is that it appears to be easy to reproduce the loss curve when the high-frequency data is missing. Figure 9.1 shows that even when these are available the far infrared region in terms of loss appears only as a slight shoulder on the main peak. The opposite is true in $\alpha(\omega)$ representation, which obliterates the Debye loss. It is essential therefore to measure both $\alpha(\omega)$ and $\epsilon''(\omega)$ and *interpret them together*, with a suitable mathematical model for $C_\mu(t)$. This is what we mean in the chapter by zero–THz spectroscopy.

The realization of the importance of the far infrared power absorption coefficient will remove the false impression that the intricacies of liquid state molecular interactions can be described more than superficially by elementary algebraic models (i.e. by human preconception, by simple ideas). The description of $\alpha(\omega)$ and $\epsilon''(\omega)$, and of the effect of the reaction field (over, of course, the complete temperature and pressure range of the existence of the liquid), may just be within the capability of the most powerful available computers using *ad hoc* forms for each molecular potential. (Such a description is not known at present.) However, the recent results of Reid and Evans (1979) for small dipolar solute molecules in ultra-viscous and vitreous solvents confound even this expectation, because the zero–THz spectrum is extended over an enormous range of frequency. This reflects a molecular dynamical evolution of staggering complexity, whereby motions taking place on the picosecond time scale (γ processes) evolve into much slower manifestations (β and α processes) taking place on a scale of seconds and ultimately years. Despite the enormous sweep of time involved, the (α, β, γ) loss peaks are related features of the same overall correlation function $C_M(t)$.

It takes of the order of an hour on the most powerful available computers to simulate $C_M(t)$ from $t=0$ out to picoseconds using the technique of molecular dynamics. It is doubtful therefore whether it will be possible to simulate molecular motions which are manifesting themselves on the time scale of seconds and longer. (This would need a run lasting 10^9 years.)

Faced with this, empirical correlation is a powerful technique of data analysis and reduction which will be used extensively in this chapter. It is particularly useful when looking for signs of anomalous behaviour such as hydrogen-bonding, known to be present from independent sources.

Figure 9.1 clearly shows that the internal field, according to Fatuzzo and Mason at least, does not affect the *shapes* of $\epsilon''(\omega)$ and $\alpha(\omega)$ at all severely.

It is therefore rational to neglect its influence entirely when dealing with correlation functions, since these are normalized to unity at the time origin. Theoretical support for this comes from a paper by Kivelson and Madden (1975) which shows that $C_{\mathbf{M}}(t)$ and $C_{\boldsymbol{\mu}}(t)$ are identical when plotted on a reduced time scale and when calculated using successively more realistic approximations of the Liouville equation. We shall therefore concentrate on producing naive ideas for $C_{\boldsymbol{\mu}}(t)$, the dipole autocorrelation function. Simple ideas do not imply simple mathematics, and further approximations usually have to be made to translate them into zero–THz spectra.

Finally, we are well aware of, but shall not concern ourselves with, the phenomenon of induced absorption. This may be briefly summarized as the induction of temporary dipoles by interacting molecular potentials. The induced dipole moments vary in both magnitude and direction, and are responsible, for example, for the broad far infrared band observable in nondipolar liquids, such as benzene and carbon disulphide (Davies and Evans, 1976). To minimize the effect of induced absorption on the spectra of permanent dipoles in which we are interested it is expedient to choose a strongly dipolar species, such as methylene chloride, in dilute solution. Solution spectra in general form the backbone of this chapter.

9.1.1 *The far infrared (Poley) absorption*

The all-important peak in the far infrared $\alpha(\omega)$ was discovered in the sixties independently by more than one group of investigators (see Muller and Rothschild, 1971; Chantry, 1971). Characteristically, the maximum absorption in the liquid lies at higher frequency ($\bar{\nu}_{\max}$) than in the gas. This is a direct consequence of the hindering of free rotation, a phenomenon which may be measured in terms of a root mean square torque. It is essential that any mathematical model of the liquid state reproduces the shift of $\bar{\nu}_{\max}$. We know now that m and J diffusion models developed by Gordon (1968) do not shift $\bar{\nu}_{\max}$ because of the assumptions of uncorrelated, impulsive collisions which periodically send the torque to infinity. It has also become clearer that models such as these can be catalogued (Evans *et al.*, 1980) in terms of a continued fraction expansion of the Liouville equation due to Mori (1965). Rotational diffusion is technically a zeroth approximant of such an expansion and m and J (or extended) diffusion a first approximant. We need at least a second approximant to be able to reproduce theoretically the shift in $\bar{\nu}_{\max}$. Details of these expansions are given in the appendices.

The peak of $\alpha(\omega)$ referred to as the Poley absorption (Poley, 1955) is characteristic of all dipolar liquids, which indicates that its origin lies in whole molecule (end over end) roto-translation rather than in specific forms of intramolecular vibration. Datta and Barrow (1968), who obtained some of the first peak positions, $\bar{\nu}_{\max}$, of these bands (for some very light

molecules), discovered a correlation between $\bar{\nu}_{\max}$ and the rotational constants of the molecules involved. This was taken as evidence for their rotational origin. Gordon (1965) has considered the general relation between a spectral bandshape and the correlation function of the dipole or transition dipole responsible. For the pure rotational modes of motion a sum rule (Gordon, 1963) for the total (integrated) absorption was derived without consideration of the internal field correction. The sum rule is (in standard notation):

$$\int_{\text{band}} \alpha(\omega)\,\mathrm{d}\omega = \frac{N\pi}{6c\epsilon}\left\{\frac{(\mu_a^2+\mu_b^2)}{I_c}+\frac{(\mu_b^2+\mu_c^2)}{I_a}+\frac{(\mu_c^2+\mu_a^2)}{I_b}\right\}. \tag{9.5}$$

Equation (9.5) usually only accounts for between 50% and 80% of the observed integrated absorption intensity. The reasons for this may be summarized as the neglect of internal field, of induced absorption, and of associated factors. Recently the application of the rule has been criticized by Hill (1977). However, a classical derivation by Brot (1975) substantiates Gordon's equation (9.5).

The increments of reorientation of a molecule in the ensemble are not uncorrelated, because as pointed out by Van der Elsken and Wegdam (1972) this would imply that $\bar{\nu}_{\max}$ would not shift its position away from the gas phase value. The motion must therefore be librational in origin (i.e. torsional oscillatory). If $\bar{\nu}_{\max}$ is considered to be the mean frequency of libration we may estimate for any given system a maximum limit for the mean amplitude of libration (Reid, 1979a). If the motion is assumed to be harmonic then the energy of the librator is $E=\frac{1}{2}I\dot{\theta}(t)^2+\frac{1}{2}k\theta^2(t)$, or $kT=\frac{1}{2}I\dot{\theta}_{\max}^2$ on average where $\dot{\theta}_{\max}$ is the angular velocity at the equilibrium position. If the frequency of libration is $c\bar{\nu}_{\max}$ then for a mean aperature of $\theta_{\max}$, the mean angular velocity is $2\theta_{\max}c\bar{\nu}_{\max}$. Hence $2kT/I \geqslant (2\theta_{\max}c\bar{\nu}_{\max})^2$, giving an estimate of the maximum value of $\theta_{\max}$ for a suitable choice of inertia I. Such values are typically less than 0.6 radians except for very small molecules such as CH_2Cl_2, NH_3, or HBr, where the rotational motion seems to be less hindered.

The assumption of harmonic librations of dipolar molecules more or less fixed in preferred orientation by their neighbours corresponds to the rotational site model of Darmon *et al.* (1970). Such a model considers the microwave loss process to arise from activated jumping between such sites. Libration is necessitated by considerations of entropy. If the potential barrier V is associated with the activation enthalpy ΔH, then for a multiplicity of n sites, a molecule of inertia I will undergo planar libration with frequency given by $\nu=(n/2\pi)\sqrt{V/2I}$. This very simple model therefore actually predicts from thermodynamic considerations the librational motion in the far infrared. For the 'planar' rotator phases of hexa-substituted pentachlorobenzenes, the predicted values are very close to the centres of

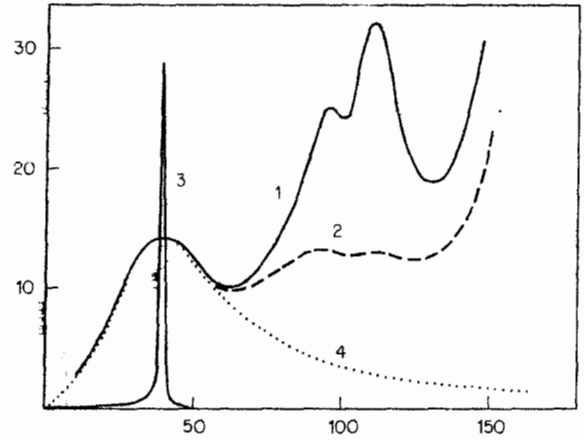

Figure 9.3 The harmonic model spectrum with reference to data for rotator phase pentachloronitrobenzene (293 K): (1) experimental absorption of pressed disc specimen; (2) absorption of a single crystal specimen (notice the relative diminution of proper modes at about 100 cm^{-1}); (3) harmonic model libration frequency predicted from the position and behaviour of the loss peak (at kHz frequencies); (4) itinerant oscillator (4-variable) fit (Section 9.6). Ordinate: neper cm^{-1}; abscissa: wavenumber cm^{-1}

the observed bands (Evans *et al.*, 1978) (Figure 9.3). The harmonic, delta function in the far infrared produced theoretically is of course too narrow for this model to be considered realistic. However, the concept of potential wells still provides a simplistic model of the long time cooperative motions in the denser phases and several attempts at generalization have been made. One model for rotator phases has been detailed by Brot (1967), whose formulation of the orientational time correlation function for a thermally perturbed librator in a multi-site potential provides a better description of the far infrared data as measured by Larkin (1973).

For liquids, the diffusive nature of such sites can be incorporated through the concept of itinerant oscillation, whereby a central dipole librates harmonically within a cage of neighbours, the whole undergoing rotational diffusion. One analytical approximation of this model, due to Wyllie (1971), has been compared with experimental data by Larkin (1973) who also investigated the Brot model. It was found that such models could only simulate the Debye/Poley features if the form for the potential was made temperature-dependent by the inclusion of an adjustable well-narrowing parameter. For both models, the approximation of impulsive (momentarily

infinite) torques leads to an orientational correlation function which contains all time-odd terms higher than t^2. Such a form is therefore badly behaved at short times (Figure 9.4) where classically it should be an equilibrium time-even function. This failure is observed spectrally as a too-gradual return to transparency at high frequencies compared with the experimental absorption. A more recent analysis of the itinerant oscillator type of model (Calderwood and Coffey, 1977), where full account is taken of the moment of inertia of the librating molecule, proves more satisfactory and will be considered in detail later.

Before leaving the concept of site models we should perhaps discuss the origin of the potential barriers. In one sense, a site model is incomplete because it does not specify, in molecular terms, the cause of the asymmetry. In a liquid, the temporary sites intuitively arise from the translational degrees of freedom of neighbouring molecules which are diffusing on a slower time scale than the rotational diffusion and are mutually cooperative. As such motions are not directly involved in spectral absorption their effect

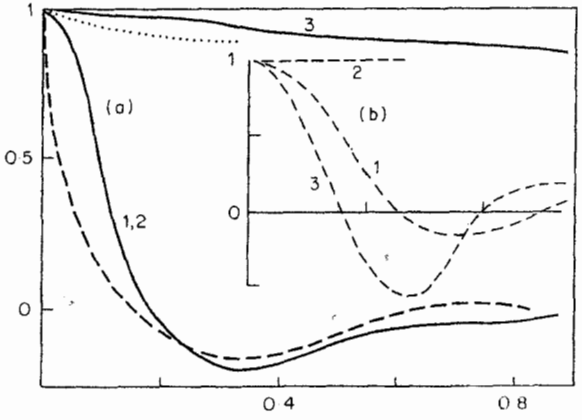

Figure 9.4 The time correlation functions: their relative behaviours in liquid and gaseous media (with reference to methyl chloroform data) and zeroth order model simulations. Curves 1 are rotational velocity a.c.f. Curves 2 are angular velocity a.c.f. Curves 3 are orientational a.c.f. (a) liquid methyl chloroform at 293 K ——— experimental data, — — — — Larkin–Brot model simulation of curve 1 (a similar curve is obtained for a diffusion model), ... Debye type orientation and rotational velocity a.c.f.'s. (b) gas phase methyl chloroform 293 K: free rotor (Kummer) functions which generally well simulate dilute gas data (note conservation of angular momentum gives $\langle \omega(0)\omega(t)\rangle$ 1). Abscissae: time (ps)

may either be rigorously included by defining appropriate roto-translational correlation functions, or more simply by choosing an appropriate time-averaged interaction potential (site-model). The relaxation process is invariably considered to be due to activated jumping, the breadth of the process reflecting a distribution of potential barrier heights. However, the barriers themselves fluctuate and are created and destroyed by the same motions that allow libration and relaxation.

It is then too easy, in the more complex behaviour of supercooled liquids, to consider the α and β processes as arising from two distinct sets of molecules in different environments or in some other manner (Williams and Hains, 1971) where causality becomes lost. On the other hand, the Arrhenius (or Eyring) behaviour of the loss process is most simply explained in terms of potential barriers. (The Debye model simply shifts the argument to consider η as an activated process rather than τ_D.) Further, the best fit values of barrier height V that satisfy both the microwave and far infrared data of the rotator phases and liquids studied by Larkin and Evans (1974) are clearly in approximate proportion to the size of the substituent groups. Site models can thus suggest that the far infrared peak position depends on the bulkiness of the molecule in question, and consequently the hindrance to rotation. A highly hindered molecular rotation would thus lead to a large separation of the Debye and far infrared peaks and further emphasize their existence as an entity. This is illustrated in Figure 9.5.

An alternative viewpoint of molecular motion in liquids is that of a complex sequence of collision processes. Gordon's well-known models for linear molecules (Gordon, 1965) assume (for mathematical tractability) that such collisions are Poisson distributed and are such that they either randomize the magnitude of the angular velocity (m diffusion) or randomize

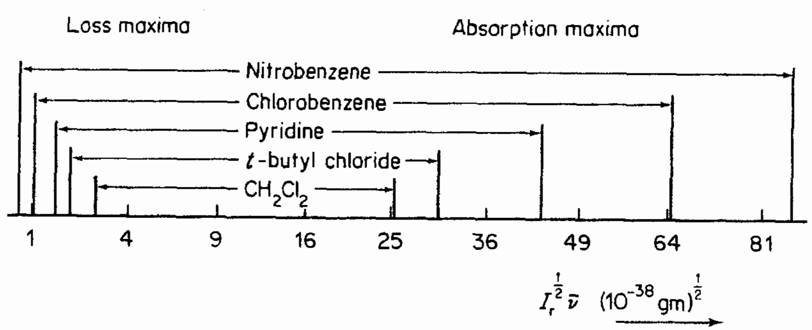

Figure 9.5 Illustrating how separation between loss and absorption maxima varies with solute size (and mean square torque): 1, nitrobenzene; 2, chlorobenzene; 3, pyridine; 4, t-butylchloride; 5, CH_2Cl_2. Abscissa: normalized frequency $10^{18} I_r^{\frac{1}{2}}\bar{\nu}(g^{\frac{1}{2}})$. (Reproduced from C. J. Reid, Ph.D. thesis (copyright))

both the magnitude and direction of the angular velocity (J diffusion) at each impact. Unfortunately, these assumptions leave the mean square torque undefined, as discussed above. Leroy *et al.* (1967), who were amongst the first to obtain essentially complete spectral profiles in the zero–THz range, tackled this problem by superposing a distribution of resonance forms on the Poisson distribution of collisions. For several liquid systems, they observed an experimental correlation between a parameter λ_2 (related to the correlation time of the collisions) and the wavelength at which the far infrared absorption had dropped to half the peak value. This parameter was model-related to the Debye critical wavelength λ_1 by $\lambda_1\lambda_2 = 2\pi^2c^2I(kT)^{-1}$. Hence by knowing that the Debye loss peak frequency decreases exponentially with temperature (Arrhenius behaviour) it follows that $\lambda_1 T$ increases and hence λ_2 decreases with temperature. The model thus 'predicts' that the librational band shifts to higher frequency with lowering temperature, i.e. in the opposite direction to the loss peak. Similarly, the relation predicts solvent shifts in the far infrared, counterbalancing the known solvent shifts in the dielectric regime.

Apart from Leroy's model, which is tractable only for the extreme cases of predominantly inertial behaviour, the above collisional models fail in general on two counts. Firstly, because the hard sphere collisions create impulsive torques, so giving rise to slow recovery of transparency, and secondly because the model collisions are not correlated. To proceed we need to consider a more rigorous statistical mechanical approach, as outlined in the appendices. The Mori reformulation of the Liouville equation governing the N-body dynamics is particularly useful in this respect because the complicated multi-molecular dynamical problem is approximated in terms of a few thermodynamic averages calculated at equilibrium.

9.2 Relation of spectra to correlation functions

According to the fluctuation-dissipation theory of Kubo (1965) applied to spectral behaviour by Glarum (1960), the dissipative response (susceptibility χ^*) that we observe is primarily related to the fluctuation of macroscopic polarizability:

$$\chi^*(\omega) = \frac{1}{kT}\int_0^\infty e^{i\omega t}\langle \mathbf{M}(0)\,.\,\dot{\mathbf{M}}(t)\rangle\,dt. \qquad (9.6)$$

Brot (1975) has explained how this result may be used to produce:

(9.7)

where

$$\mathscr{L}_a[-\dot{\phi}] = -\int_0^\infty e^{-i\omega t}\dot{\phi}(t)\,dt; \qquad \phi(t) = \frac{\langle \boldsymbol{\mu}(0) \cdot \sum \boldsymbol{\mu}(t)\rangle}{\langle \boldsymbol{\mu}(0) \cdot \sum \boldsymbol{\mu}(0)\rangle}.$$

Here $\epsilon^*(\omega) = \epsilon'(\omega) - i\epsilon''(\omega)$ is the complex dielectric permittivity. Using equation (9.7) it is easy to see that if $\phi(t)$ decays exponentially with a single relaxation time τ we obtain the Debye equation:

$$\frac{\epsilon^*(\omega) - \epsilon_\infty}{\epsilon_0 - \epsilon_\infty} = \frac{1}{1 + i\omega\tau_{exp}} \quad \text{where} \quad \tau_{exp} = \left(\frac{\epsilon_0 + 2}{\epsilon_\infty + 2}\right)\tau.$$

Debye's treatment means that

$$\langle \boldsymbol{\mu}(0) \cdot \sum \boldsymbol{\mu}(t)\rangle = \langle \boldsymbol{\mu}(0) \cdot \boldsymbol{\mu}(t)\rangle$$

is assumed implicitly.

Alternative treatments of the internal field are available, but none are particularly realistic. However, if we take $\epsilon_0 \doteqdot \epsilon_\infty$ (i.e. a dilute solution of a dipolar solute in a nondipolar solvent) then the simple relation:

$$\frac{\epsilon^*(\omega) - \epsilon_\infty}{\epsilon_0 - \epsilon_\infty} = -\int_0^\infty e^{-i\omega t}\langle \mathbf{u}(0) \cdot \dot{\mathbf{u}}(t)\rangle\,dt \tag{9.8}$$

can be deduced from a variety of internal field formalisms. From equation (9.8),

$$\frac{\epsilon^*(\omega) - \epsilon_\infty}{\epsilon_0 - \epsilon_\infty} = 1 - i\omega\int e^{-i\omega t}\langle \mathbf{u}(0) \cdot \mathbf{u}(t)\rangle\,dt$$

or

$$\epsilon''(\omega)/\omega = (\epsilon_0 - \epsilon_\infty)\,\text{Real}\int_0^\infty e^{-i\omega t}\langle \mathbf{u}(0) \cdot \mathbf{u}(t)\rangle\,dt. \tag{9.9}$$

Here $\mathbf{u} = \boldsymbol{\mu}/|\boldsymbol{\mu}|$, the dipole unit vector. The $\epsilon''(\omega)/\omega$ factor is directly dependent on the orientational correlation function through a Fourier transform. This illustrates the central role played by the correlation function.

Equation (9.9) is not particularly sensitive to the spectral details at far infrared frequencies as the $\epsilon''(\omega)/\omega$ representation reduces this to insignificance. However, by twice integrating equation (9.9) by parts and using

$$\frac{d^2}{dt^2}\langle \mathbf{u}(0) \cdot \mathbf{u}(t)\rangle = -\langle \dot{\mathbf{u}}(0) \cdot \dot{\mathbf{u}}(t)\rangle$$

we find that

$$\alpha(\omega) \quad \frac{\epsilon_0 - \epsilon_\infty}{n(\omega)c}\,\text{Real}\int_0^\infty e^{-i\omega t}\langle \dot{\mathbf{u}}(0) \cdot \dot{\mathbf{u}}(t)\rangle\,dt \tag{9.10}$$

where $\langle \dot{\mathbf{u}}(t) \cdot \dot{\mathbf{u}}(0)\rangle$ is often known as the *rotational* velocity autocorrelation function (Darmon *et al.*, 1970) to distinguish it from the *angular* velocity a.c.f. which it sometimes resembles. Some authors attempt to include in (9.10) an internal field correction which has the effect of Figure 9.1.

Some orientational and rotational velocity correlation functions for gaseous and liquid states are illustrated in Figure 9.4, together with the angular velocity autocorrelation function drawn for comparison. For the liquid the rotational velocity a.c.f. decays very rapidly compared with the a.c.f. of orientation. Its evolution is not well matched by either the Debye model or by the Larkin–Brot or Gordon models although, as will be seen, adequate simulatory forms may be obtained from a second approximant of the Mori continued fraction of Appendix 9B—the planar itinerant oscillator model. Rotational diffusion corresponds to a delta memory function for angular momentum. The Brot site model and m-diffusion model in the limit of frequent collisions both correspond to the first approximant of the orientational Mori series where the memory function is an exponential. This does not define the mean square torque, because the Taylor series of the analytic auto-correlation function of orientation is not time even.

Equation (9A.3) is particularly useful in describing zero–THz data with three parameters $\phi_0(0)$, $\phi_1(0)$, and γ_u. This type of model was first used by Levesque *et al.* (1973) to describe the results of a computer simulation on N_2 using site–site Lennard–Jones interactions.

An alternative approach is that of planar itinerant libration, discussed in Appendix 9B. The spectrum is now described in terms of the parameters $K_0(0)$, $K_1(0)$, and γ, which can be related to physical concepts as in the appendix. It is reasonable to associate ω_0 of Appendix 9B with the observed band centre $2\pi c\tilde{\nu}_{max}$, while the annular relaxation may be associated with the macroscopic relaxation time τ_{exp} through $\beta = kT\tau_{exp}/I_1$. A suitable choice of I_2 and I_1, where I_2 is the moment of inertia of the encaged molecule harmonically bound to a diffusing entity of moment of inertia I_1, should be sufficient to fix the parameters $K_0(0)$, $K_1(0)$, and γ. In this way the basic idea of the model can be evaluated directly with the zero–THz spectral data.

9.3 Solution spectra of small rigid molecules

The far infrared $\alpha(\omega)$ profiles of pure dipolar liquids at ambient temperature are generally asymmetric and peak at a wavenumber ($\tilde{\nu}_{max}$) determined principally by molecular size and inertia (Reid, 1979b). Similar factors are at play in determining the loss peak frequencies. For example, in methylene chloride (CH_2Cl_2) the loss peaks above 110 GHz at 293 K, while nitrobenzene (consisting of much larger molecules) peaks at about 4 GHz at the same temperature. For linear and symmetric top molecules the dipolar

reorientation primarily involves a single moment of inertia I_B so that the variation of $\bar{\nu}_{max}$ with I_B can be studied quantitatively. In the more general case of the asymmetric top such comparisons require an average over the three principal moments of inertia, I_A, I_B, I_C.

A natural average in the limit of free rotation (or at times very close to the arbitrary $t=0$) is the *reduced moment of inertia*, defined as:

$$I_r^{-1} = (u_B^2+u_C^2)I_A^{-1} + (u_C^2+u_A^2)I_B^{-1} + (u_A^2+u_B^2)I_C^{-1} \qquad (9.11)$$

where $u_{A,B,C}$ denote unit dipole vector components along the axes of the principal moments of inertia. The latter intersect at the centre of mass with $I_A \leqslant I_B \leqslant I_C$. $\bar{\nu}_{max}$, the far infrared peak wavenumber, depends not only on I_r, but is obviously affected by the intermolecular interaction responsible for shifting it away from the free rotor ($J \rightarrow J+1$) band centre. This can be rationalized in terms of a mean square torque, the derivative with respect to orientation ($\boldsymbol{\Omega}$) of the mean intermolecular potential energy. In solution there are contributions from the solute, solvent, and cross-terms. All three may be kinematic or electrodynamic or both. The measured $\bar{\nu}_{max}$ of a dipolar solute in a nondipolar solvent varies markedly therefore with concentration (Figure 9.6). This can be useful in identifying the librational band

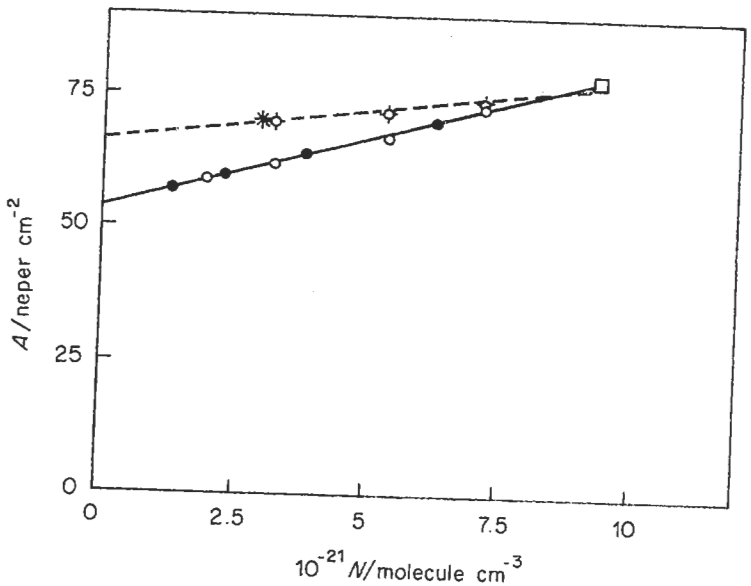

Figure 9.6 The solvent shift for dichloromethane in decalin (and C.O.C.): ——— in decalin solvent, — — — — in cholesteryl oleyl carbonate (all curves corrected for solvent). Concentrations in 10^{21} molecules/ml: (1) pure CH_2Cl_2; (2) 7.22; (3) 4.93; (4) 1.97; (5) 0.94 (10% v/v). Ordinate: neper cm^{-1}; abscissa: wavenumber cm^{-1}. From (Evans *et al.*, *JCS Faraday II*, 1978, **74**, 337)

when proper modes of intra-molecular vibration are present. It is fruitful to intercompare different solutes in a common solvent at the same temperature and same low concentration because we can discern the effect of solute molecular shape on the position of $\bar{\nu}_{max}$ under standardized conditions (Reid and Evans, 1980a).

From the early work of Datta and Barrow it is known that the $\bar{\nu}_{max}$ depends on $I_B^{-1/2}$. We may also infer from the studies by Larkin and Evans that the potential barrier V determines both $\bar{\nu}_{max}$ and τ and is dependent on molecular geometry. Therefore $\bar{\nu}_{max}$ is proportional to the mean square torque $\langle\Gamma(0)^2\rangle$. For itinerant libration constrained to a plane:

$$K_0(0) = (2\pi c\bar{\nu}_{max})^2 = I^{-2}\langle\Gamma(0)^2\rangle_z/(kT/I).$$

In general, for asymmetric-top space reorientation, the following result by Reid (1979b) is useful:

$$\langle\Gamma(0)^2\rangle/(16\pi^2c^2kT) = I_r\bar{\nu}_{max}^2 \equiv 10^{-38}T_q. \qquad (9.12)$$

In what follows $I_r\bar{\nu}_{max}^2$ is called the torque factor, which at constant T is an approximate measure of the mean square torque acting on the solute. If the molecule is taken as a rigid, inpenetrable particle then it can be shown that the mean square torque is proportional to a solute-dependent factor V^2, where V is an averaged volume of rotation. The proportionality factor P is mainly dependent on the environment, so for a given solvent and temperature the mean square torque is expected to increase proportionally with solute size.

Using the product $I_r\bar{\nu}_{max}^2$ as a basis for quantitative discussion, Reid (1979b) has studied a number of dipolar solutes in cis-decalin solvent, chosen for their rigidity and absence of spectral complications such as low frequency proper-modes. Decalin is a particularly useful solvent in such work because its cross-sectional absorption is always low compared with the solute contribution. The criterion of solute rigidity (in the sense that the dipole vector $\boldsymbol{\mu}$ remains fixed in the molecular frame) limits the choice of molecules to substituted methanes or ethanes or their inorganic analogues, and aromatic cyclics. The latter solutes can be grouped according to the parent ring size, i.e. five-membered heterocyclics, benzene derivatives and pyridine (six-membered, and the 1 halogenonaphthalenes. The group of six-membered cyclics can be further subdivided according to the size of substituents, while for the acyclics a subdivision depending both on size and on the dipolar orientation within the molecule was found convenient. Eight groups are considered in what follows, the different substituents (or heteroatoms) within each group forming an ordered sequence.

The variation of $I_r\bar{\nu}_{max}^2$ (for mostly 10% v/v solutions in decalin at 293 K) within and between the eight groups, is shown in Figure 9.7. The general indication is that the $I_r\bar{\nu}_{max}^2$ values are smallest for the acyclic groups A to D

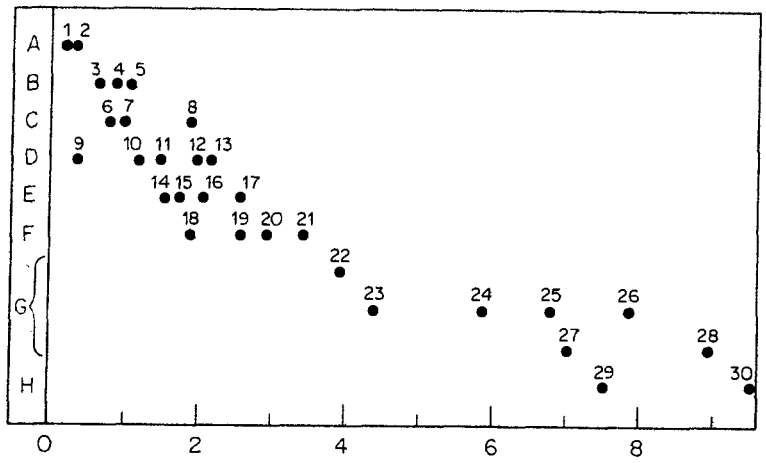

Figure 9.7 Tq values for various molecules in decalin illustrating variation with geometry classified as: A, diatomic linear; B, small ellipsoids; C, pseudospherically substituted methanes; D, elongated; E, five membered aromatic cyclics; F, six membered aromatic cyclics with single atom substituent; G, six membered cyclics with bulkier substituents; H, halonaphthalenes. Numbered as in Table 9.1. Abscissa: $10^{35} I_r \bar{\nu}^2_{max}$ (g)

with values as low as 100×10^{-38} g for HCl (in cyclohexane), and increase gradually to values as high as $10\,000 \times 10^{-38}$ g for 1 chloronaphthalene. Groups E and F in particular show the expected increase of mean square torque (proportional to $I_r \bar{\nu}^2_{max}$) with increasing solute size as either the heteroatom or substituent changes. Such comparisons validate to some degree the underlying model of itinerant libration.

Considering the data in Figure 9.7 in more detail we note several comparisons that appear to lie outside the pattern above. In particular, for group F, the trend that begins with pyridine (whose geometry is approximately equivalent to the benzene ring) is reversed when we consider the chloro- and bromo-benzenes. A similar effect is found for the 1 halogenonaphthalenes. The bromine substituent is roughly equivalent in volume to the methyl group, yet $I_r \bar{\nu}^2_{max}$ in toluene is much bigger than in bromobenzene. This is due to the fact that the bromo group is much more massive than $-CH_3$ and shifts the centre of mass in C_6H_5Br appreciably away from its centre of volume. For the cyclics of groups F and G the volume centres are close to the ring centres. In condensed media the rotational motion of such solutes is perhaps typified by Ewing's (1969) discussion of the HCl molecule. Here the centre of mass is close to the chlorine atom and consequently asymmetrically placed within the solvent

cage. As the HCl molecule rotates in the fixed cage the centre of mass has to continually translate to maintain the molecule in a low energy environment. This is an example of what we term rotation/translation coupling. Steele (1976) has emphasized that, in condensed media, rotation occurs about torque-determined principal axes which are different from the inertial axes more relevant to the gaseous states. In monosubstituted benzene rings the time-averaged torque-determined axes intercept at the 'volume centre', close to the centre of the parent ring. In general, the centre of mass is not the same and this is reflected in I_r. The changes are greatest for derivatives involving heavy substituents, e.g. I_r increases by 50% for C_6H_5Br, but only 9% for toluene. The discrepancies in Figure 9.7 can therefore be explained with a suitable choice of axes.

To look at the translation–rotation coupling, Reid has suggested the use of covalent radii spheres to define a molecular surface. These do not overlap significantly so their contributions to a calculated volume of rotation are almost additive. The surface defined in this way is more appropriate to the dynamical problem at hand. The volume of rotation (V) appropriate to general rotation about the set of principal axes can be taken as the reciprocal average of those about each axis which contributes to dipolar relaxation. In terms of V, equation (9.12) becomes:

$$I_r \bar{\nu}^2_{max} = 8\pi^2 c^2 kTPV^2 \tag{9.13}$$

where P is expectedly a constant for constant solvent and temperature. A plot of $I_r \bar{\nu}^2_{max}$ against these volumes squared is shown in Figure 9.8, where both I_r and V are computed for inertial axes. The majority of the data fall on a straight line that passes through the origin. Points corresponding to molecules with massive substituents lie well below this straight line. If axes are chosen to minimize V the only significant changes occur for the halo compounds, t-butyl chloride and nitrobenzene. The corresponding increases in T_q are given in Table 9.1, and the change from inertial to 'centre of volume' axes are seen graphically in Figure 9.8 by dotted arrows. For the chloro and phenyl compounds, the reduction of V^2 is large compared with the increase in I_r so that it is very likely that these molecules rotate predominantly about ring centre (or centre of volume) axes. Nitrobenzene, on the other hand, would suffer a relatively larger change in I_r compared with the change in V^2 on rotating about ring centre axes so that, here, rotation/translation coupling is less likely to occur. On the assumption that coupling occurs for the chloro and bromobenzenes and naphthalenes but not for nitrobenzene or the other solutes, the new data points are now well represented by the straight line of Figure 9.8. The representation can now form a basis for prediction of far infrared behaviour of other rigid solute molecules in dilute decalin solution at 293 K.

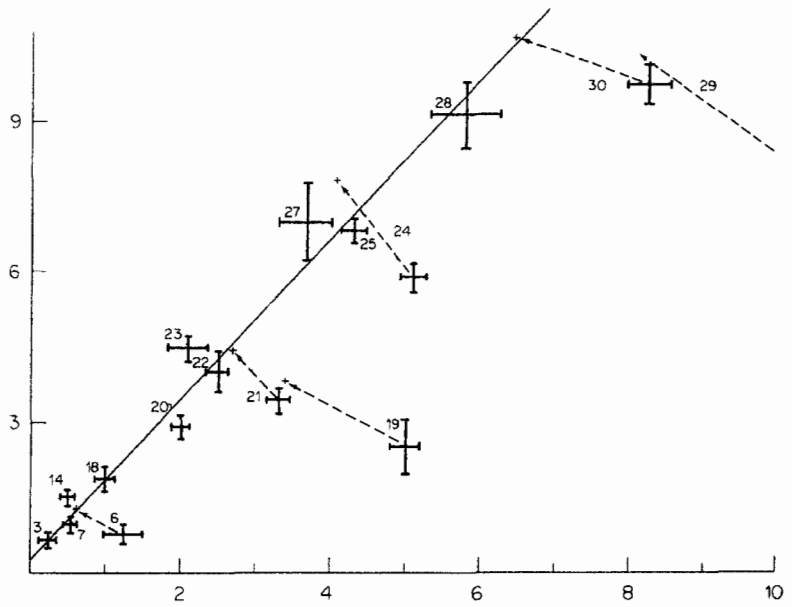

Figure 9.8 Mean square torque factor ($I_r\bar{\nu}^2_{max}$) variation with solute volume of rotation squared (V^2): evidence for roto-translation coupling. Points numbered as in Table 9.1: ——— best straight line through data of non-coupled systems, — — — shift of points on considering torque determined rotational axes (roto translation coupling). Arrow heads correspond to maximum coupling. Ordinate: $10^{35} I_r\bar{\nu}^2_{max}$(g); abscissa: $10^{-3} V^2$(Å^6)

Such predictions are based on the assumption that the environmental interactions in weakly polar systems are essentially kinetic with no long-range interactions. One may therefore expect that for more complex systems such as aniline or pyrrole in decalin, where independent evidence exists for the persistence of H-bonding even in dilute solution, some deviations may occur. Far infrared comparisons between systems containing mono-disperse solutes and those where association may occur are therefore becoming very important in assessing the dynamic effect of the latter (Reid, 1980). One such comparison can be made between solutions of pyrrole in decalin and the other five-membered cyclics of group E. Pyrrole, with its basic N–H ring-segment has the lowest molecular weight and yet the highest (pure liquid) boiling point of the series: pyrrole (NH segment); furan (O); thiophen (S); and thiazole (S and O segments). There is also NMR and vibrational spectrographic evidence for the persistence of H-bonding in solution (Chenon *et al.*, 1972; Paolo and Sandorfy, 1974). In decalin or cyclohexane solvents, the far infrared spectrum of pyrrole (at 10% v/v concentration) is

Table 9.1

	Solute	Dipole moment (D)	Reduced inertia $10^{38}T_r$ (g cm^2)	$\bar{\nu}_{max}$ (cm^{-1})	T_q	V^2 (Å^6)	$\frac{\Delta T_q}{\Delta V^2}$
1	$HCl/(C_6H_{12})$		0.013	125	200	8.3	
2	HBr/SF_6		0.024	108	280	15.6	
3	CH_2Cl_2	1.6	0.24	53	674	250	
4	CH_2Br_2		0.3	55	925		
5	SCl_2	1.61	0.48	50	1187		
6	t-butyl chloride	2.15	1.43	24	823 (1028)	1225 (600)	0.33
7	chloroform	1.1	1.26	30	990	552	
8	2 chloro nitro propane	3.69	1.96	33	1915	3326	
9	MeCl/ethane		0.28	37	376	321	
10	$SOCl_2$		1.19	32	1218		
11	Acetone		0.53	53	1495		
12	MeI		0.5	60	1800	460	
13	CH_3CN/CCl_4	3.39	0.435	70	2131	324	
14	Furan	0.67	0.6	51	1560	552	
15	Thiazole	1.79	0.83	45	1687	725	
16	Thiophene	0.53	0.96	46	2040	812	
17	Pyrrole	1.8	0.6	65	2577	600	
18	Pyridine	2.23	0.96	45	1857	1011	
19	phBr	1.56	4.43	24	2551 (3784)	5093 (3406)	0.73
20	phF (ph ≡ C_6H_5)	1.4	1.92	39	2923	2019	
21	phCl	1.58	2.97	34	3433 (4427)	3314 (2737)	1.72
22	pentafluoro benzene	1.4	4.4	30	3160	2510	
23	α-picoline	2.04	1.22	60	4393	2144	
24	Nitrobenzene	3.97	3.9	39	5932 (7878)	5168 (4109)	1.84
25	phCN	4.03	3.07	47	6781 (8173)	4353 (4304)	
26	Aniline	1.13	1.92	64	7864	3433	26
27	Toluene	0.36	1.92	60	6912	3697	
28	o-xylene	0.64	2.3	60	6912	5848	
29	1-Bromonaphthalene	1.56	5.17	38	7464 (10 194)	11 320 (8150)	0.86
30	1-Chloronaphthalene	1.58	4.43	47	9786 10 647	8216 6496	0.5

shown in Figure 9.9 compared with the solution spectra of furan and thiazole. The former band of librational absorption is centred at higher frequency and is clearly broader than that of the geometrically almost equivalent furan solute. There may in fact be two (or more) components within the band. Forming the product $I_r\bar{\nu}^2_{max}$ (where $\bar{\nu}_{max}$ is the band centre

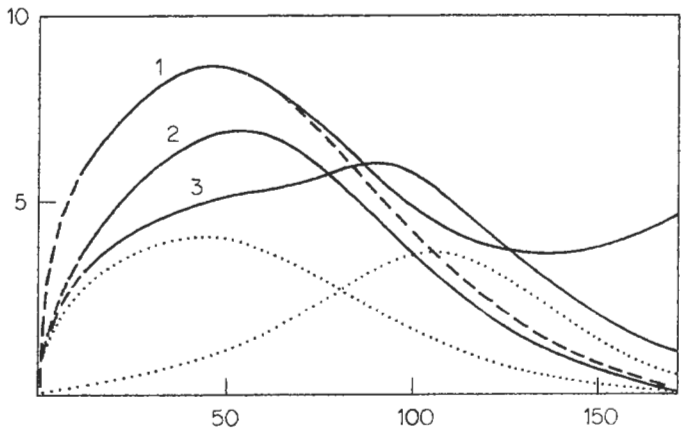

Figure 9.9 Spectral absorptions of three geometrically similar solutes: furan, thiazole, and pyrrole in decalin, the comparison suggesting association effects in the latter. (1) Thiazole; (2) furan (trebled intensity); (3) pyrrole: ——— experimental data, — — — extrapolation of libration bands, ... a possible (arbitrary) separation of curve 3 into free and complexed solute contributions. Ordinate: neper (cm^{-1}); abscissa: wavenumber (cm^{-1})

rather than the position of maximum absorption), we see in Figure 9.10 that this is anomalous. Similarly, a high value of the torque product occurs for aniline in the group F/G series and for acetonitrile in the series of elongated molecules. These and other H-bonded systems (including water) are particularly important and will be considered again below. For the present we confine our discussion to systems which we believe are monodisperse, having only short-range (kinematic) interactions and which are therefore more appropriate to the theory at hand.

9.4 Comparison of spectral profiles and Debye relaxation times

We have so far considered only the mean librational frequency $\bar{\nu}_{max}$ and shown this to be a useful parameter from which we may deduce the presence of mode coupling or long range interactions. To obtain information on the dynamic evolution of the interactions involved we need to consider the complete spectral profile or, equivalently, the appropriate time correlation functions derived numerically from such a profile. Our first concern is whether the three-variable Mori/I.O. theory can adequately simulate such profiles which for simple liquids extend over some three to four decades of

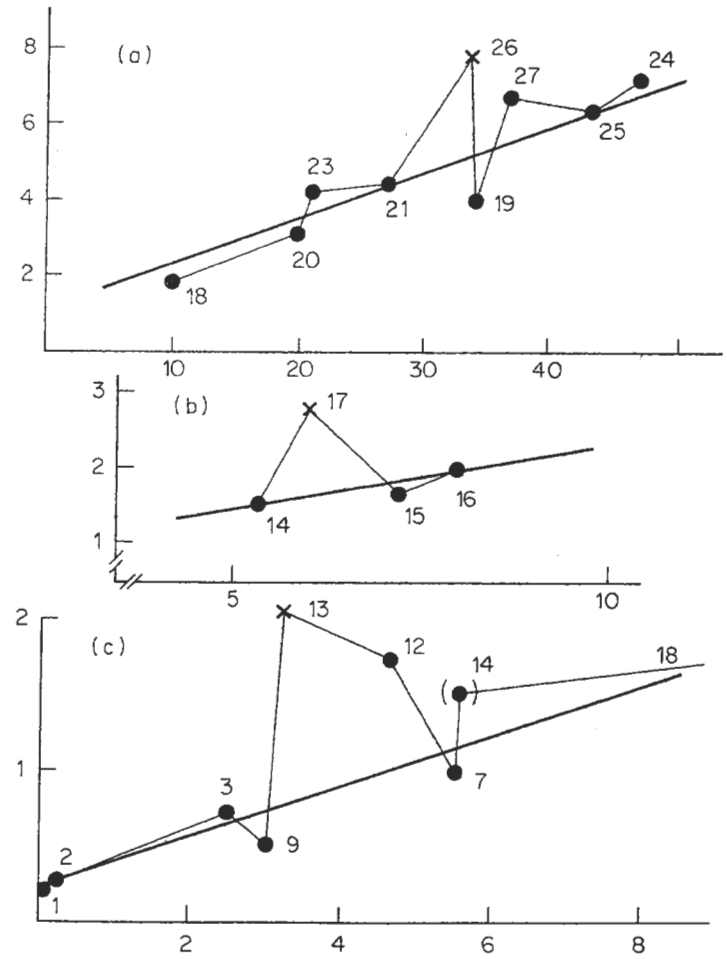

Figure 9.10 Mean square torque factor ($I_r\bar{\nu}^2_{max}$) versus V^2 for sets of geometrically similar solutes in decalin: (a) the F/G series; (b) the E series; (c) the acyclics. Points numbered as in Table 9.1; the heavy lines (generally parallel to the line in Figure 9.8) indicate the trends in each series. Points × are anomalous and may reflect solute association in these systems. Ordinate: $10^{35} I_r\bar{\nu}^2_{max}(g)$; abscissa: $10^{-2}V^2(Å^6)$

frequency. For planar rotation the relation:

$$\langle \mathbf{u}(0) \cdot \mathbf{u}(t) \rangle = \langle \cos \theta(t) \rangle = \exp\left| \int_0^t (t - s) \langle \boldsymbol{\omega}(0) \cdot \boldsymbol{\omega}(t) \rangle \, ds \right|$$

between the orientation and angular velocity autocorrelation function gives

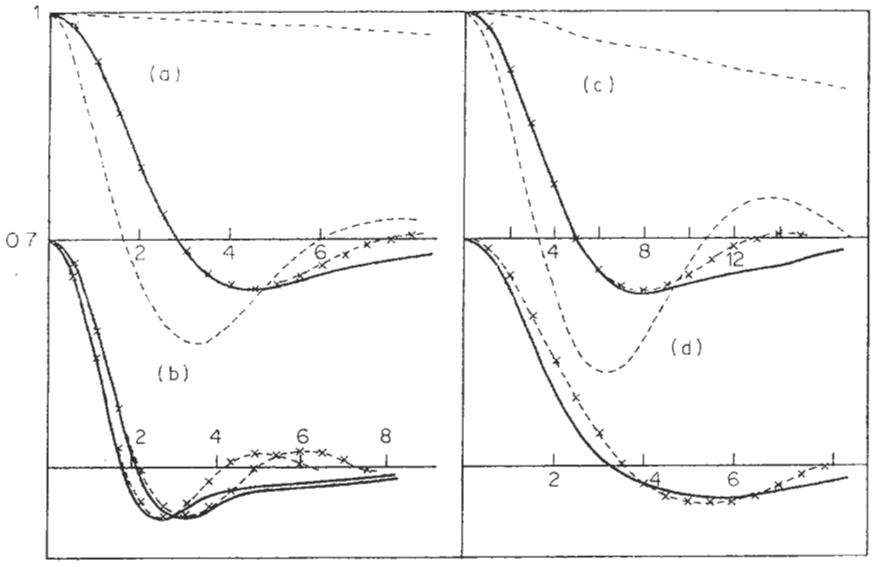

Figure 9.11 Itinerant oscillator simulation of rotational velocity a.c.f.'s for four solutes in decalin at 293 K: ——— experimental data (equation 9.10), —×××— analytic rotational velocity a.c.f. (see Appendix 9A), — — — — analytic angular acceleration a.c.f., —·—·—· analytic orientational a.c.f. (the analytic angular velocity a.c.f. is found to be identical to that of rotational velocity in all examples). (a) Pyridine; (b) chlorobenzene (for alternative choices of reduced inertia I_r); (c) dichloromethane; (d) chloroform. Abscissae: $10(kT/I_r)^{\frac{1}{2}}t$

(see Appendix 9A) a cumbersome form for the former which has been used to fit the solution data measured by Reid (1979a). Some typical fits are shown in Figure 9.11, where, for the pyridine and chlorobenzene system, the two curves coincide over the first half period of the oscillation, gradually diverging at longer times where both tend to zero.

For CH_2Cl_2 in solution the shallowness of the correlation function indicates an almost gas-like behaviour of these molecules, although similar forms for chloroform solution and other weakly polar systems with absorption maxima below 30 cm^{-1} may indicate appreciable band distortions due to induced absorption. The adequacy of equation (9A.3) when attempting to fit the experimental time correlation functions (at least where such functions have pronounced maxima as in Figure 9.11 is an improvement over other previously used models of far infrared behaviour. From the best fit parameters we are able to form the analytic approximations of other relevant correlation functions such as those of angular velocity, orientation, and torque. These are shown for the pyridine and CH_2Cl_2 systems in Figure 9.11 together with the form of the first memory function (the correlation function

of random torques). As can be seen, the latter is non-Gaussian although the second memory function is Gaussian by approximation.

The analytic spectral profile corresponding to a set of best-fit parameters is generally twin peaked as illustrated by the fit obtained for 10% fluorobenzene in decalin at 293 K, Figure 9.2. Here, the analytical curve has been matched in intensity to the experimental curve to emphasize how, despite the spectral distortion, there is at least some similarity with regard to the bandwidth and high-frequency fall-off. If we were to disregard absolute magnitudes completely (in view of our uncertainty concerning internal field factors) we could now attempt to explain why the model spectrum apparently consists of two components: a 'Debye shoulder' and a librational absorption, which have not fully merged. To some extent this is due to the planar nature of the model which is a method of avoiding the nonlinearities of the Euler equations in three dimensions. However, the approximant to the infinite, governing continued fraction is an early one. It does not describe well enough the evolution from deterministic quasi-free rotation at short times to stochastic behaviour. This shows up in the very far infrared.

The theoretical absorption intensity cross-section is generally much lower than the true absorption to the extent illustrated in Figure 9.12 using data for 10% dichloromethane in decalin. This is the internal field problem illustrated in Figure 9.1 which is responsible for the failure of sum rules, such as those of Gordon, to reproduce the complete cross-section.

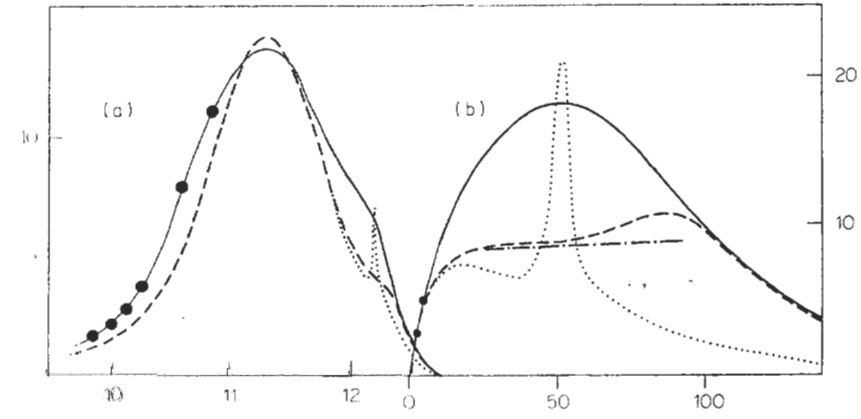

Figure 9.12 Itinerant oscillator spectral simulation of dichloromethane in decalin (293 K): (a) attenuation per frequency representation; (b) absorption; ——— interferometric data, ● ● microwave points, — — — I.O. model fit (parameters of Table 9.2), ... alternate fit based on a more literal interpretation of the I.O. model with a massive annulus (see Appendix 9A), ——·—·—· Debye plateau. (a) Ordinate: $10^3\alpha'/f$ in cm^{-1}; abscissa: $\log_{10}(f/\mathrm{Hz})$. (b) Ordinate: nepers fem^{-1}; abscissa: wavenumber fem^{-1})

In loss representation (Figures 9.2 and 9.12) the theoretical and experimental curves are well matched, the former having a Debye-type profile (except at THz frequencies) and peak intensity of $(\epsilon_0 - \epsilon_\infty)/2$. For CH_2Cl_2 this match at low frequencies is seen in the absorption representation as a juxtaposition of curves below 5 cm^{-1}. Above this frequency the analytical curve follows, and generally rises above, the plateau level of rotational diffusion, reaching a maximum at around 50–80 cm^{-1} before tailing off to higher frequency. The model therefore reproduces the basic features of (i) a Debye loss process, (ii) a resonance (libration) above the Debye plateau, and (iii) an inertial fall-off.

The contribution of induced-absorption to these bands is often overemphasized. In view of the dramatic shifts observable in these peaks to higher frequency with lowering temperatures (Section 9.6) it is thought more likely that the excess intensity is due to fluctuations in magnitude of the permanent dipole itself, i.e. the value of dipole moment responsible for far infrared absorption differing from that which gives rise to the loss process. This interpretation gives some justification for using spectral profiles rather than cross-sections in the evaluation.

Having demonstrated that the Mori/I.O. model describes short-time molecular dynamics and spectral profiles fairly adequately we have proceeded to evaluate the parameters γ, $K_0(0)$, and $K_1(0)$ using nonlinear least mean squares algorithms. The results are shown in Table 9.2. From $K_0(0) = \langle \Gamma(0)^2 \rangle / (4kTI_r)$ we can associate the reduced value $\bar{K}_0(0) = (I_r/kT)K_0(0)$ with the mean square torque. Indeed, in Table 9.2 we find that $\bar{K}_0(0)$ does generally increase with the molecular size as suggested by the analyses of the previous section. The larger value of $\bar{K}_0(0)$ found when rotation is assumed to be about centre of volume rather than centre of mass axes is not a significant result except in that it reflects the degree of uncertainty posed by the question of mode–mode coupling in those molecules concerned. What is significant is that, for all the systems, the ratio $K_0(0)/(2\pi c\bar{\nu}_{max})^2$ is not unity as would be expected from the phenomenological aspect of the theory. This means that the assumption that the observed peak frequency $2\pi c\bar{\nu}_{max}$ corresponds to the mean libration frequency is not correct. It does appear, however, that the ratio $K_0(0)/(2\pi c\bar{\nu}_{max})^2$ is reasonably constant with values centred about 2.5. Thus we may still take $\bar{\nu}^2_{max}$ to be in proportion to $K_0(0)$ and the result summarized as equation (9.13) is not significantly altered.

A further result may be drawn from the data of Table 9.2 where for all the systems $K_1(0)$ is greater than $K_0(0)$. In terms of the itinerant oscillator model this implies that the moment of inertia I of the annulus is less than that of the central disk containing the dipole ($I_2 < I_r$) and therefore contravenes the more literal model assumption that the annulus consists of a given number of nearest-neighbour molecules. In model terms the annulus is only a mathematical convenience to describe the interaction between the

Table 9.2 Mori/I.O. model best fit data for data for decalin systems at 293 K

		$(I_r/KT)^{1/2}$	$\bar{K}_0$	$\bar{K}_1$	$\bar{\gamma}$	$K_0/(2\pi c\nu_{max})$	τ_{Mori}	τ_{exp}
1	CH_2Cl_2	0.24	13.4	23.4	6.7	2.6	0.95	1.1
2	CH_2Br_2	0.27	15.7	23	6.9	2.0		
3	t butylchloride	0.59	26.4	67.6	12.9	3.7	3.0	3.4
4	chloroform	0.55	32.6	86.9	15.2	3.36	3.1	4.2
5	2 chloro-2-nitro propene	0.7	49.7	104	16	2.6		
6	methyl iodide	0.37	35.9	56.2	11.9	2.05		
7	furan	0.38	34.3	60	12.2	2.56	2.6	2.0
8	thiazole	0.45	35.9	66	12.8	2.46		
9	pyridine	0.48	41.5	81.8	14.2	2.5	3.35	3.1
10	bromobenzene	1.04	82	224	23.5	3.7	8.5	16.2
		1.27	147	333	28.6	4.4	16	
11	fluorobenzene	0.69	61	118	17.1	2.37	6.0	4.0
12	chlorobenzene	0.85	77.7	130	18	2.6	9.2	10.7
		0.97	110	176	21	2.84	12.7	
13	pentafluorobenzene	1.04	129	232	24	3.7	13.8	9.8
14	α picoline	0.55	69.4	93	15.5	1.8	6.5	8.5
15	nitrobenzene	0.98	147	277	26.2	2.8	13.6	20
		1.15	211	398	31.4	2.94	19	
16	phCN	0.87	135	218	23.4	2.26	12.6	27
17	aniline	0.69	94.5	94.3	11.6	1.35		
18	toluene	0.69	100	112	17.3	1.64	10.7	9
19	oxylene	—	—	—	—	—	—	12
20	chloronaphthalene	1.0	141	193	22.3	1.73	16.6	29
21	bromonaphthalene	1.13	149	239	24.5	2.27		
		1.32	207	322	28.5	2.3		

dipolar molecule and its environment, the best-fit analyses now showing how on average such a region contains less than one molecular centre. Intuitively we do not expect a dipolar molecule in the liquid state to be permanently encaged by (say) six neighbours constrained to rotate cooperatively in a circular motion about the common centre. Rather, at random instants there may be one or more neighbours coupled to the dipole and giving rise to librational motion, such instances being interspersed with periods in which the dipole undergoes a less restricted rotation. The annulus envisaged is therefore neither permanent nor rigid, although at times shorter than those required for appreciable translational diffusion it may approximate to these conditions. At longer times, the disregard of diffusive interchange of neighbouring molecules is expected to result in partial failure of the itinerant oscillator model, especially for systems where the libration and relaxation processes are on appreciably different time scales. Such breakdown of the Mori/I.O. theory is illustrated in Section 9.6 where we present data for some very viscous and glassy systems. Use of a modified I.O. theory involving a fourth parameter to partly account for the effects of a nonrigid annulus does, however, allow a more reasonable description of such systems.

The implication, from $K_0(0) < K_1(0)$ of a tenuous annulus, places a serious doubt on the ability of the original itinerant oscillator concept to simulate both the short-time (far infrared) and long-time dynamics of molecules in liquid. The latter may be most appropriately described in terms of the orientational correlation function whose analytic form is given in equation (9B.11). At long times this equation becomes purely exponential with a single relaxation time τ_{Mori} given in terms of the molecular parameters as $\tau_{\text{Mori}} = (kT/I)K_1(0)/(\gamma K_0(0))$. Theoretically (Quentrec and Bezot, 1974), the three parameters could be determined from spectral measurement at a minimum of three separate frequencies although practically, as shown above, they are more accurately determined by best-fitting in the time domain. Sufficient spectral data to perform a numerical transformation and best fit analysis may be obtained from a single far infrared interferometric experiment (20–200 cm^{-1}) so that it is possible to predict long-time behaviour from the short-time details reflected in far infrared profiles (Reid and Evans, 1980). In addition to providing a critical test of the I.O. model by comparing τ_{Mori} values with the Debye times τ_{D} found from independent microwave measurements, the approach emphasizes the causal nature of the libration-relaxation process.

Table 9.2 gives several comparisons of τ_{Mori} and τ_{D}, the latter having been obtained from τ_{exp} by correction with the Cole field factor $(2\epsilon_0+\epsilon_\infty)/3\epsilon_0$ (Cole, 1965). Except for C_6H_5F and C_6HF_5 τ_{Mori} and τ_{D} are within 30% of each other, these two being within 50%. The agreement is not so good for benzonitrile and 1 chloronaphthalene (within a factor of two only). In addition, for chloro-, bromo-, and nitrobenzene systems, the parameters obtained by choosing the larger reduced inertias appropriate to torque-determined axes give significantly larger and more realistic values of τ_{Mori}. This further evidences translation/rotation coupling.

The Mori/I.O. can therefore simulate both the long and short time details of a large number of solutes in decalin at 293 K. In terms of absorption the two peaks do not merge completely to give the single observed absorption band, which is partly a consequence of translation/rotation coupling and the cog-wheel effect of large angled motions.

It may be argued that although Debye's model of rotational diffusion (Debye, 1929) involving τ_{D} is not sufficiently general and must be replaced by a non-Markovian model, the continued use of τ_{D}, the long-time decay constant in the orientational autocorrelation function, serves as a simple measure for describing molecular dynamics in several fields of study and thus has a technological interest. We have indicated how the loss peak is linked to the far infrared peak and how their frequency and separation depends on the degree of rotational hindrance (mean square torque). To illustrate this dependency we may note the wavenumbers of both peaks, and, to compare with other systems, these may be normalized by multiplying

each by the root of the solute reduced inertia. We then find (Figure 9.5), using this coordinate, that the pair of peaks for CH_2Cl_2 in decalin are close together, while for the nitrobenzene system they are more widely separated due to the increased rotational hindrance. A similar peak separation occurs for a given system with lowering temperature. We now attempt to derive a direct relationship between τ_{D} and its associated far infrared peak position.

The underlying equation of motion is a generalized Langevin equation of the form:

$$I\ddot{\theta}(t) = -\int_0^t K_0(\tau)\dot{\theta}(t-\tau)\,\mathrm{d}\tau + \Gamma(t).$$

In the long-time diffusion limit the central term reduces to $\alpha\dot{\theta}(t)$ where α is the 'friction constant' which (by analogy with the theory of linear diffusion) is related to the correlation function of $\boldsymbol{\Gamma}(t)$, the random torque:

$$\alpha = (2kT)^{-1}\int_{-\infty}^{\infty} \langle \boldsymbol{\Gamma}(0)\,.\,\boldsymbol{\Gamma}(t)\rangle\,\mathrm{d}t.$$

It may also be shown that α is related to the mean square displacement by $\alpha = 2kT\langle\dot{\theta}^2\rangle^{-1}t$ and hence kT/α is the rotational diffusion constant. As τ_{D} is the averaged time required for a dipole to rotate by 1.2 radians (the angular values which causes $\langle\cos\theta(t)\rangle$ to decay to e^{-1}) then it must be equal to α/kT (within a geometric constant). Using Reid's result that $\langle\boldsymbol{\Gamma}(0)\,.\,\boldsymbol{\Gamma}(t)\rangle$ may be factored into $V^2P(t)$ where $P(t)$ is the a.c.f. of torque-per-unit-volume-of-rotation, we have finally:

$$\tau_{\text{D}} \doteq V^2(kT)^{-2}\int_0^{\infty} P(t)\,\mathrm{d}t.$$

Under conditions of common solvent and temperature $P(t)$ is expected to evolve in a similar manner for all the solute systems studied so that τ_{D}, V^2, and $I_r\bar{\nu}^2_{\max}$ are all in proportion. To confirm this behaviour, the relaxation times of Table 9.2 have been plotted against their respective V^2 values in Figure 9.13. In addition the figure shows the Mori predicted values, which, for those solutes where two possible values of I_r and V^2 were considered, are linked by dashed lines. The resulting distribution of points appears to be well correlated, although not as well as for the almost linear distribution found between $I_r\bar{\nu}^2_{\max}$ and V^2. This is expected in view of the more complex (cooperative) behaviour at long times and the consequent dependency of τ_{D} not only on the far infrared peak position but also on its band-shape. It seems that it is possible to use a curve such as in Figure 9.13 to predict the relative values of τ_{D} from a simple consideration of solute geometry and to a better accuracy than that predicted by Debye's model.

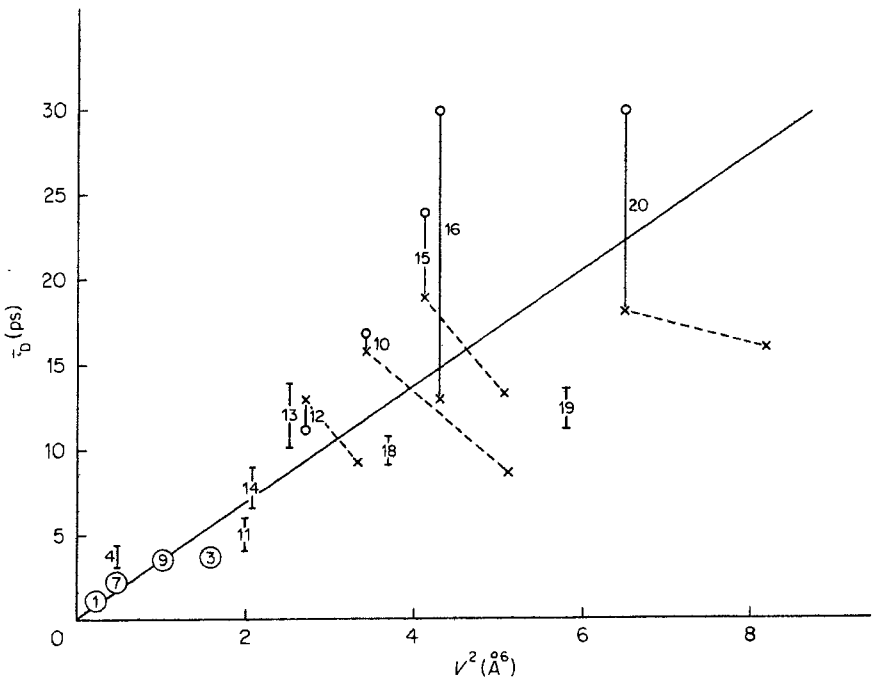

Figure 9.13 The variation of macroscopic relaxation times with solute size numbered as in Table 9.2 × Mori predicted values; ● experimental values. Ordinate: τ_D(ps); abscissa: $10^{-3}V^2$(Å^6)

9.5 Hydrogen bonding and far infrared spectroscopy

9.5.1 *Water and aniline*

These have been discussed by Pardoe (1969). Subsequently, a number of spectra of aqueous systems have been taken by Hasted (1972) and Afsar *et al.* (1976). In pure liquid water the spectrum is a broad band whose portion up to about 200 cm^{-1} appears as a shoulder on a very extended absorption centred at about 658 cm^{-1}. Although liquid water is a very intense absorber, its integrated absorption is much lower than is predicted by the Kroon and Van der Elsken (1967) relationship for the integrated absorption intensity, based on the sum rule devised by Gordon, who extended in turn the Thomas–Reiche–Kuhn sum rule:

$$A = \int_0^\infty \alpha(\bar{\nu})/N \, d\bar{\nu} = \frac{\pi}{3c^2} \sum \mu_z^2 \left(\frac{1}{I_x} + \frac{1}{I_y}\right).$$

Here I_x and I_y are the moments of inertia about axes perpendicular to that

containing the electric moment μ_z. The integration is carried out over the complete range of rotational modes occurring in the liquid and therefore includes both the Debye peak in the dielectric loss (at low frequencies) and the Poley peak in the power absorption coefficient $\alpha(\bar{\nu})$ (neper cm^{-1}) which appears in the range up to 200 cm^{-1} for non-hydrogen-bonded liquids.

The problem in liquids such as water is to isolate the Poley absorption from other low frequency modes due to the nature of the extensive network of H-bonds. The gas phase integrated intensity at a density corresponding to that of the liquid at ambient temperature and pressure is calculated from the sum rule as 60×10^{-18} cm. This is an order of magnitude greater than the total experimental intensity as measured by Pardoe (1969) up to 200 cm^{-1} (4.2×10^{-18} cm). The gas phase intensity is that in the absence of interaction, using the dipole moment and moment of inertia of the isolated molecule. However, in the liquid state extensive hydrogen-bonding will increase the effective moment of inertia thus leading to a greatly reduced absorption intensity. The hydrogen-bonding can be largely eliminated by dilution. This isolates the absorption of free water, which is, not surprisingly, vastly different from that of bound water. This is dealt with in more detail later.

The experimental absorption in the far infrared of pure liquid aniline, also studied by Pardoe (1969), contrasts with that of water in that the integrated intensity is much greater than expected on the basis of the rotational motion of a gas phase molecule. A similarly structured and dipolar, but non-hydrogen-bonded, molecule is chlorobenzene. The two molecules have very similar moments of inertia and virtually identical dipole moments: μ chlorobenzene (in benzene) = 1.58 D whilst μ aniline (in benzene) = 1.53 D. The former has a maximum of $\alpha = 16.8$ neper cm^{-1} at 44 cm^{-1}, whereas aniline is 45 neper cm^{-1} at this wavenumber, and peaks with 80 neper cm^{-1} at $\bar{\nu} = 100$ cm^{-1}. Pardoe explains this as being due to the relaxation of the NH$_2$ group at frequencies higher than the whole molecule (Debye) relaxation.

Garg and Smyth (1967) have studied liquid aniline in the dielectric region (microwave and lower frequencies). The loss peaks at about 7 cm^{-1} but bears little resemblance to a Debye loss curve due to the vibrational deformation of the N–H $\cdots$ N hydrogen bonds and the librational contributions at higher frequencies. Dilute solutions of aniline in cyclohexane (Pardoe, 1969) show a considerably greater absorption per molecule than does the pure liquid. This is expected because hydrogen-bonding results in an increased effective moment of inertia, thus moving the whole-molecule relaxation to lower frequencies and stopping the high-frequency rotation or inversion process.

9.5.2 *The alcohols*

These have been widely studied (Davies, 1971) over the complete zero THz range (radio, microwave, and far infrared frequencies) over a broad range of

temperature. The alcohols may be supercooled easily, and at low temperature the major dispersion is at radio frequencies. At ambient temperatures there is a large discrepancy between ϵ_∞ of the Cole–Cole plot and the square of the refractive index n_D^2 at high frequencies. For example, $\epsilon_\infty = 5.4$ for 1-propanol ($n_D^2 = 1.92$). In loss representation, the far infrared absorption of the alcohols appears as a small supplementary 'foot' on the high frequency side of the Cole–Cole arc.

The alcohols were extensively studied in the far infrared by Davies and methanol by Mandel and Mazur (1958) in the range 100 to 500 wavenumbers. For liquid methanol an absorption was observed at 120 cm^{-1} with a shoulder at 250 cm^{-1}. On cooling to 173 K the peak at 120 cm^{-1} 'sharpened up' and shifted to 163 cm^{-1} whilst the shoulder at 250 cm^{-1} became a sharp absorption centred around 350 cm^{-1}. Both bands are hydrogen-bond stretching modes. The intensity of the 163 cm^{-1} band remains constant from solid to liquid, which suggests that most of the methanol molecules are also H-bonded in the liquid. Below a concentration of 0.12 mole $litre^{-1}$ in dilution the band at 120 cm^{-1} disappears.

In the far infrared the absorption spectra of the n alkyl alcohols up to n-octyl alcohol show the same featureless absorption whose intensity increases with increasing frequency up to 100 cm^{-1}. The data by Davies agree well with microwave points at 4.5 cm^{-1} and 3.1 cm^{-1}. The absorption is a rising continuum to 120 cm^{-1}. Apart from the first two primary alcohols—methanol and ethanol—the integrated absorption intensity per molecule, A (in cm), is seemingly constant. According to Davies this establishes that the absorption in the far infrared is primarily dependent on the hydroxyl group and not on other molecular features such as the moments of inertia of the molecule. This result is in agreement with a similar study of Pardoe's (1970) on primary and secondary alkyl bromides. In this, all primary alkyl bromides with the exception of bromoethane were shown to have the same integrated absorption intensity. The prime difference between the bromides and the alcohols is that the former all peak below 60 cm^{-1}, whereas the alcohols all have maxima above 120 cm^{-1}. This means that Pardoe was able to estimate the integrated intensity of the total zero–THz absorption due to the C–Br dipole, whereas in the alcohols the intensity estimate is restricted to the absorption occurring below 100 cm^{-1}. In view of the spectral effect of replacing Br by OH it would seem that the absorption in the alcohols is determined by the OH groups involved in extensive H-bonded aggregation. Davies gives further support to this argument by comparing the integrated absorption intensities per molecule for butan-1-ol and 1-bromobutane between 0 and 100 cm^{-1}. For the former ($\mu = 1.71$ D), this is 60.7×10^{-20} cm, for the latter ($\mu = 2.0$ D) $A = 46.9 \times 10^{-20}$ cm which does not accord with the *a priori* expectation that the A would be proportional, by the sum rule, to the square of the dipole. Therefore it seems that association (with subsequent increase in the effective moment of inertia) is occurring in the alcohol.

In order to clarify the origins of these far infrared bands a dilution study was carried out of n-butanol in cyclohexane by Davies (1971) over the frequency range 20 to 180 cm^{-1} (Figure 9.14). The pure alcohol peaks at 150 cm^{-1} but this disappears at a concentration of 0.005 mole $litre^{-1}$. At 0.088 mole $litre^{-1}$ the n-butanol molecules are still associated in solutions because there is no linear dependence either of absorption coefficient or integrated intensity on concentration: the absorption is not due to the libration of single molecules.

The tert-butyl-alcohol is known for its inability to form a complex H-bonded system—only a dimer—and its zero–THz spectrum clearly peaks at 70 cm^{-1} when expressed in terms of power absorption coefficient. There is an extra absorption (Figure 9.15) at 145 cm^{-1} which Davies attributes to association, i.e. a low frequency mode of the dimer hydrogen-bond. If this is correct the intensities of the two bands should change with respect to each other on dilution.

Davies emphasized that the complete zero–THz region should be considered when analysing the spectral features for the information they contain on molecular motion and interaction. A consequence of this is his calculation of the foot observed by Garg and Smyth (1967) in n-propanol. In order

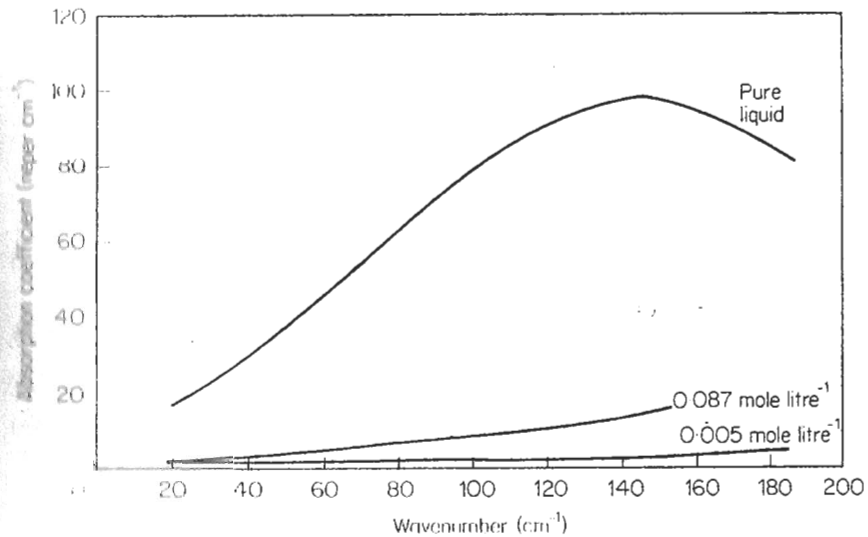

Figure 9.14 Graph of power absorption coefficient against wavenumber. Far infrared dilution spectrum of n-butanol (Reproduced by permission from G. J. Davies, Thesis, University of Wales, 1971)

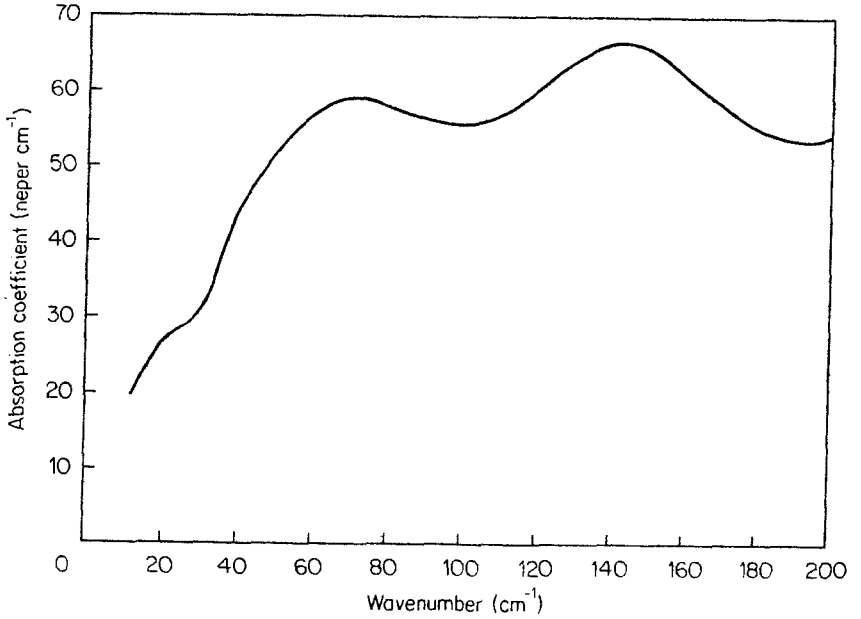

Figure 9.15 Far infra-red spectrum of t-butanol (Reproduced by permission from G. J. Davies, Thesis, University of Wales, 1971)

to convert the absorption coefficient into both dielectric loss and permittivity it was necessary to use the Kramers–Kronig relation

$$\int_0^\infty (\epsilon''(\bar{\nu})/\bar{\nu})\,\mathrm{d}\bar{\nu} = \frac{\pi}{2}(\epsilon_0 - \epsilon_\infty). \tag{9.14}$$

In terms of absorption coefficient this is:

$$\int_0^\infty (\alpha(\bar{\nu})/\bar{\nu}^2)\,\mathrm{d}\bar{\nu} = \frac{\pi^2}{n(\bar{\nu})}(\epsilon_0 - \epsilon_\infty) \tag{9.15}$$

and by defining the limits of the integral more specifically, say between $\bar{\nu}_1$ and $\bar{\nu}_2$, the relation is modified to:

$$\int_{\bar{\nu}_1}^{\bar{\nu}_2} (\alpha(\bar{\nu})/\bar{\nu}^2)\,\mathrm{d}\bar{\nu} = \frac{\pi^2}{n(\bar{\nu})}(\epsilon_1 - \epsilon_2) \tag{9.16}$$

where ϵ_1 and ϵ_2 are the dielectric permittivities at the frequencies $\bar{\nu}_1$ and $\bar{\nu}_2$ respectively. From the plot of $\alpha/\bar{\nu}^2$ vs. $\bar{\nu}$ for n-propanol the value of the integral was evaluated between specific limits and the permittivities at the higher frequency ϵ_2 was deduced. This procedure was repeated until the

frequency end of the zero-THz band. The corresponding dielectric loss was then calculated from the Maxwell relation:

$$\epsilon''(\bar{\nu}) = 2n(\bar{\nu})(\alpha(\bar{\nu})/4\pi\bar{\nu}).$$

The complete Cole–Cole arc is shown in Figure 9.16 together with an enlarged diagram of the high frequency portion. From this it can be seen that the presence of a 'foot' is established beyond doubt; also the shape is well defined. The fall off to n_D^2 is not gradual but more of a distinct portion of a semicircle. A large semicircle can be drawn through the low-frequency points as well as through the high-frequency data. However, this type of construction is being replaced by modern approximants of the Liouville equation, as explained in the appendices. The complexity of the molecular dynamics in hydrogen-bonded media such as the alcohols is evident and molecular dynamics simulation should be useful in untangling the various threads in the leaven of the far infrared spectra. In this respect the method of dilution is a useful simplification and has proven especially useful in the case of water.

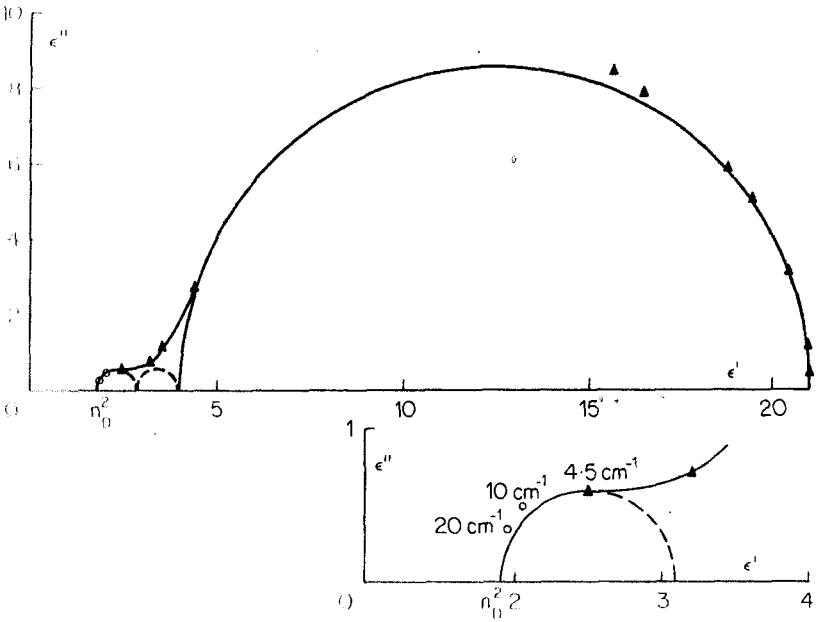

Figure 9.16 Complete Cole–Cole plot for n-propanol, as calculated by G. J.

9.5.3 *The molecular dynamics of water free from hydrogen bonding*

The hydrogen-bonding in pure liquid water means that the observed Cole–Cole plot takes its apparently semicircular form from the combined motion of many molecules. At far infrared frequencies, however, the Cole–Cole plot is considerably more complicated—and has been drawn in detail by Hasted (1972) (Figure 9.17). However, if water is dissolved in organic solvents such as cyclohexane, benzene, and carbon tetrachloride the hydrogen bonding between water molecules is removable (Evans, 1976). The zero–THz spectrum of a dilute solution of water in, for example, carbon tetrachloride is informative in the sense that the motion of individual water molecules free from H-bonding is revealed directly. The difference between the hydrogen-bonded and free water loss curves is illustrated in Figure 9.17. The dielectric loss of the latter type peaks at *over* $100\,cm^{-1}$, well above the microwave peak frequency of the former. The corresponding reorientational correlation function, $\langle \mathbf{u}(t) \cdot \mathbf{u}(0) \rangle$ ($\mathbf{u}$ being the water dipole unit vector), is not exponential so that the intermolecular dynamics cannot be described by the classical Debye/Stokes/Einstein picture of rotational diffusion requiring infinitely fast, infinitesimally small changes in the angular orientation of an individual

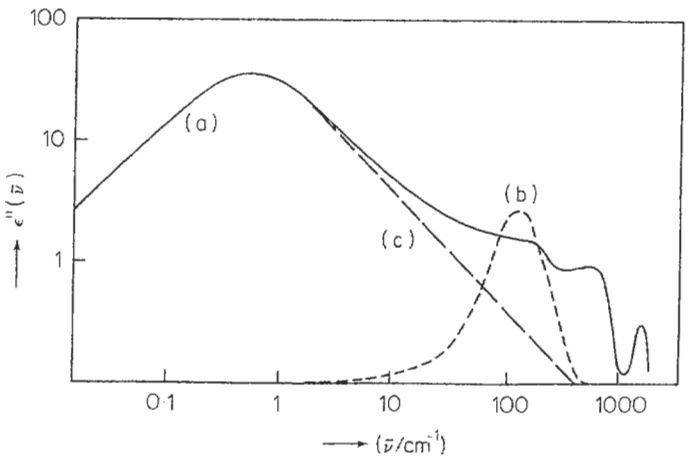

Figure 9.17 Dielectric loss for: (a) pure liquid water; (b) a dilute solution of water in cyclohexane; (c) Debye theory, behaviour at high frequency (Reproduced by permission of the Royal Society of Chemistry from M. W. Evans *et al.*, *J. Chem. Soc. Faraday Trans. II*, 1978, **74**, 337, and *J. Chem. Soc. Faraday Trans. II*, 1980, **76**, 667) (Note this diagram is also being used in Evans et al "Molecular Dynamics", Wiley/Interscience, N.Y., 1982)

dipole moment. The correlation time:

$$\tau_M = \int_0^\infty \langle \mathbf{u}(t) \cdot \mathbf{u}(0) \rangle \, dt \equiv \int_0^\infty \phi_u(t) \, dt$$

is of the order of 0.1 ps in the three solutions measured by Pardoe and Gebbie (1970) (carbon tetrachloride, benzene, and cyclohexane). Such a short value is expected for a molecule with the inertial properties of water but with the hydrogen-bonding absent. (The average moment of inertia of water is only 2×10^{-40} g cm^2 about axes perpendicular to that of the dipole.)

Loss curves ($\epsilon''(\omega)$) and correlation functions can be calculated analytically by fitting the far infrared absorption data of Pardoe and Gebbie to a theoretical curve generated using the continued fraction representation of the reorientational memory function. This is a theory developed by Nee and Zwanzig (1970) and is described in Appendix 9A.

The far infrared absorption data of Pardoe and Gebbie for very dilute solutions of water in cyclohexane, carbon tetrachloride, and benzene were fitted to equation (9B.4) using a nonlinear least-mean-squares minimization program (N.A.G. E04 FAA). The results are illustrated in Figure 9.18 where the corresponding correlation function $\langle \mathbf{u}(t) \cdot \mathbf{u}(0) \rangle$ is also displayed. Table 9.3 shows the values of $\phi_1(0)$ and γ needed for each fit together with the correlation time τ_u. The memory functions are displayed in Figure 9.19 together with the dielectric loss curves $\epsilon''(\omega)$ calculated from $\alpha(\omega)$ Figure 9.20.

Here $\epsilon''(\omega)$, the dielectric loss, and $n(\omega)$, the frequency dependent refractive index, is virtually constant, near the D-line value, for these low absorbing systems.

The value of $\phi_0(0)$ is in each case close to the theoretical symmetric top value of $2kT/I_B$, the water molecule being in reality an asymmetric top. In contrast, the torque-dependent parameter $\phi_1(0)$ is solvent-dependent to a greater extent.

The motion of the dipolar water molecule cannot be described as rotational diffusion because the correlation functions $\langle \mathbf{u}(t) \cdot \mathbf{u}(0) \rangle$ are not exponential. In cyclohexane, there is a probability that a majority of molecules will have moved through greater than $\pi/2$ rad. at $\geq$0.11 ps because $\phi_u(t)$ becomes negative before oscillating to zero at about 0.4 ps. The overall correlation time is 0.10 ps, much shorter than the Debye relaxation time in pure water, where many molecules are simultaneously contributing to the relaxation process. The loss curve in cyclohexane is asymmetric when plotted on a log scale, and peaks at about 140 cm^{-1}.

Oscillations in $\phi_u(t)$ are apparent also in solution in carbon tetrachloride, but here the correlation function remains positive, implying that the H_2O molecule has slightly less angular freedom ($\phi_1(0)$ is slightly higher) than in cyclohexane, and jumps of smaller amplitude are possible. This conclusion is

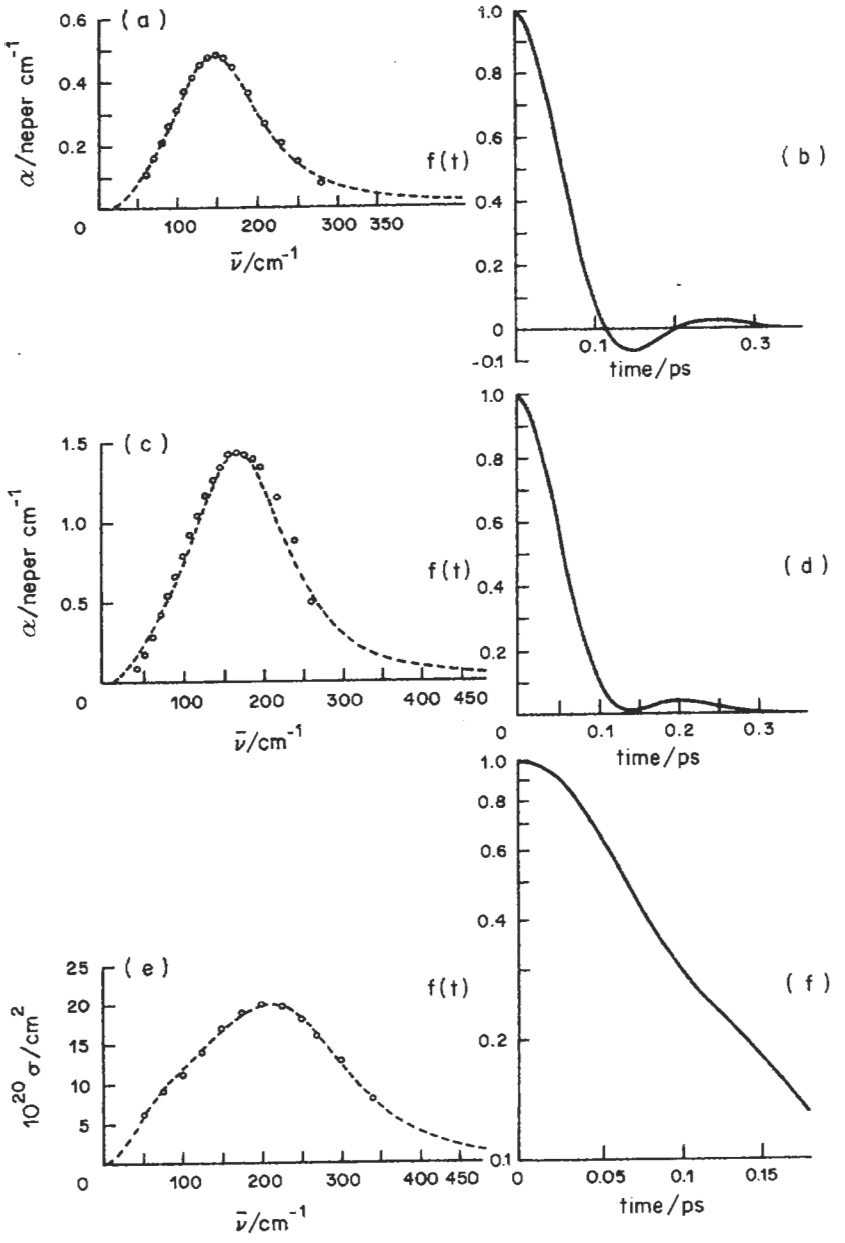

Figure 9.18 (a) Absorption of a 0.011% W/w solution of water in cyclohexane at 296 K, corrected for solvent. (b) Orientational autocorrelation function $\langle u(t) \, . \, u(0) \rangle$ for the absorption of (a). (c) 0.01% W/w solution of water in CCl_4 at 300 K, corrected for solvent. (d) $\langle u(t) \, . \, u(0) \rangle$. (e) 0.06% W/w solution of water in benzene at 300 K. (f) $\langle u(t) \, . \, u(0) \rangle$ for H_2O/benzene. (Reproduced by permission of the Royal Society of Chemistry from M. W. Evans *et al.*, *J. Chem. Soc. Faraday Trans. II*, 1978, **74**, 337, and *J. Chem. Soc. Faraday Trans. II*, 1980, **76**, 667)

Table 9.3 Parameter for water free of hydrogen bonding*

Solution	T (K)	$\phi_0(0)$	$\phi_1(0)$	γ	τ_μ (ps)
H_2O + cyclohexane (0.011% w/w)	296	1.11	3.00	2.58	0.10
$H_2O + CCl_4$ (0.01% w/w)	300	1.18	3.39	2.37	0.08
H_2O + benzene (0.06% w/w)	300	1.16	6.19	2.82	0.09

* normalized.

open to uncertainty since the original fit is not as satisfactory as for the solution in cyclohexane.

The oscillations in $\phi_u(t)$ are damped out almost completely in the benzene solution, but the semi-logarithmic plot shows that the correlation function is not exponential, so that Debye-type relaxation is not taking place. The loss curve is highly asymmetric and peaks at 70 cm^{-1}, considerably lower than in cyclohexane and carbon tetrachloride solutions. The shape of $\phi_u(t)$, the correlation function, is independent of $\phi_0(0)$, and depends upon the torque $\phi_1(0)$ and width parameter γ only, at each time t.

The autocorrelation function and its associated memory function describe a system of molecular reorientations where past events have a bearing on what happens at future times, unlike Debye relaxation, where $\mathbf{u}(t)$ is Markovian and $\langle \mathbf{u}(t) \, . \, \mathbf{u}(0) \rangle$ is purely exponential. Since $\phi_u(t)$ is an even, equilibrium function of time, it can be shown that the memory function must also have the same property, and subsequently its Maclaurin expansion must ideally contain even powers of t only. The $\phi_0(t)$ used in generating the loss curves of Figure 9.19 is even up to t^2, but contains a term in t^3, and the orientational autocorrelation function contains a term in t^5. Therefore both are approximations to the theoretically even functions, but are reasonably adequate for present needs.

There are few memory functions available for comparison with those of Figure 9.19, but Kushick and Berne (1973) have computed these for the velocity of selfdiffusion of an argon molecule in a Lennard–Jones fluid at several number densities. The overall form of these functions of argon molecular diffusion and the rotational water memory functions are similar. For lower molecular number densities, the translational memory function for argon has a shallow negative region and is damped to zero with slight oscillations. These features are reproduced in our rotational $\phi_u(t)$, the oscillation being most pronounced in the benzene solution. The memory function becomes negative after 0.10 ps in cyclohexane, 0.08 ps in CCl_4, and

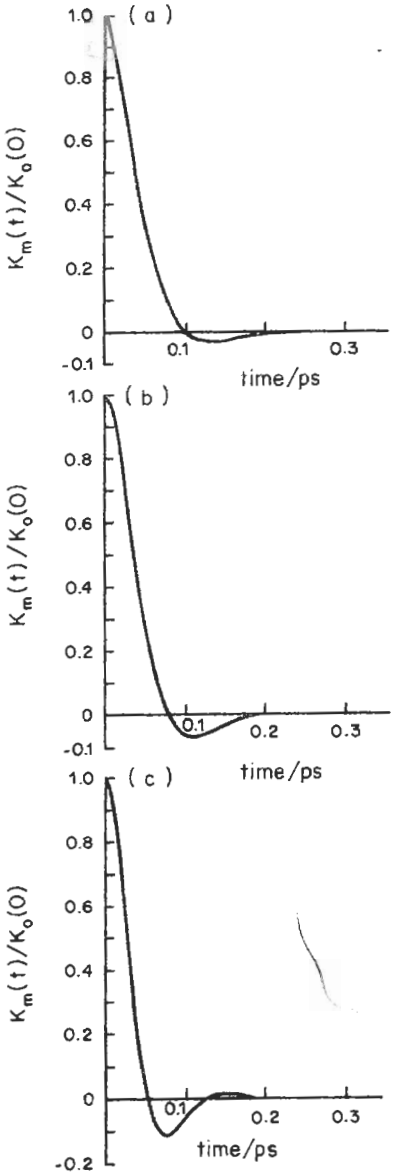

Figure 9.19 (a) Normalized memory function for H_2O/cyclohexane of Figure 9.18. (b) As for (a), H_2O/CCl_4. (c) Memory function for H_2O/benzene at 300 K. (Reproduced by permission of the Royal Society of Chemistry from M. W. Evans *et al.*, *J. Chem. Soc. Faraday Trans. II* 1978, **74**, 337, and *J. Chem. Soc. Faraday Trans. II*, 1980, **76**, 667)

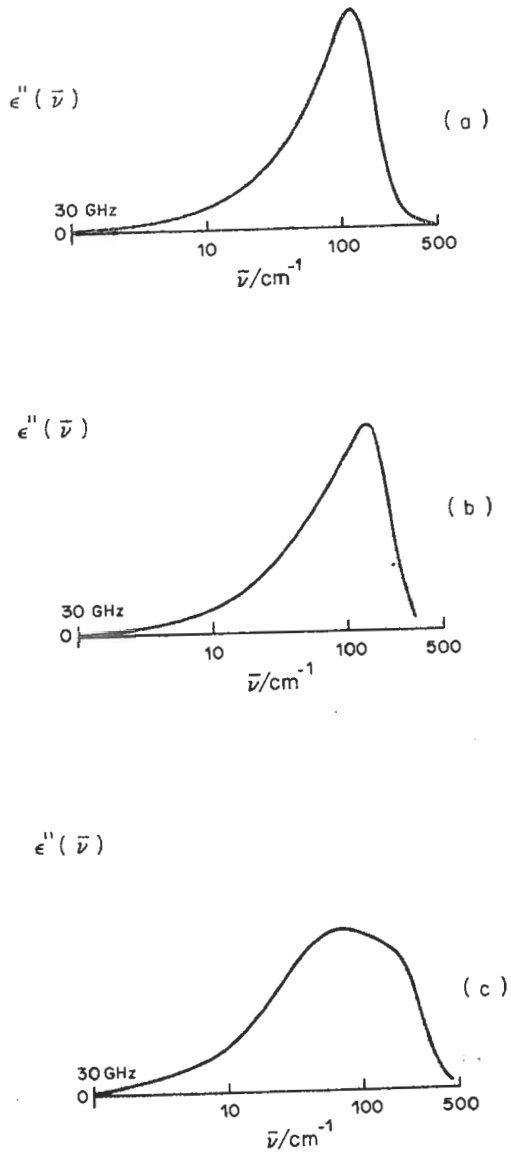

Figure 9.20 (a) Loss curve estimated for Figure 9.19(a). (b) Loss curve of Figure 9.19(b). (c) Loss curve for H_2O/benzene, Figure 9.19(c). (Reproduced by permission of the Royal Society of Chemistry from M. W. Evans *et al.*, *J. Chem. Soc. Faraday Trans. II*, 1978, **74**, 337, and *J. Chem. Soc. Faraday Trans. II*, 1980, **76**, 667)

0.05 ps in benzene, suggesting that the 'collision' process in the latter solution is shortest lived, since instantaneous inertialess events would correspond to a delta function for $\phi_0(t)$ at $t = 0$. This is evidence for the effect of anisotropy of solvent molecules in the motion of the solute H_2O.

9.6 Molecular motion in ultra-viscous and vitreous environments. Dynamical evolution from ps to years

The dynamical evolution from an arbitrary initial $t = 0$ of an ensemble of small dipolar molecules in a low temperature, ultra-viscous environment is slowed enormously in comparison with that at room temperature. Johari (1973), Johari and Smyth (1972), Johari and Goldstein (1972), Williams and Hains (1971), and Williams *et al.* (1977) have shown that at low frequencies in a wide range of solutions the dielectric loss in the ultra-viscous and vitreous environments peaks more than once. There is a secondary relaxation which appears at higher frequencies than the main dielectric loss. The latter's activation energy plot is nonlinear and high compared with that of the higher frequency (β) relaxation, for which these plots are linear. The lower frequency peak is termed the α process. Both α and β peaks appear at very low frequencies (Hz–kHz) compared with observable loss at room temperature, which for small dipolar solutes appears in the microwave (GHz) region.

This has widespread implications in fields of spectroscopy which give insights into aspects of molecular dynamics other than dipolar rotational relaxation. These include infrared and Raman bandshape analysis (roto-vibrational relaxation), incoherent and coherent inelastic scattering of thermal neutrons (rototranslational motions), depolarized light scattering (single particle and collective rotational modes of motion and their interrelation), Brillouin spectroscopy of scattered light and acoustic relaxation (dispersion of thermally propagated sound waves), mechanical visco-elastic relaxation, and others, including the rapidly developing techniques using laser pulses on the time scale of picoseconds to measure directly the equilibration of some property of a molecule initially put out of equilibrium by the laser pulse.

However, both the α and β peaks are manifestations of the nature of the dipolar dynamical evolution at elapsed times which are relatively very long, i.e. at low frequencies. The properties of the classical autocorrelation function, however, imply that *there will be another peak in the far infrared analogous to that discussed in Sections* 9.1–9.5 *for liquids at room temperature.*

In the ultra-viscous and vitreous states of matter therefore the complete dielectric loss process consists of a *continuous* band, covering many decades of frequency, which must peak at least twice, and sometimes three times. The α peak appears at lowest frequencies, the broad β peak lies at

intermediate frequencies, and the *relatively* sharp far infrared peak, which we shall designate 'the γ process', always remains at THz frequencies. In contrast, at room temperature, the dielectric broad-band spectrum consists of the main microwave (GHz) peak, with a barely resolved THz γ shoulder at higher frequencies. The γ peak (but not the α and β—see Section 9.1) is within range of the spectral techniques mentioned above, and of computer simulation methods.

The existence of three peaks in the extreme broad-band dielectric spectrum challenges much of the current mathematical thought on modelling, i.e. approximating the Liouville equation describing the dynamics of many interacting molecular potentials. The (α, β, γ) triad is observable in *small, simple rigid,* dipolar molecules such as the halogenobenzenes or methylene chloride and a model must be able to describe effectively the complete (zero frequency to THz) dielectric spectrum under all conditions where end over end dipole reorientation is still possible. If such a model describes satisfactorily the spectrum under conditions of low viscosity, *then it should also be able to produce an* (α, β, γ) *profile as the viscosity rises.*

The existence of a relaxation process at low frequencies must, irrespective of its detailed origin, be associated with a short-time process which will appear in the far infra-red. The α and β features are causally related, i.e. they and the γ peak are manifestations of the same underlying dynamic process and are representable in terms of a single orientational correlation function, which has a natural non-exponential behaviour at long and short times.

Some γ peaks are illustrated in decalin glass at 110 K in Figure 9.21 and at room temperature (296 K). The glass phase spectra are much more symmetric than those of the liquid solutions due to the proximity of the main microwave (GHz) loss in the latter. The spectra of Figure 9.21 detail the short-time molecular movements which in ultra-viscous and vitreous media eventually evolve into motions taking place on an immensely slower time scale observable as (α, β) features in the dielectric loss. The complete dynamical process is governed mathematically by Liouville's equation. It is not enough to approximate this using rotational diffusion.

This point is emphasized by the very large shift between liquid and glass in the peak frequencies, $\tilde{\nu}_{max}$, of Figure 9.21. These are proportionately different for each solute, being 18 cm^{-1} (46% increase) in C_6H_5F solute, 19 cm^{-1} (56%) for C_6H_5Cl, and 20 cm^{-1} (87%) in C_6H_5Br. This frequency is not defined with rotational diffusion, there is no theoretical peak, only a plateau, but the observed changes reflect environmental effects on molecular dynamics in detail.

By determining the rate of shift of the α and β features to give activation energies we may reasonable extrapolate to yield the complete dielectric loss spectra of Figure 9.22 whose far infrared portion appears as the feature

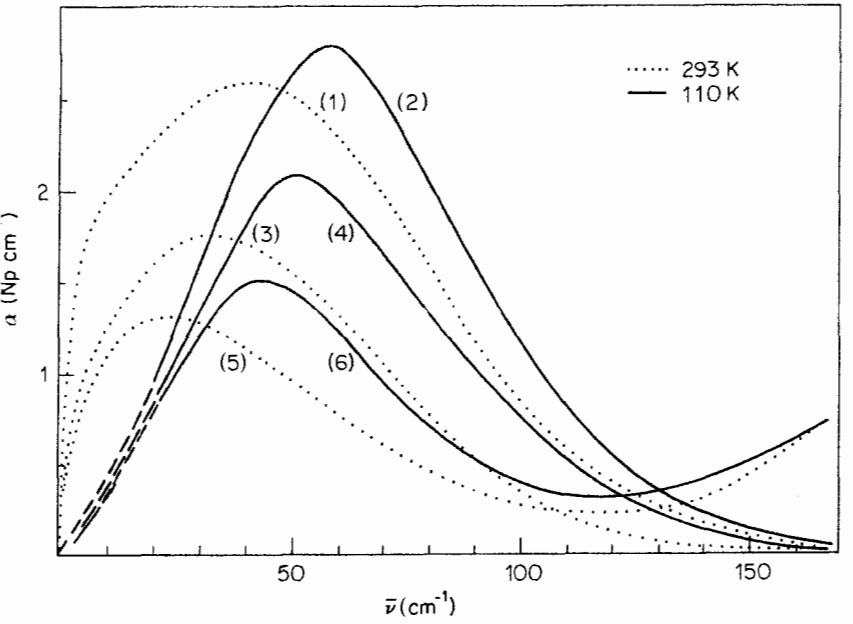

Figure 9.21 Power absorption coefficient $\alpha(\omega)$ (neper cm^{-1}) vs. $\bar{\nu}$ (sec^{-1}) for halogenobenzenes in decalin (10% v/v concentration): (1) fluorobenzene/decalin at 293 K ($\bar{\nu}_{max} = 39\ cm^{-1}$); (2) at 110 K, $\bar{\nu}_{max} = 57\ cm^{-1}$, vitreous solution; (3) chlorobenzene/decalin at 293 K ($\bar{\nu}_{max} = 34\ cm^{-1}$); (4) at 110 K ($\bar{\nu}_{max} = 53\ cm^{-1}$); (5) bromobenzene/decalin at 293 K ($\bar{\nu}_{max} = 23 \pm 3\ cm^{-1}$); (6) at 110 K ($\bar{\nu}_{max} = 48\ cm^{-1}$). (Reproduced from C. J. Reid, Thesis, University of Wales, 1979, copyright: C. J. Reid, University of Wales)

Figure 9.22 (a) Zero–THz dielectric loss spectrum for 10% v/v fluorobenzene in decalin, illustrating the (α, β, γ) triad at 143 K in the supercooled solution. At 293 K the spectrum is made up only of β and γ components, as is the case in the glass at 110 K and 77 K, the α component in the latter two cases having moved to 'immeasurably' low frequencies. Plots of $\log_{10}(\epsilon'')$ against $\log_{10}(f/Hz)$: (1) 77 K; (2) 110 K; (3) 143 K; (4) 293 K.

(b) Zero–THz dielectric loss spectrum of 10% v/v chlorobenzene in decalin: (1) 120 K (glass); (2) 130 K (glass); (3) 138 K (ultra-viscous supercooled liquid); (4) 143 K (supercooled); (5) 293 K. Note the decreased amplitude compared with (a) of the β process of curve (4).

(c) Bromobenzene/decalin (10% v/v): (1) 110 K (glass); (2) 145 K (ultra-viscous liquid); (3) 293 K (liquid)

Source as for Figure 9.21

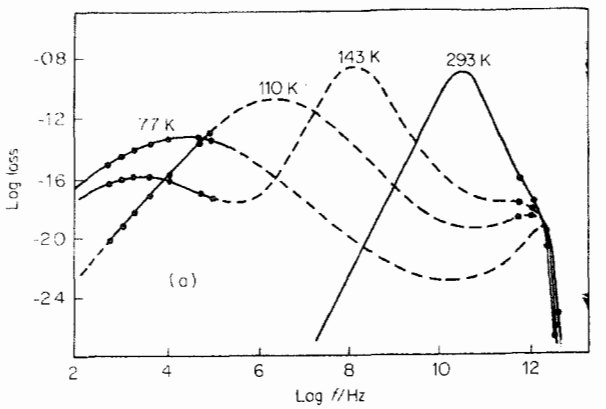

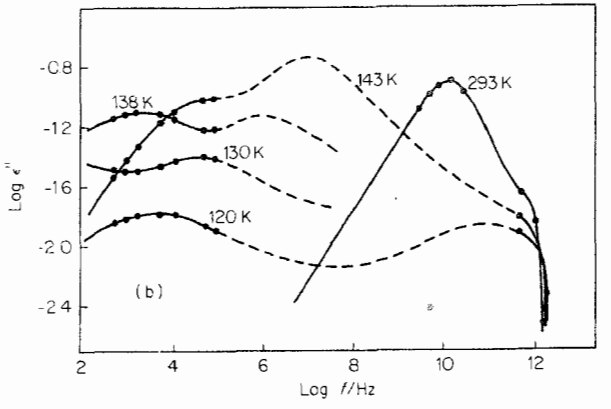

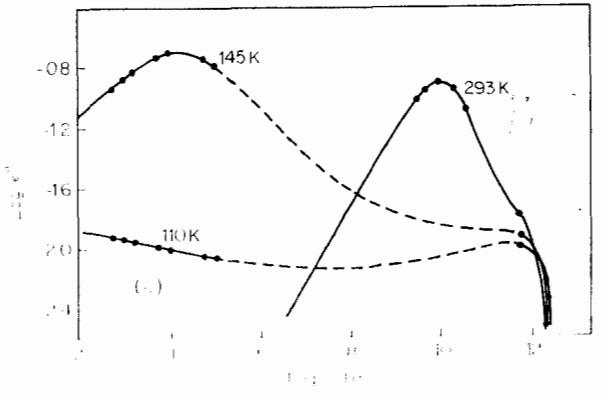

labelled γ. At 148 K in supercooled C_6H_5F/decalin, 15 K above T_g, the glass transition temperature, the loss in the kHz range is dominated by the α feature of three decades half-width. If the measurement temperature is lowered this moves out of range to lower frequencies while the shoulder of the β loss approaches from higher frequencies. At our lowest accessible temperature of 77 K the β process may be distinguished as a band of four decades half-width.

Figure 9.22 illustrates how the microwave (or Debye) loss in room temperature liquid becomes resolved from the γ feature (which shifts, Figure 9.21, with decreasing temperature in the opposite direction), eventually resolving also the α and β features at about 180 K. At this temperature the viscosity of the supercooled liquid solution is a few orders of magnitude higher than in the ambient liquid. At 143 K, where the α process is measurable, we can estimate the β peak to be at 10^8 Hz (by virtue of activation enthalpy). It is of course desirable to check this estimate with more data measured at low temperatures throughout the technically difficult MHz–GHz region. However, the estimate is based soundly on the well-known linearity of the β peak frequency vs. temperature plot. Some features of both peaks at 137 K (4 K above T_g) may be seen in Figure 9.23, and possibly a shoulder of the α process at 27 K (6 K below T_g in the glass). The α loss maximum in the glass must be at extremely low frequencies, as indicated by the Arrhenius plot of Figure 9.24. At 10 K (23 K below), the β process centres at about 3 MHz, and ϵ_0 is falling due to the progressive freezing-in of all large-angled molecular motion. This means that the molecular mean square torque is larger and that the γ peak shifts to higher frequencies as in Figure 9.21. The whole process, from picoseconds to koloseconds (or years), provides us with a new challenge of adequately approximating the Liouville equation in the course of any analytical description. *It is clear that dynamicists are currently restricting their model evaluations to a much too narrow range of both macroscopic viscosity and frequency.* There is no mathematical description currently available to explain even the gross features of the (α, β, γ) triad in terms of the motion of individual molecular dipoles. The fastest computers (e.g. the CRAY) are wholly inadequate to simulate motions over the decades of Figure 9.22. It seems a matter of some urgency therefore that a range of experimental techniques should be brought to bear on molecular motion in the vitreous and ultra-viscous states of matter.

To end the discussion on C_6H_5F/decalin we note that the activation energy (ΔE) for the β process, 12 kJ mole^{-1}, is similar to that derived from measurements in the microwave region at around room temperature, while ΔE for the α process is (90 ± 15) kJ mole^{-1}, with no temperature dependence over a limited range of kHz frequencies. The linearly extrapolated intercept of the α and β plots is about 130 K, this being approximately where the two features become resolved in the supercooled liquid.

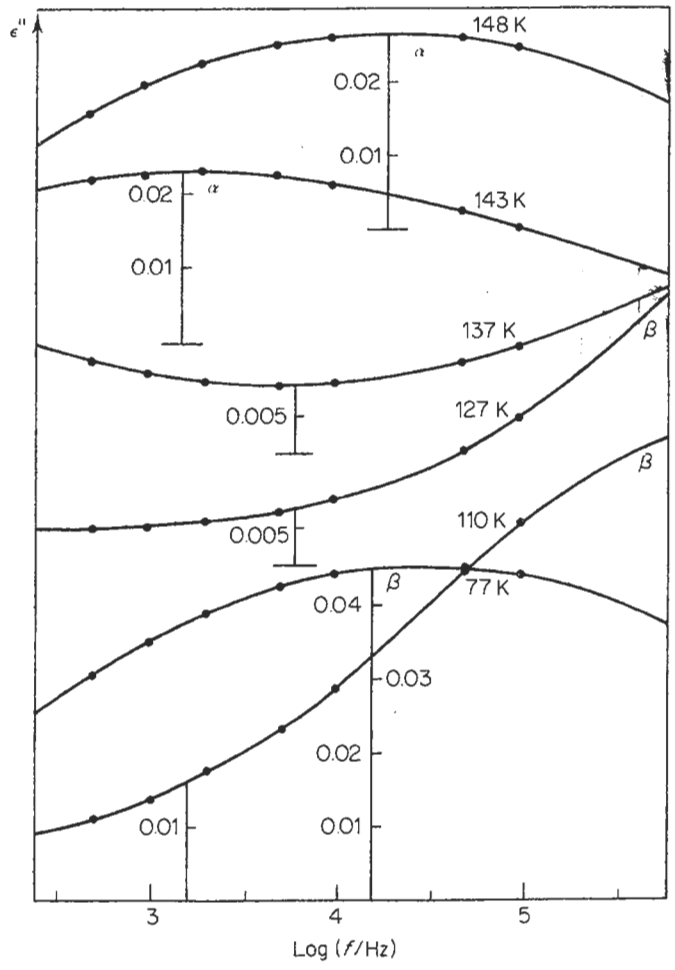

Figure 9.23 Isothermal low frequency loss spectra for 10% v/v fluorobenzene in decalin: (1) 148 K; (2) 143 K; (3) 137 K; (4) 127 K; (5) 110 K; (6) 77 K. Glass transition temperature = 133 K. Plots of ε'' vs. $\log_{10}(f/\text{Hz})$ (Source as for Figure 9.21)

The zero–THz loss spectra for the C_6H_5Cl/decalin system are shown in Figure 9.22. At kHz (audio) frequencies the results have been checked with those of Johari and Goldstein (1972), and are very similar. At 143 K the α and β peaks are only just resolved at a much lower temperature than for C_6H_5F in decalin. The decrease in intensity of the β process as it moves into range from higher frequencies is more than in C_6H_5F/decalin, while ΔE for the α peak is again about seven times that for the β.

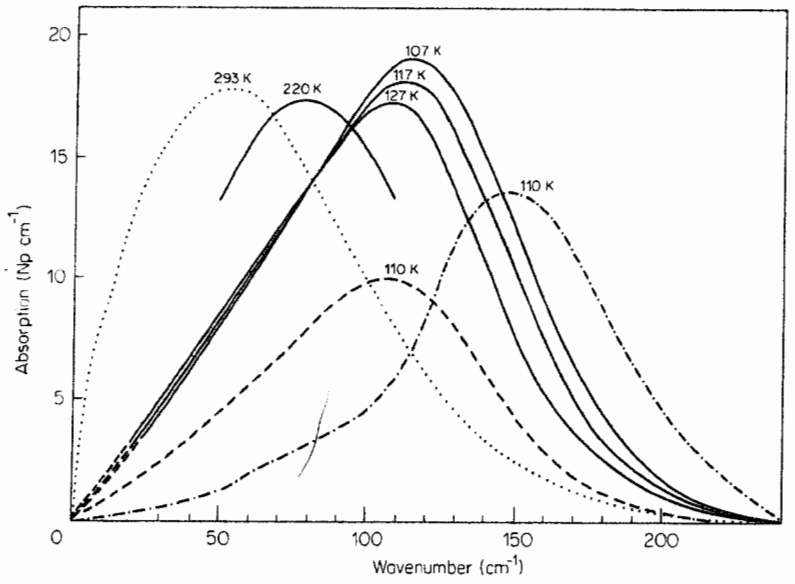

Figure 9.24 Far infra-red spectrum of CH_2Cl_2 systems: ..... At 293 K, ——— 10% v/v CH_2Cl_2/decalin, — — — 5% v/v CH_2Cl_2/decalin at 110 K, — · — · — · — 10% v/v CH_2Cl_2 (10% pyridine/toluene)

Dielectric measurements on C_6H_5Br/decalin reveal in Figure 9.22 only the single presence of the α peak whose behaviour at low frequencies compares well with Johari's measurements. In the glass at 110 K only the wing of this absorption, with possibly losses due to impurities and inherent d.c. conduction, are present at low frequencies. There is no discernible β process but the high frequency far infrared γ process is well defined (Figure 9.21), indicating torsional oscillation at these frequencies. This is not cooperative, and the γ peak is not a crystalline lattice mode whose dielectric loss adjunct lies at an immeasurably low frequency because the relaxation processes in a single crystal occur on a geological time scale of tera-seconds or longer.

To summarize the results for the halogenobenzenes, in C_6H_5F/decalin there is a well-defined β process, in C_6H_5Cl/decalin it is much less intense, and in the bromide it is either unresolved or vanishingly small. We therefore form the hypothesis that it exists only for small ratios of solute to solvent size. This hypothesis may be evaluated by using smaller molecules in decalin. Such a molecule is methylene chloride, a rigid dipolar asymmetric top.

The far infrared power absorption coefficient of a rapidly cooled, transparent and presumably mono-disperse sample of 10% CH_2Cl_2 in decalin at

107 K is shown in Figure 9.24 to peak at $\bar{\nu}_{max} = 114\ cm^{-1}$ compared with its liquid phase value (at 293 K) of $53\ cm^{-1}$. This 113% increase makes this system ideal for studying the variation of the far infrared $\bar{\nu}_{max}$ with temperature, and curves for three intermediate temperatures are also shown. The rate of peak shift in the glass is similar to the overall shift from the room temperature shift, about $3\ cm^{-1}$ per 10 K.

The kHz loss process (β) in the glass is dramatically temperature dependent. The peak is observable at 110 K and shifts across the two decades of measurement for only a 4 K increase in temperature. By 118 K the glass phase kHz losses are again small, and remain so until at 20 K higher a second loss process becomes apparent. Before this can be characterized, crystallization occurs at 140 K and the losses at this temperature slowly reduce with time. If this temperature is not reached, the loss spectra are reproducible upon cooling and intensities do not vary between samples if they are rapidly cooled. The observed peak at the lowest temperatures was thus interpreted as the β process, the magnitude of which was estimated to account for one third of the total polarization. In view of the very high apparent activation energy ($\Delta E = 100\ kJ\ mole^{-1} \pm 10\%$) its nature is different from those of the halogenobenzene systems discussed earlier. The low-frequency loss processes are illustrated in Figure 9.25.

The origins of this β process may be investigated further by using

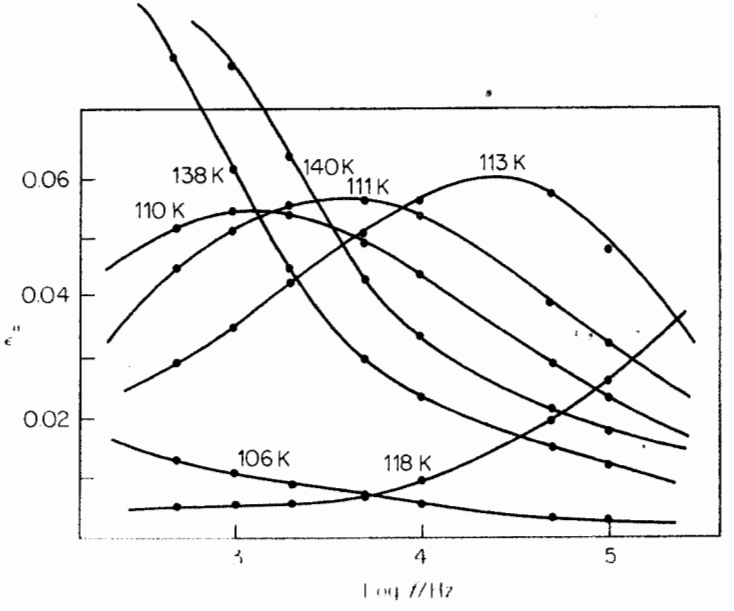

Figure 9.25 kHz loss spectra for 10% CH_2Cl_2 in decalin

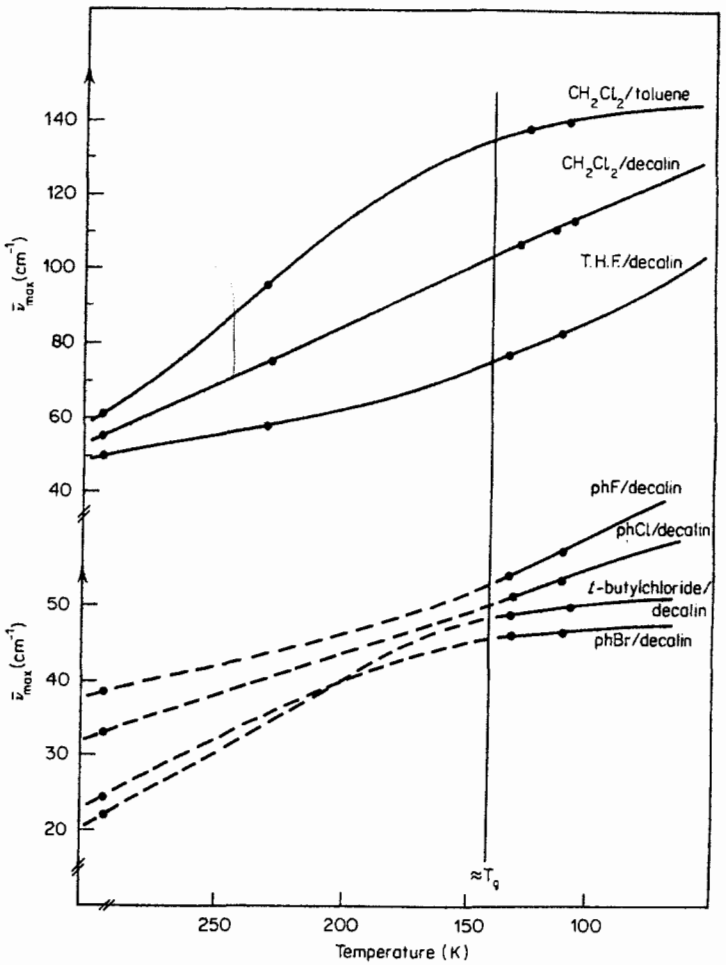

Figure 9.26 Variation of γ absorption peak with temperature

different glassy solvents. For this purpose toluene is useful, and also mixtures of pyridine and toluene (10% of the former). A 10% v/v solution of CH_2Cl_2 in toluene/pyridine solvent produces a very large shift in $\bar{\nu}_{max}$ of the far infrared (Figure 9.24) as the temperature is lowered from ambient to 110 K in the glass (53 cm^{-1} to 140 cm^{-1}). The loss peak, clearly observable in decalin, has, however, disappeared. In the far infrared it appears that the rate of shift of $\bar{\nu}_{max}$ has reduced in the glassy state compared with its value in the liquid, and thus differs from the CH_2Cl/decalin system which shows a linear dependence of ν_{max} on T throughout the accessible range.

The far infrared behaviour is reflected in that of the dielectric process in that the CH_2Cl_2/pyridine/toluene system has no β process of measurable intensity, the rotational motion being frozen-in as indicated by the nondispersive low values of $\epsilon'(\omega)$ obtained, close to that of the solvent. In other words the activation energy (barrier height) for the process is very high, and this can be associated with the large shift of $\bar{\nu}_{max}$ and the convexity of this dependence ($d^2\bar{\nu}_{max}/dT^2 < 0$) in Figure 9.26. The C_6H_5Br/decalin system also has a slight convexity of slope (and no β process) while the curve for C_6H_5Cl/decalin is more linear and that for C_6H_5F/decalin (with prominent β process) is of concave slope.

The results for several systems can be summarized in terms of the molecular mean square torque which is proportional to $I_r\bar{\nu}^2_{max}\ T$ (equation 9.11). Although several more accurate measurements are required to complete these plots the indication is that for systems where a β process is absent, i.e. of such weak intensity that it is not resolved, the plots reach their maximum values in the supercooled viscous phase above T_g, the glass transition temperature, while for systems with prominent β peaks the curves are generally of overall negative gradients which suffer discontinuities at or below the glass transition range.

The β loss process in CH_2Cl/decalin is classified as such because of its occurrence (at kHz frequencies) at a temperature much lower than the glass transition temperature of the solvent (137 K) and because the presence of a lower frequency region of loss may be discerned at a temperature just above 137 K and prior to crystallization. The activation energy (100 kJ mole^{-1}) for the process is however very high compared with anything reported previously and is comparable with the values found by Johari for α processes, so that its designation as a β process must be substantiated. In defending this assignment it may be argued that as CH_2Cl_2 is a molecule of very different geometry to those studied by Johari *et al.* the high value of activation enthalpy is not necessarily anomalous. It is, however, remarkable that no similar β processes have yet been observed for similar solute molecules (such as CH_2Br_2, SCl_2, and $SOCl_2$). These solute molecules are only slightly larger than CH_2Cl_2. To confirm the existence of the β peak in CH_2Cl_2/decalin the solution was monitored for loss and permittivity at a fixed frequency (1 kHz) while rapid cooling from room temperature was effected (about 10 K per minute at T_g). Under these conditions measurement of temperature is less accurate and gradients may exist in the sample. However, the permittivity is observed to rise from 2.6 at 293 K to 3.3 at about 160 K, below which the value decreases and appreciable loss is observed. The loss is again minimal at about 136 K until at lower temperatures the second peak appears. The main (α process) loss is clearly seen at 160 K to 130 K, and is distinct from the loss at 110 K which must therefore be of a secondary (β) nature.

A study of CH_2Cl_2 in more stable decalin/toluene or decalin/cholesteryl oleyl carbonate solvents allows both α and β processes in CH_2Cl_2 to be characterized. The latter appears in the kHz region at the same temperature as for the present system and its activation energy has the same large value as in decalin.

In view of the possible plasticizing effect of CH_2Cl_2 solute on the fluidity of decalin, the glass transition temperature was measured for 5% and 10% v/v solutions. No appreciable lowering of T_g (<10 K) was found so that the β process at 110 K is a property of the glassy state of this system. Finally, the process may be associated with the presence of aggregates of CH_2Cl_2 rather than the mono-disperse solute rotation. That it is not due to normal crystalline CH_2Cl_2 is inferred from the reduced intensity of the peaks seen after a sample has been annealed at 140 K for some time.

The far infrared spectrum for the 4% v/v CH_2Cl_2/decalin system peaks at 95 cm^{-1} at 114 K, which is appreciably lower than the spectrum for a 10% v/v solution. A measurement for a 5% v/v concentration also given in this figure confirms this variation with concentration and thus indicates that 'solvent shifts' may occur even in a rigid environment and apparently with greater effect, the shift on dilution from 10% to 5% at 107 K being 10 cm^{-1} while at room temperature it is only 2 cm^{-1}. A concentration effect was also found in the kHz region as a broadening of the peak from 3.6 decades of half-width to 4.0 decades, but without any apparent change in activation energy. (The broadening may arise in part from inadvertent experimental factors such as the presence of thermal gradient in the samples.) Whether the effects are due to dipole–dipole interactions or the presence of a larger number of smaller molecules in the system (density and microviscosity changes) may be usefully investigated in the future.

To further attempt to verify the hypothesis made for the β process, that it occurs only for favourable solute to solvent geometry and size ratios, the motion of CH_2Cl_2 was studied in several mixed solvents. To create only slight changes in the decalin solvent environment, neo-pentane or cyclohexane (both nondipolar, nearly spherical molecules) decalin mixtures were used as solvents. The former gave glassy solutions in all proportions with decalin and the latter at least up to 50% v/v. Despite the differences in glass transition temperature (as low as 120 K for 50% neo-pentane), the process was still observed at kHz frequencies at about 110 K with the same high activation energy and slightly increased intensity (30%). Again crystallization prevents spectral observation of the α process seen transiently on cooling. However, by combining decalin with the lath-like molecules of cholesteryl oleyl carbonate a more stable system with CH_2Cl_2 may be formed and both α and β processes have been observed. For 10% v/v CH_2Cl_2 in 1:7 cholesteryl oleyl carbonate/decalin, the α peak is observed at 150 K to 146 K (Figure 9.27), while almost 40 K lower the β peak is

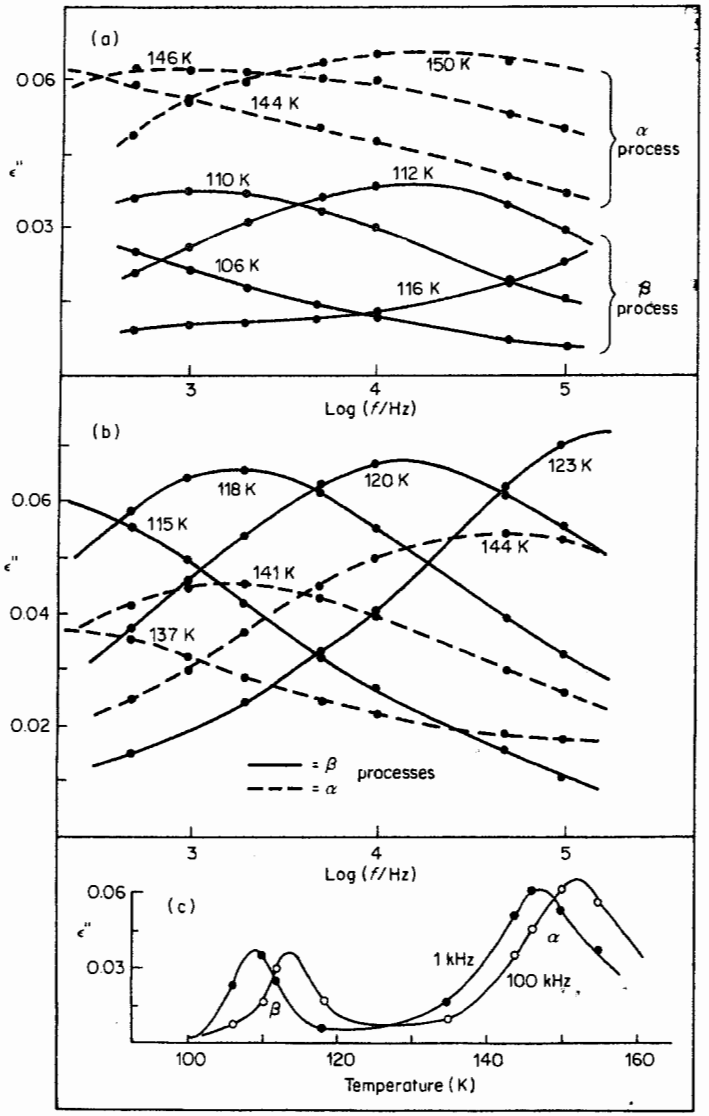

Figure 9.27 Dielectric data for 10% v/v CH_2Cl_2 in mixed glass forming solvents. (a) Loss spectra for CH_2Cl_2 in 1:7 C.O.C./decalin; (b) loss spectra for CH_2Cl_2 in 1:9 toluene/decalin; (c) loss versus temperature for (a)

observed with the same activation energy and a lower intensity than for the CH_2Cl_2/decalin system (by 50%). The α process involves relaxation of both CH_2Cl_2 ($\mu = 1.6$ D) and cholesteryl oleyl carbonate ($\mu = 1.14$ D) although the latter appears from pure solution measurement to contribute less than 20%. For 10% CH_2Cl_2 in 1:3 cholesteryl oleyl carbonate/decalin, the β process disappears and only a more intense α process is observed. A similar behaviour occurs for toluene/decalin solvent as shown in Figure 9.27b. For 10% CH_2Cl_2 in a 1/9 toluene/decalin solvent the system is stable and both α and β peaks may be characterized. Less than 10% of α peak intensity is estimated to be due to toluene so that an activation energy of 119 kJ mole^{-1} may be associated with CH_2Cl_2 motion in this solvent and can be compared with values of from 138 to 170 kJ mole^{-1} for solutes in decalin. The β process has an activation energy of 107 kJ mole^{-1} and is of greater intensity than for the concentration in decalin. In a 2/8 toluene/decalin solvent the β peaks have lost intensity to the α process while in a 3/7 toluene/decalin system the β peak is absent and the α peaks are of variable intensity and over three times the height of those in the 1/9 toluene/decalin system (Figure 9.27). One particular feature of the (3/7 toluene/decalin) solvent system is that the activation energy plot is decidedly nonlinear (Figure 9.28). The initial slope implies 28.5 kJ mole^{-1} which increases at 129 K to 120 kJ mole^{-1}. The estimate of T_g for this system (by calorimetry) is 127 K, so it appears that at 129 K the α and β processes separate, the β process being unobserved (unresolved) but presumed to evolve along the line of lowest slope.

The gradual reduction of CH_2Cl_2 β-process intensity by the replacement of decalin with the molecules of toluene or cholesteryl-oleyl-carbonate may be due to their more laminar molecules preventing the formation of suitable sites for liquid-like rotation in the medium or there may be a dipolar interaction between these weakly polar molecules and CH_2Cl_2. A parallel may be drawn with a concentration effect on sites found by Moliton (1972) for solid solutions of diethyl-ether in n-pentane. This study revealed kHz dielectric absorptions at low temperatures up to 30 K below the melting point (142 K) whose intensities initially increased linearly with concentration but above 2.5% fall sharply to a negligible level above 4%. The activation energy for each concentration remained at a value of 30.7 kJ mole^{-1}. In the present comparison of CH_2Cl_2 systems, the polarity has been increased by adding toluene or cholesteryl oleyl carbonate to a point where the CH_2Cl_2 absorption has become negligible but without change in ΔE. (Moliton's measurements have been repeated for 2% ether concentration to confirm this rotation in the solid phase, and a higher activation energy of 76 kJ mole^{-1} was obtained.)

As the activation energy of the unique CH_2Cl_2/decalin process does not vary significantly with partial solvent changes it could be that the solute

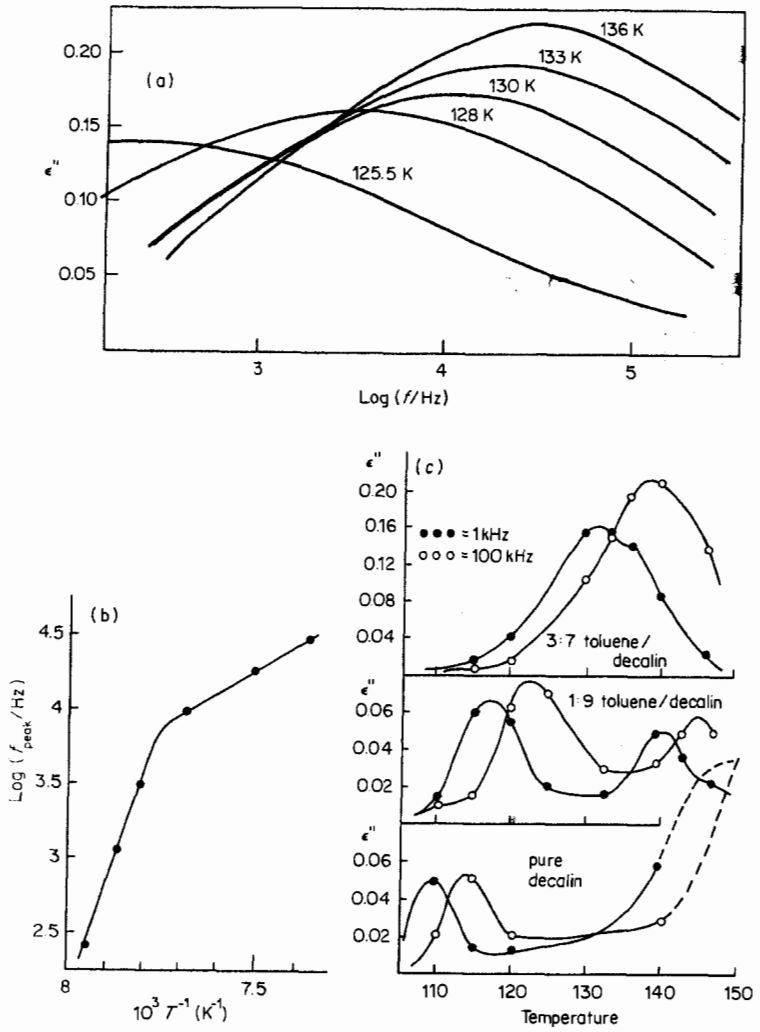

Figure 9.28 Dielectric data for 10% v/v CH_2Cl_2 in toluene/decalin solvents. (a) Loss spectra for CH_2Cl_2 in 3:7 toluene/decalin; (b) Arrhenius plot for the peaks observed in (a); (c) comparison of peaks in glasses of increasing toluene content

becomes associated in some way with decalin molecules. Cis-decalin is a particularly flexible molecule, as may be seen using a skeletal model, and the small CH_2Cl_2 molecules could become 'locked' within this flexing mechanism. However, the β intensity is not reduced when up to 50% of the decalin is replaced by isopentane, cyclohexane, or methylcyclohexane, so polarity must be a principal factor. In addition the behaviour in mixed solvents

appears to be specific to CH_2Cl_2 systems as a 10% solution of fluorobenzene in 1:1 cholesteryl-oleyl-carbonate:decalin system still revealed both α and β processes. Finally, one is left with the possibility that this process may be caused by aggregation of CH_2Cl_2 into dimer or polymer clusters. The structures of these would have to be different from that of the normal crystalline solid as no dielectric absorptions were found for pure

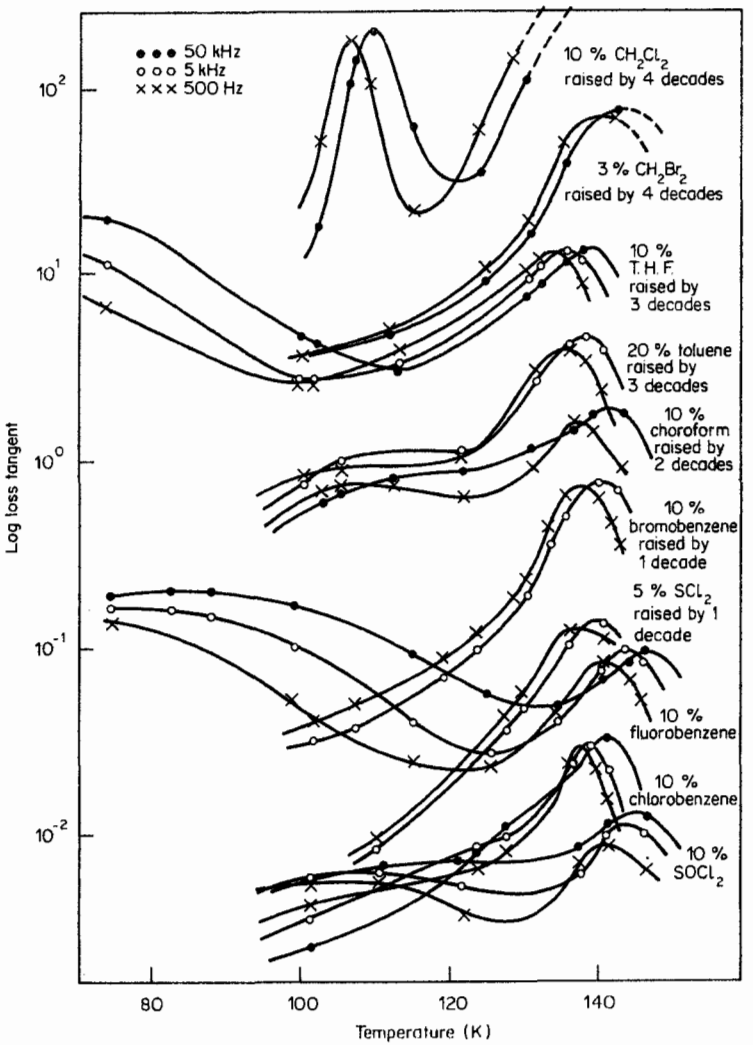

Figure 9.29 Log loss tangent showing α and β processes in decalin glass

CH_2Cl_2 at these temperatures. Possibly if clusters do form in the decalin environment they are weakly bound and act as rotator phases, while, in a decalin/toluene environment, solvation is more effective and CH_2Cl_2 solutes are mono-disperse (and without a β process). To clarify the mechanism of the β process a study will be made in the future to search for subtle differences in far infrared behaviour.

It is clear that further accurate work would help explain the apparent uniqueness of the β processes observed. For the other solutes studied the most common manifestation of the β process is as a high-frequency shoulder on the main α process, as exemplified by the 10% chlorobenzene/decalin system. The results for several more solutes are presented in Figures 9.29 and 9.30. The activation energies for these β shoulders are between 24 and 30 kJ mole^{-1}, values which are intermediate between the low ones found for tetrahydrofuran and C_6H_5F and the high value for CH_2Cl_2. Arrhenius plots are shown in Figure 9.30: all the α processes converge to 'zero frequency' as T_g is approached. A variety of relaxation behaviour is exhibited in the decalin glass medium, for various solutes, but none has so high an activation energy as that of CH_2Cl_2.

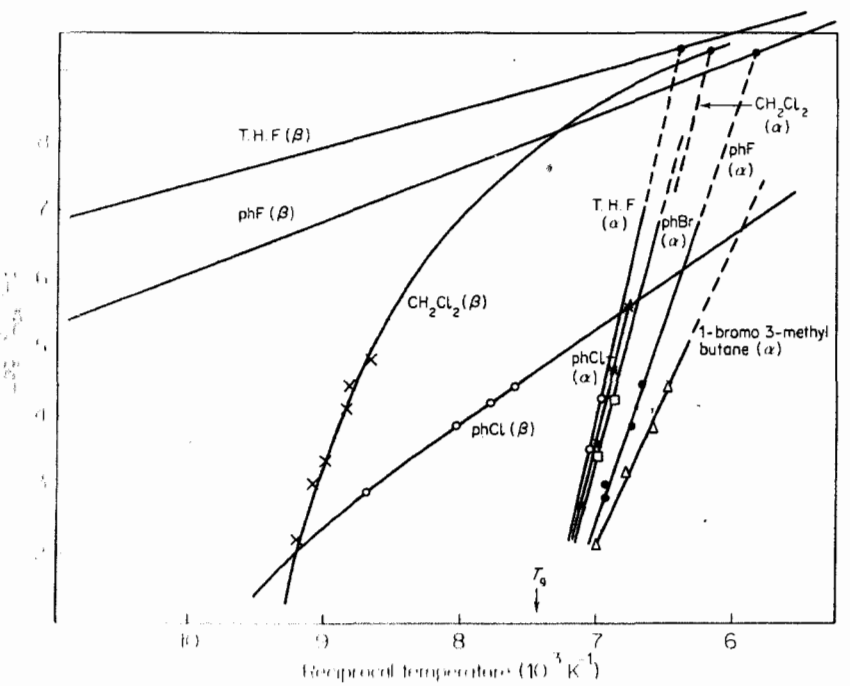

Figure 9.30 Activation energy plots for decalin systems

A semi-empirical approach to these spectral features has been developed based on the itinerant oscillator and Reid's relation between the mean square torque and the volume of rotation. A distribution is assumed of non-equivalent time-independent sites (Johari's view) and implies that the glassy systems are non-ergodic, i.e. the averages over time and over molecules are not equivalent. However, this does not prove capable of producing an (α, β, γ) triad in the loss, but only two, as illustrated in Figure 9.31.

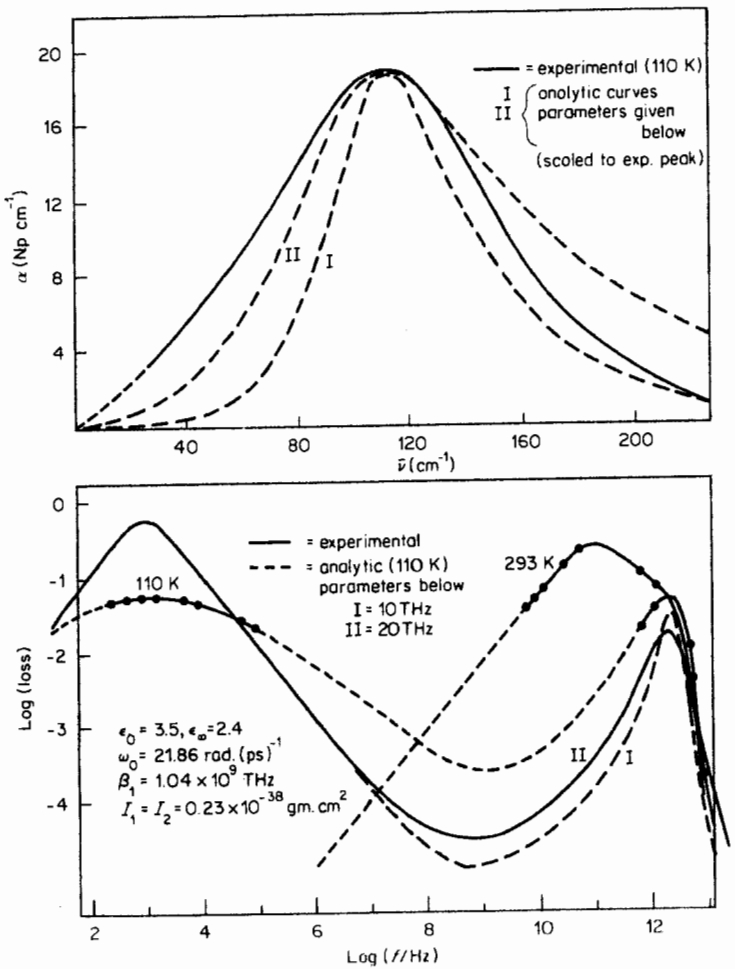

Figure 9.31 I.O. model simulation of 10% v/v CH_2Cl_2 in decalin glass. (a) Two fittings in the FIR absorption representations; (b) zero THz log loss representation

The development of adequate mathematical techniques may be facilitated by comparing directly the behaviour of CH_2Cl_2 in different glasses. In this final section we make a comparison of results in three glasses at 107 K. The temperature shift of the γ peak for solutes in pyridine/toluene is greater than for those in the other solvents. If we define a torque increment by $\Delta T_q = T_q$ (107 K)/T_q (293 K) then ΔT_q is large in this glass. (This is true also for the other solutes, specifically C_6H_5F (10%), CH_3CN (3%), pyridine (10%), $C_6H_5NO_2$ (5%), C_6H_5CN (3%), all v/v). The low frequency dielectric decrement, defined by $\Delta\epsilon' = (\epsilon_0 - \epsilon')/(\epsilon_\theta - \epsilon_\infty)$ is also correspondingly high. The question still remains as to whether it is the greater polarity of the pyridine/toluene medium that prevents rotation in this glass compared with decalin or o-terphenyl, or whether it is the kinematic effects of differing solvent molecular structure. From our results on solvent effects in the far infrared the latter is less likely.

9.7 Computer simulations of molecular motion

The use of fast and very powerful computers has brought an entirely new dimension to the traditional methodology of comparing analytical theory with experimental data because it has become possible to simulate the motion of a very large number of interacting potentials. This is of the order of 10^3 in the latest algorithms, and potentials as complicated as flexible alkyl halides are now being used. Any description of the technical aspects of such computer methods is outside the scope of this chapter, but the results are stored usually on magnetic tapes in the form of information about dynamical variables of interest. These include:

(i) Orientation and position.
(ii) Angular and linear velocity.
(iii) Derivatives up to the order of the predictor–corrector algorithm used.

The use of the simulation technique can be demonstrated by following a paper by Evans (1980) on the Mori theory as applied to orientation. In this work the equations of motion for 108 interacting triatomic molecules were solved using an algorithm due originally to Singer and Renaud (1979). The intermolecular potential used was a three-centre atom–atom where a Lennard-Jones form is used for each of nine interatomic interactions. The Newton equations were then solved using a two-step predictor/corrector algorithm based on Gear's method with periodic boundary conditions. These mean that a molecule which leaves the finite volume under consideration by the computer (usually a cube) is replaced mirror-image-wise by another. The reader is referred to the technical literature for more details. In this way the volume under consideration is kept constant. The temperature and pressure are monitored and scaled at intervals during the run.

The simulation proceeds in time-steps of 10^{-15} s (0.01 ps) from an initial lattice configuration of high energy which melts over the first 2000 or so steps to a more stable liquid configuration. Information about the latter is stored on file and the simulation restarted. A further 3000 or so steps are run, the dynamical information at each step being stored on magnetic tape for statistical analysis. In this way only data at thermodynamic equilibrium are used in building up the averages of interest.

The molecule used in the simulation may be described as follows:

with $AB = BC = 10^{-10}$ m, $M_A = 2.5 \times 10^{-25}$ kg,

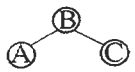

$ABC = 60°$, $M_B = M_A = M_C$, with Lennard–Jones parameters $= 3.0 \times 10^{-10}$ m, $\epsilon/k = 173.5$ K. The temperature of the sample was set at 220 K, the molar volume being 10^{-4} m^3.

Calculation of Autocorrelation function

In calculating autocorrelation functions such as $\langle \mathbf{a}(t) \cdot \mathbf{a}(0) \rangle$ a running-time average is used. If we define by $a_{x,j}$ the x coordinate of $\mathbf{a}_j$ the value of $\mathbf{a}$ for the jth particle, we may construct the following products:

$$\boxed{1}\boxed{1} = \sum_{j=1}^{108} a_{x,j}^2(1) + a_{y,j}^2(1) + a_{z,j}^2(1)$$

$$\boxed{1}\boxed{2} = \sum_{j=1}^{108} a_{x,j}(1)a_{x,j}(2) + a_{y,j}(1)a_{y,j}(2) + a_{z,j}(1)a_{z,j}(2),$$

the number of molecules used here being 108. The computer then proceeds to evaluate the correlation function using loops in the following manner.

First loop

DATA (1) $= \boxed{1}\boxed{2}$;
DATA (2) $= \boxed{1}\boxed{3}$; . . . ;
DATA (2000) $= \boxed{1}\boxed{2000}$
This gives $\langle \mathbf{a}(0) \cdot \mathbf{a}(0) \rangle$ as the sum of all these.

Second loop

DATA (1) $= \boxed{2}\boxed{3} +$ DATA (1) $= \boxed{2}\boxed{3} + \boxed{1}\boxed{2}$
DATA (2) $= \boxed{2}\boxed{4} +$ DATA (2) $= \boxed{2}\boxed{4} + \boxed{1}\boxed{3}$
DATA (2000) $= \boxed{1}\boxed{2000}$

2000th loop

DATA (1) $= \boxed{1}\boxed{2} + \boxed{2}\boxed{3} + \cdots + \boxed{1999}\boxed{2000}$
DATA (2) $= \boxed{1}\boxed{3} + \boxed{2}\boxed{4} + \cdots + \boxed{1998}\boxed{2000}$
DATA (2000) $\boxed{1}\boxed{2000}$
We have DATA (1) $= \langle \mathbf{a}(1) \cdot \mathbf{a}(0) \rangle$;
DATA (2) $= \langle \mathbf{a}(2) \cdot \mathbf{a}(0) \rangle$ etc. to $\langle \mathbf{a}(2000) \cdot \mathbf{a}(0) \rangle$.

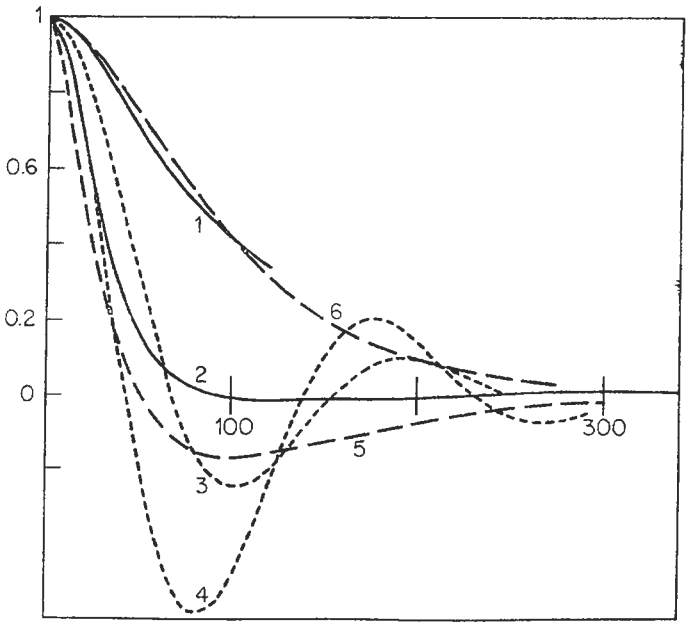

Figure 9.32 Simulated and analytical autocorrelation functions at 220 K. These are normalized at the origin. (1) Simulated orientational autocorrelation function $\langle \mathbf{e}_A(t) \cdot \mathbf{e}_A(0) \rangle$. Here $\mathbf{e}_A$ is the unit vector along the axis of the least principal moment of inertia. (2) Simulated rotational velocity a.c.f. $\langle \dot{\mathbf{e}}(t) \cdot \dot{\mathbf{e}}(0) \rangle$. - - - - (6) Least mean squares best fit to the orientational a.c.f. of Mori three-variable theory. - - - - (5) The angular momentum a.c.f. calculated from the best fit (6). (3) Calculated torque a.c.f. using $\phi_1(0)/\phi_0(0)$ from the best fit (6). (4) Calculated torque a.c.f. using $\phi_1(0)/\phi_0(0) = 1.57$. Ordinate: $C(t)$; abscissa time steps

Note that the autocorrelation function calculated in this way is reliable up to about DATA (1000) only, because progressively less data is used in its calculation. The calculation takes a large amount of the computer time in the largest available machines, such as the UMRCC CDC 7600.

In order to evaluate the orientational Mori theory of Appendix 9B, correlation functions were calculated (Figures 9.32–9.34) using these data and methods for the orientation vector $\mathbf{e}_A$, the angular momentum $\mathbf{J}$, the torque $\mathbf{T}_q$ and the derivative $\dot{\mathbf{e}}_A = \mathbf{J} \times \mathbf{e}_A$. The fluctuations of the squared angular momentum and squared torque over 3.0 ps are illustrated in Figures 9.35 and 9.36. We have the mean values (in reduced units):

$$\langle \mathbf{J}(0) \cdot \mathbf{J}(0) \rangle = 2.8 \times 10^{1}$$

$$\langle \mathbf{T}_q(0) \cdot \mathbf{T}_q(0) \rangle = 9.1 \times 10^{1}$$

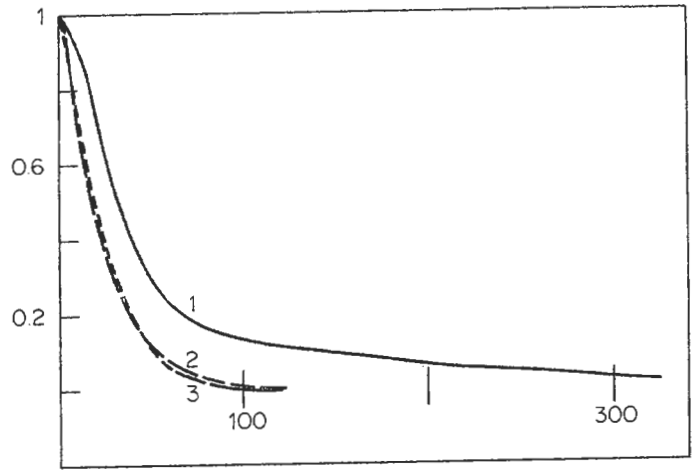

Figure 9.33 Simulated (1) and analytical (2, 3) autocorrelation functions: (2) $\phi_1(0)/\phi_0(0) = 1.57$; (3) calculated from a least mean squares best fit. Ordinate: $C(t)$; abscissa: time steps

for the asymmetric top. Taking a 'spherical top equivalent' moment of inertia, after Lobo *et al.* (1973), then $\phi_1(0)/\phi_0(0) = 1.6$ (see Appendix 9B).

By making a three-variable fit on the molecular dynamics data with γ_u, $\phi_0(0)$, and $\phi_1(0)$ as parameters we obtain the result $\phi_1(0)/\phi_0(0) = 67.75/3.2$ and the curves of Figures 9.32 and 9.33. The three-variable iteration fit of Figures 9.32 and 9.33 is such that the orientational a.c.f. is followed well, at least up to the mid-range of its decay sequence, but only the general

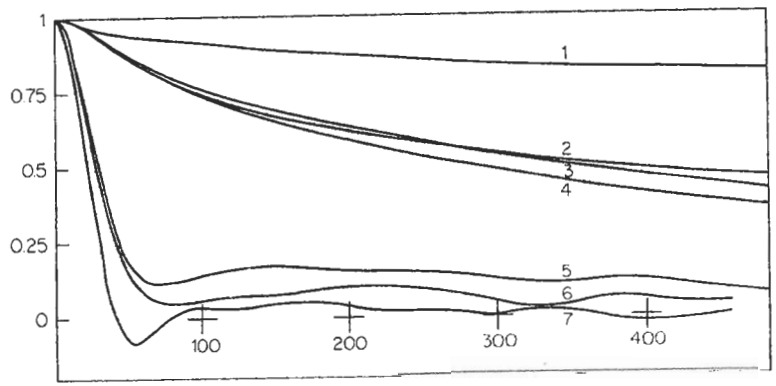

Figure 9.34 Simulated autocorrelation functions at 100 K: (1) $\mathbf{r}_{cm}$, centre of mass; (2) $\mathbf{e}_x$; (3) $\mathbf{e}_y$; (4) $\mathbf{e}_\wedge$; (5) $\mathbf{J}$; (6) $\dot{\mathbf{e}}_\wedge$; (7) $\mathbf{V}$. Here the $\mathbf{e}$ vectors are those along the principal axes of inertia, $\mathbf{J}$ is the angular momentum, and $\mathbf{V}$ the linear velocity

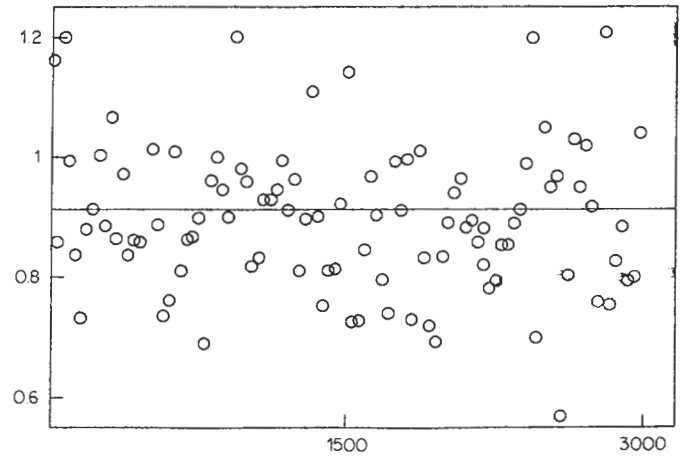

Figure 9.35 Simulated mean square torque over 3000 time steps. The horizontal bar denotes the mean level. Ordinate: mean square torque in reduced units; abscissa: time steps

features are reproduced for the related a.c.f.'s (rotational velocity, angular velocity, and torque). In particular the characteristic negative tail of the rotational velocity a.c.f. is greatly exaggerated. The initial decay of the angular velocity a.c.f. is too sharp analytically. The torque a.c.f. is, not surprisingly, badly reproduced from the orientational a.c.f., the negative lobe being absent in the simulation. As a crude approximation the analysis is fairly useful. As a quantitative measure of its efficiency we can compare the

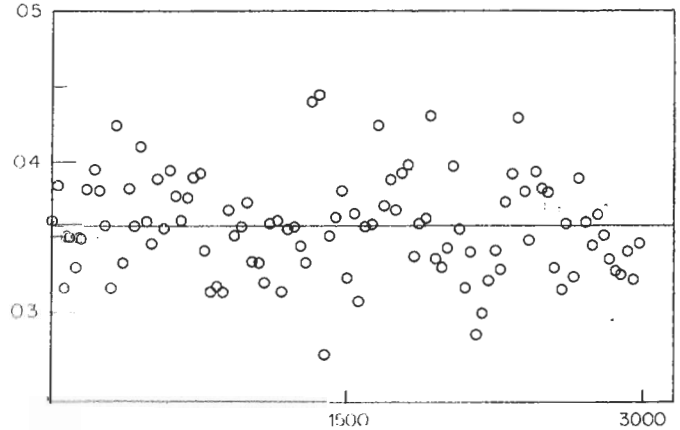

Figure 9.36 Simulated mean square angular momentum over 3000 time steps, as for Figure 9.35. Ordinate: mean square angular momentum in reduced units; abscissa: time steps

ratio $\phi_1(0)/\phi_0(0)$ from the three-variable fit and from the simulation. These are 21.5 and 1.6 respectively. It would clearly be advantageous to have available the rigorous formalism (a generalization of that by Favro, 1961) for the asymmetric top so that the uncertainties caused by linearizing the Euler equations (substituting spherical top geometry) can be eliminated. For the present we may conclude that the molecular dynamics method is easily capable of exposing the shortcomings of the three-variable Mori theory.

In order to improve the analytical treatment it would be advantageous to take into account the asymmetric top nature of the CH_2Cl_2 molecule and to generalize the Favro equation for the probability density function P:

$$\frac{\partial}{\partial t} P(\mathbf{\Omega}, t) = -\hat{M} \cdot \mathbf{D} \cdot \hat{M} P(\mathbf{\Omega}, t) \qquad (9.17)$$

to include inertial and memory effects. Here $\mathbf{D}$ is the asymmetric top diffusion tensor and $\hat{M}$ is identical with the quantum mechanical angular momentum operator. In the case of the symmetric top the eigenstates of the diffusion operator $\hat{\Gamma} = \hat{M} \cdot \mathbf{D} \cdot \hat{M}$ are provided by the Wigner rotation matrix elements $D^{(L)}_{MK}(\mathbf{\Omega})$, where $\mathbf{\Omega} = (\alpha, \beta, \gamma)$, the set of Euler angles. The results for the asymmetric top may be obtained by a perturbation of those for the symmetric top. If we denote by $|\alpha\rangle$ the eigenstates of the diffusion operator in the case of the symmetric top, the general solution of equation (9.17) is

$$|P(\mathbf{\Omega}, t)\rangle = \sum_{\alpha\alpha'} C_{\alpha'} |\alpha\rangle\langle\alpha|\pi\rangle\langle\bar{\pi}|\alpha'\rangle e^{-E_\pi t}$$

where $|\pi\rangle$ and E_π are eigenstates and eigenvalues of $\hat{\Gamma}$, respectively. The vector $\mathbf{C} = (C_1, C_2, \ldots)$ denotes the initial condition of the physical system. The operator $\hat{\Gamma}$ is endowed with an eigenvector whose eigenvalue vanishes, the other eigenvalue being represented by positive real numbers. If we look at the state $|\mathbf{A}\rangle = (|\alpha_1\rangle, |\alpha_2\rangle, \ldots)$, equation (9.17) may be written in the matrix form:

$$\dot{\mathbf{A}} = \hat{\Gamma}\mathbf{A} + \mathbf{f} \qquad (9.18)$$

where the rapidly fluctuating force $\mathbf{f}$ can be replaced by its time average, which is vanishing. Inertial and memory effects may now be included by considering equation (9.18) as a Markov limit of:

$$\dot{\mathbf{A}} = \int_0^t \mathbf{\Phi}(t, \tau)\mathbf{A}(\tau)\, d\tau + \mathbf{f}(t)$$

the structure of the 'memory kernel' $\mathbf{\Phi}$ being defined by the continued fraction expansion of its Laplace transform as demonstrated by Mori. By using the continued fraction (see Appendix 9A), the above equation may be replaced by a multi-Markovian form:

$$\dot{\mathbf{V}}(t) + \mathbf{A} \cdot \mathbf{V} + \mathbf{S} \cdot \mathbf{V}(t) = \mathbf{F}(t) \qquad (9.19)$$

as demonstrated by Grigolini and Ferrario (1980). In equation (9.19), **A**, **S**, and **F** are in general supermatrices, whose elements are themselves matrices, and are defined fully elsewhere (Evans *et al.*, 1980; Shimizu, 1968). The fluctuation-dissipation theorem corresponding to equation (9.19) is defined by:

$$\langle \mathbf{F}(t)\mathbf{F}(s)^T \rangle = 2\gamma\delta(t-s).$$

It is possible to use equation (9.19) to take care of inertial and memory effects by truncating at various levels the supermatrices.

In summary, therefore, the simulation of rotational autocorrelation functions by molecular dynamics is a powerful method of exposing the shortcomings of early Mori approximants of the Liouville equation of motion. It may be possible to reproduce fairly accurately one of a set of autocorrelation functions but the others, as in Figure 9.32, are not satisfactorily described. Also the computed and least mean squares fitted ratios $\phi_1(0)/\phi_0(0)$ are not in agreement.

In this respect the molecular dynamics simulation is more incisive than any spectroscopic technique used in isolation, and, possibly, more so than several in combination. However, the spectra have the advantage of dealing with the real world without first having to model the intermolecular potential.

9.8 Future trends

In view of the many techniques now available for studying molecular relaxation it seems probable that a project should be initiated with the following aims.

(i) To study by various spectroscopic techniques a dipolar fluid (gas/liquid) at thermodynamic conditions which are to be agreed upon by each laboratory involved and adhered to thereafter. The end result will be a collection of bandshapes, for example, which are to be analysed for the information they contain about molecular motion and interaction.

(ii) The bandshapes should be simulated by the technique of molecular dynamics under the same thermodynamic conditions. Various model potentials should be used by various groups, so that sensitivity of the simulated spectral features to changes in interaction potential can be estimated by direct comparison between laboratories.

(iii) An analytical model should be developed in an attempt to describe the range of data from (i) and (ii).

(iv) Second virial coefficients and related thermodynamic measurements should be carried out to aid the choice of potential for the simulations.

(v) The end results should be discussed in a conference convened for this purpose.

The choice of molecule is interesting, but narrows considerably if the drawbacks associated with each technique are to be circumvented. In the (zero–THz) experiment, for example, there is a need to choose a molecule which is an intense absorber (free from the effects of induced absorption) and free from overlapping proper modes. An intensively-studied specimen is methylene chloride, whose atoms are all amenable to study by N.M.R. spectroscopies of different kinds, and whose hydrogens are useful for neutron scattering experiments. Its symmetry is that of water, so that the existing water algorithm could be adopted for use with CH_2Cl_2 quite easily. It is also easily studied by a variety of other techniques, such as acoustic relaxation, light scattering, Kerr effect spectroscopy, and pulsed high-field dielectric relaxation. We have shown how the behaviour of CH_2Cl_2 in glassy and supercooled liquid solvents is especially interesting.

At the time of going to press, attempts are being made to organize and fund such a coordinated effort with CH_2Cl_2, and the symmetric tops CH_3F and CH_3I.

9.9 Appendix 9A Derivation of the Mori equation from the Liouville equation of motion. Continued fraction

The derivation of the Mori equation usually proceeds classically from the Liouville theorem, which can be written as:

$$\mathrm{D}f = \frac{\partial f}{\partial t} + \sum_r [\dot{\mathbf{q}}_r \partial f/\partial \mathbf{q}_r + \dot{\mathbf{p}}_r \partial f/\partial \mathbf{p}_r]$$

$$\mathrm{D}f = \frac{\partial f}{\partial t} + \sum_r \left[\frac{\partial H}{\partial \mathbf{p}_r}\frac{\partial f}{\partial \mathbf{q}_r} + \frac{\partial H}{\partial \mathbf{q}_r}\frac{\partial f}{\partial \mathbf{p}_r}\right] \qquad (9A.1)$$

$$\equiv \frac{\partial f}{\partial t} + [H, f] \equiv \frac{\partial f}{\partial t} + \hat{\mathscr{L}} f = 0.$$

Here $\mathbf{q}_r$ is the coordinate and $\mathbf{p}_r$ the momentum of the rth particle. H is the Hamiltonian, [ ] the classical Poisson bracket, and $\hat{\mathscr{L}}$ the Liouville operator. Equation (9A.1) describes the statistical behaviour of a classical macroscopic assembly under the action of external and internal forces. f is a probability distribution in $2N$ dimensions where N is the number of degrees of freedom of the system.

For analytical purposes it is necessary to modify equation (9A.1) by limiting the degrees of freedom to a small but representative set of thermodynamic averages which define the potential part of the Hamiltonian successively more accurately. In this appendix this eventually leads us to the Mori continued fraction. Df/Dt vanishes because of the nature of the interaction between the set considered and the background. Of the various possible types of intermolecular interaction one widely investigated is the

class of adiabatic collisions, which are of such short duration in comparison with other explicitly considered time intervals that they can be treated as instantaneous. Linear Brownian motion is an example where the collisions do not alter the positions of the particles, and their velocities are altered by such small amounts as to be infinitesimal. Correlation between successive impulses is negligible, the effect of such collisions appears as a viscous retardation, $\mathrm{d}\mathbf{v}/\mathrm{d}t = -\beta\mathbf{v}$ where $\mathbf{v}$ is the centre of mass linear velocity and β the friction coefficient. If this is applied to the description of rotating molecules in a dipolar fluid using the method of Debye then the consequences at far infrared frequencies are in spectral terms disastrous (Figure 9.2) because the theoretical power absorption coefficient does not regain spectral transparency. The mathematical reasons behind this inconsistency in classical Debye theory are now well known to be embodied in the manner in which equation (9A.1) was approximated, this being Gaussian/Markovian in the distribution function f. In the literature of the last decade there have been various attempts to lift these restrictions by modelling the molecular dynamics more realistically. The use of projection operators for this purpose has proven incisive.

Projection operators

Their use has been discussed lucidly by Berne and Pecora (1976) and what follows is a brief summary. To proceed we write the Liouville equation making use of the definition:

$$\mathrm{i}\hat{\mathscr{L}} = \sum_r \left[\frac{\partial H}{\partial \mathbf{p}_r}\frac{\partial}{\partial \mathbf{q}_r} - \frac{\partial H}{\partial \mathbf{q}_r}\frac{\partial}{\partial \mathbf{p}_r}\right]. \qquad (9A.2)$$

Define a point $\mathbf{\Gamma} = (\mathbf{q}_1, \ldots, \mathbf{q}_r, \mathbf{p}_1, \ldots, \mathbf{p}_r)$. The Liouville equation now takes the standard form:

$$\dot{\mathbf{\Gamma}} = [\mathbf{\Gamma}, H] = \mathrm{i}\hat{\mathscr{L}}\mathbf{\Gamma}.$$

Consider now a linearly independent set $[A_j(t), j = 1, \ldots, n,$ of real valued implicitly time-dependent, dynamical variables of the given r-particle system. The set of all possible dynamical variables is a real Hilbert space. Now construct an ensemble average in this space, denoted by the brackets $\langle\ \rangle$. This is an *inner product*, so that

$$(A, B) = \langle A(0)B(t)\rangle$$

where A and B are separate variables. We can write the inner product (or correlation function) in terms of, for example, the equilibrium *canonical distribution function*, defined by:

$$f(\mathbf{\Gamma}_0) = \exp(-H(\mathbf{\Gamma}_0)/kT) \Big/ \int e^{-H(\mathbf{\Gamma}_0)/kT}\,\mathrm{d}\mathbf{\Gamma}_0$$

where Γ_0 is Γ at $t=0$. We have:

$$(A^*, B) = \int d\Gamma f(\Gamma) B(\Gamma) A^*(\Gamma)$$

where A^* is the complex conjugate of A. The properties A and B (or A^* and B) depend on time only through the dependence of the state Γ on time—they are implicitly time-dependent. It follows that:

$$\dot{A} = [A, H] = i\hat{\mathscr{L}}A$$
$$A(\Gamma, t) = \exp(i\hat{\mathscr{L}}t)A(\Gamma, 0).$$

In Berne's notation the time auto-correlation function of A may now be defined as:

$$C(t) = (A(t), A^*) = (e^{i\mathscr{L}t}A(0), A^*)$$
$$= \int d\Gamma f(\Gamma) A^*(\Gamma) e^{i\mathscr{L}t} A(\Gamma).$$

Because of the formal identity of $C(t)$ with the scalar product of matrix mechanics (Heisenberg), mathematical techniques of quantum mechanics may be used with classical time-correlation functions with the following formal analogies.

(1) A and B are orthogonal if $(A^*, B) = 0$.
(2) The propagator $\exp(i\hat{\mathscr{L}}t)$ is an orthogonal operator.
(3) If $(A^*, A)^{1/2}$ is unity then A is normalized.
(4) The quantity $f^{1/2}A \equiv \psi_A(\Gamma)$ is the 'wavefunction'.
(5) The linear, hermitian, operator $\hat{\mathscr{L}}$ is the Liouvillian.
(6) $C(t)$ is the 'expectation value' of $\exp(i\hat{\mathscr{L}}t)$ in the 'state' ψ_A.
(7) The operator $\exp(i\hat{\mathscr{L}}t)$ preserves the norm of A, i.e. is unitary.

Using these ideas Berne and Pecora show that the dynamical column vector $\mathbf{A}(t)$ evolves in time according to the equation:

$$\dot{\mathbf{A}}(t) = i\hat{\Omega}_{\mathbf{A}}\mathbf{A}(t) - \int_0^t d\tau \hat{\phi}_{\mathbf{A}}(t-\tau)\mathbf{A}(\tau) + \mathbf{F}_{\mathbf{A}}(t) \qquad (9A.3)$$

In this equation $\hat{\Omega}_{\mathbf{A}}$ and $\hat{\phi}_{\mathbf{A}}$ are operators, and $\mathbf{F}_{\mathbf{A}}(t)$ a vector of random quantities. This equation is derived using the idea of *projection* onto a sub-space of the Hilbert space we have already mentioned. This is formally identical with rotating the complex number $(r\cos\theta_1, ir\sin\theta_1) = r\exp(i\theta_1)$ to a new position defined by $(r\cos\theta_2, ir\sin\theta_2) = r\exp(i\theta_2)$. The projection of the second vector onto the first is $(r\cos(\theta_2 - \theta_1), ir\sin(\theta_2 - \theta_1))$ which may be written as $r(e^{i\theta_2}e^{-i\theta_1})/(e^{i\theta_1}e^{-i\theta_1})$. Since $A(t) = e^{i\mathscr{L}t}A(0)$ the scalar product of

the two forms a projection in Liouville space. The time auto-correlation function of A is a projection of $A(t)$ onto $A(0)$. We may project any B onto $A(0)$ using the operator $\hat{P} = (\ , A^*)(A, A^*)^{-1}A$, i.e.

$$\hat{P}B = (B, A^*)(A, A^*)^{-1}A$$

analogously with the projection in the complex plane. Note that

(1) The projection of A onto itself *at the same t* has no effect: $\hat{P}A = A$.
(2) $\hat{P}(\hat{P}B) = \hat{P}^2B = B$, therefore $\hat{P}^2 = \hat{P}$; also $\hat{P}(\hat{1} - \hat{P}) = 0$.
(3) $(\hat{1} - \hat{P})B = \hat{Q}B$ projects B on to a subspace orthogonal to A, so that $((\hat{1} - \hat{P})B, A^*) = (B, A^*) - (B, A^*)(A, A^*)^{-1}(A, A^*) = 0$.

From these properties the following operator identity may be derived:

$$e^{i\mathscr{L}t} \equiv e^{i\hat{Q}\mathscr{L}t} + \int_0^t d\tau e^{i\mathscr{L}(t-\tau)} i\hat{P}\mathscr{L} e^{i\hat{Q}\mathscr{L}\tau}.$$

Using this, equation (9A.3) follows from differentiating the Liouville equation:

$$\dot{A}(t) = e^{i\mathscr{L}t} i\mathscr{L}A(0) \equiv e^{i\mathscr{L}t}(\hat{P} + \hat{Q})i\mathscr{L}A(0)$$
$$= i\hat{\Omega}A(t) + \exp[i\hat{Q}\mathscr{L}t]\hat{Q}i\mathscr{L}A(0)$$
$$+ \int_0^t d\tau e^{i\mathscr{L}(t-\tau)} i\hat{P}\mathscr{L} e^{i\hat{Q}\mathscr{L}\tau}\hat{Q}i\mathscr{L}A(0) \qquad (9A.4)$$

where $\hat{\Omega} = (\mathscr{L}A, A^*)(A, A^*)^{-1}$ and $(F(t), A^*(0)) = \langle F(t)A^*(0)\rangle = 0$. If $\mathbf{A}(t)$ is a column vector then $\mathbf{F}$ is also a column vector of projected quantities (defined in a Hilbert subspace), and is propagated from $A(0)$. In a phenomenon involving collective motions $i\hat{\Omega}$, involving only $\hat{P}$, measures the extent to which the cooperative motion is a resonance of its components. In consequence $i\hat{\Omega}$ is a resonance operator, which is null for *auto*correlation. The integral in equation (9A.4) may be rewritten in the form of equation (9A.3) defining

$$\hat{\phi}(\tau) = (F(\tau), F(0)^*)(A(0), A^*(0))^{-1}.$$

This is known as the memory kernel, memory operator, or memory function, depending on whether A and F are scalar or vector. It is the normalized autocorrelation function of $F(t)$, which has not in general the features of Markovian statistics, i.e. the autocorrelation function $\langle A(t)A(0)\rangle$ is not in general exponential. In fact:

$$\dot{C}(t) = i\Omega C(t) - \int_0^t d\tau \phi(\tau) C(t-\tau). \qquad (9A.5)$$

where $\mathbf{\Gamma}_0$ is Γ at $t=0$. We have:

$$(A^*, B) = \int \mathrm{d}\mathbf{\Gamma} f(\mathbf{\Gamma}) B(\mathbf{\Gamma}) A^*(\mathbf{\Gamma})$$

where A^* is the complex conjugate of A. The properties A and B (or A^* and B) depend on time only through the dependence of the state $\mathbf{\Gamma}$ on time—they are implicitly time-dependent. It follows that:

$$\dot{A} = [A, H] = \mathrm{i}\hat{\mathscr{L}}A$$
$$A(\mathbf{\Gamma}, t) = \exp(\mathrm{i}\hat{\mathscr{L}}t) A(\mathbf{\Gamma}, 0).$$

In Berne's notation the time auto-correlation function of A may now be defined as:

$$C(t) = (A(t), A^*) = (\mathrm{e}^{\mathrm{i}\hat{\mathscr{L}}t} A(0), A^*)$$
$$= \int \mathrm{d}\mathbf{\Gamma} f(\mathbf{\Gamma}) A^*(\mathbf{\Gamma}) \mathrm{e}^{\mathrm{i}\hat{\mathscr{L}}t} A(\mathbf{\Gamma}).$$

Because of the formal identity of $C(t)$ with the scalar product of matrix mechanics (Heisenberg), mathematical techniques of quantum mechanics may be used with classical time-correlation functions with the following formal analogies.

(1) A and B are orthogonal if $(A^*, B) = 0$.
(2) The propagator $\exp(\mathrm{i}\hat{\mathscr{L}}t)$ is an orthogonal operator.
(3) If $(A^*, A)^{1/2}$ is unity then A is normalized.
(4) The quantity $f^{1/2}A \equiv \psi_A(\mathbf{\Gamma})$ is the 'wavefunction'.
(5) The linear, hermitian, operator $\hat{\mathscr{L}}$ is the Liouvillian.
(6) $C(t)$ is the 'expectation value' of $\exp(\mathrm{i}\hat{\mathscr{L}}t)$ in the 'state' ψ_A.
(7) The operator $\exp(\mathrm{i}\hat{\mathscr{L}}t)$ preserves the norm of A, i.e. is unitary.

Using these ideas Berne and Pecora show that the dynamical column vector $\mathbf{A}(t)$ evolves in time according to the equation:

$$\dot{\mathbf{A}}(t) = \mathrm{i}\hat{\Omega}_{\mathbf{A}}\mathbf{A}(t) - \int_0^t \mathrm{d}\tau \hat{\phi}_{\mathbf{A}}(t-\tau)\mathbf{A}(\tau) + \mathbf{F}_{\mathbf{A}}(t) \qquad (9\mathrm{A}.3)$$

In this equation $\hat{\Omega}_{\mathbf{A}}$ and $\hat{\phi}_{\mathbf{A}}$ are operators, and $\mathbf{F}_{\mathbf{A}}(t)$ a vector of random quantities. This equation is derived using the idea of *projection* onto a sub-space of the Hilbert space we have already mentioned. This is formally identical with rotating the complex number $(r\cos\theta_1, \mathrm{i}r\sin\theta_1) = r\exp(\mathrm{i}\theta_1)$ to a new position defined by $(r\cos\theta_2, \mathrm{i}r\sin\theta_2) = r\exp(\mathrm{i}\theta_2)$. The projection of the second vector onto the first is $(r\cos(\theta_2 - \theta_1), \mathrm{i}r\sin(\theta_2 - \theta_1))$ which may be written as $r(\mathrm{e}^{\mathrm{i}\theta_2}\mathrm{e}^{-\mathrm{i}\theta_1})/(\mathrm{e}^{\mathrm{i}\theta_1}\mathrm{e}^{-\mathrm{i}\theta_1})$. Since $A(t) = \mathrm{e}^{\mathrm{i}\hat{\mathscr{L}}t}A(0)$ the scalar product of

the two forms a projection in Liouville space. The time auto-correlation function of A is a projection of $A(t)$ onto $A(0)$. We may project any B onto $A(0)$ using the operator $\hat{P} = (\ , A^*)(A, A^*)^{-1}A$, i.e.

$$\hat{P}B = (B, A^*)(A, A^*)^{-1}A$$

analogously with the projection in the complex plane. Note that

(1) The projection of A onto itself *at the same t* has no effect: $\hat{P}A = A$.
(2) $\hat{P}(\hat{P}B) = \hat{P}^2B = B$, therefore $\hat{P}^2 = \hat{P}$; also $\hat{P}(\hat{1} - \hat{P}) = 0$.
(3) $(\hat{1} - \hat{P})B = \hat{Q}B$ projects B on to a subspace orthogonal to A, so that $((\hat{1} - \hat{P})B, A^*) = (B, A^*) - (B, A^*)(A, A^*)^{-1}(A, A^*) = 0$.

From these properties the following operator identity may be derived:

$$\mathrm{e}^{\mathrm{i}\hat{\mathscr{L}}t} \equiv \mathrm{e}^{\mathrm{i}\hat{Q}\hat{\mathscr{L}}t} + \int_0^t \mathrm{d}\tau \mathrm{e}^{\mathrm{i}\hat{\mathscr{L}}(t-\tau)}\mathrm{i}\hat{P}\hat{\mathscr{L}}\mathrm{e}^{\mathrm{i}\hat{Q}\hat{\mathscr{L}}\tau}.$$

Using this, equation (9A.3) follows from differentiating the Liouville equation:

$$\dot{A}(t) = \mathrm{e}^{\mathrm{i}\hat{\mathscr{L}}t}\mathrm{i}\hat{\mathscr{L}}A(0) \equiv \mathrm{e}^{\mathrm{i}\hat{\mathscr{L}}t}(\hat{P} + \hat{Q})\mathrm{i}\hat{\mathscr{L}}A(0)$$
$$= \mathrm{i}\hat{\Omega}A(t) + \exp[\mathrm{i}\hat{Q}\hat{\mathscr{L}}t]\hat{Q}\mathrm{i}\hat{\mathscr{L}}A(0)$$
$$+ \int_0^t \mathrm{d}\tau \mathrm{e}^{\mathrm{i}\hat{\mathscr{L}}(t-\tau)}\mathrm{i}\hat{P}\hat{\mathscr{L}}\mathrm{e}^{\mathrm{i}\hat{Q}\hat{\mathscr{L}}\tau}\hat{Q}\mathrm{i}\hat{\mathscr{L}}A(0) \qquad (9\mathrm{A}.4)$$

where $\hat{\Omega} = (\hat{\mathscr{L}}A, A^*)(A, A^*)^{-1}$ and $(F(t), A^*(0)) = \langle F(t)A^*(0)\rangle = 0$. If $\mathbf{A}(t)$ is a column vector then $\mathbf{F}$ is also a column vector of projected quantities (defined in a Hilbert subspace), and is propagated from $A(0)$. In a phenomenon involving collective motions $\mathrm{i}\hat{\Omega}$, involving only $\hat{P}$, measures the extent to which the cooperative motion is a resonance of its components. In consequence $\mathrm{i}\hat{\Omega}$ is a resonance operator, which is null for *auto*correlation. The integral in equation (9A.4) may be rewritten in the form of equation (9A.3) defining

$$\hat{\phi}(\tau) = (F(\tau), F(0)^*)(A(0), A^*(0))^{-1}.$$

This is known as the memory kernel, memory operator, or memory function, depending on whether A and F are scalar or vector. It is the normalized autocorrelation function of $F(t)$, which has not in general the features of Markovian statistics, i.e. the autocorrelation function $\langle A(t)A(0)\rangle$ is not in general exponential. In fact:

$$\dot{C}(t) = \mathrm{i}\Omega C(t) - \int_0^t \mathrm{d}\tau \phi(\tau) C(t-\tau). \qquad (9\mathrm{A}.5)$$

Continued fraction

Equation (9A.5) shows that any autocorrelation function may be associated via an integro-differential equation with a convolution kernel. The memory function $\phi(t)$ may be given its own memory function $\phi_1(t)$ through an equation the same as (9A.5).

$$\dot{\phi}(t) = i\hat{\Omega}_1\phi(t) - \int_0^t d\tau\phi_1(\tau)\phi(t-\tau) \tag{9A.6}$$

where ϕ_1 is the correlation function of a variable F_1, which is orthogonal to F and to A,

$$\phi_1(t) = \langle F_1(t)F_1(0)\rangle\langle F(0)F(0)\rangle^{-1}. \tag{9A.7}$$

Note:

$$F(t) = \exp[i\hat{Q}\hat{\mathscr{L}}t]\hat{Q}i\hat{\mathscr{L}}A(0)$$

$$F(0) = \hat{Q}i\hat{\mathscr{L}}A(0) = \dot{A}(0) - [\langle\dot{A}(0)A(0)\rangle\langle A(0)A(0)\rangle^{-1}]A(0)$$

$$= \dot{A}(0)$$

if we assume that $A(0)$ is real and a single molecule property, so that $\langle\dot{A}(0)A(0)\rangle = 0$, Also, $F_1(t) = \exp[i\hat{Q}_1\hat{\mathscr{L}}_1t]\hat{Q}_1i\hat{\mathscr{L}}_1F(0)$ and at $t = 0$

$$F_1(0) = \hat{Q}_1\dot{F}(0) = \hat{Q}_1\, d(\hat{Q}\dot{A}(0))/dt$$

$$= d(\hat{Q}\dot{A}(0))/dt - [\langle d(\hat{Q}\dot{A}(0))/dtF(0)\rangle\langle F(0)F(0)\rangle^{-1}]F(0)$$

$$= \ddot{A}(0) - \langle\ddot{A}(0)A(0)\rangle\langle A(0)A(0)\rangle^{-1}A(0) \tag{9A.8}$$

(with $F(0) = \dot{A}(0)$). Equation (9A.8) may be rewritten as:

$$F_1(0) = \ddot{A}(0) + \frac{\langle\dot{A}(0)^2\rangle}{\langle A(0)^2\rangle}A(0). \tag{9A.9}$$

So that, finally,

$$\langle F_1(0)F_1(0)\rangle = \langle\ddot{A}(0)\ddot{A}(0)\rangle - \frac{\langle\dot{A}(0)\dot{A}(0)\rangle^2}{\langle A(0)A(0)\rangle}.$$

If A is designated as the molecular angular momentum, for example, then the right-hand side above involves the mean square torque and the mean square torque derivative.

By taking a series of integro-differential equations to approximate the Liouville equation, the potential energy of the hamiltonian is described by successive equilibrium averages, the values of the memory function at $t = 0$. We have therefore found one way of relating the $\sim 10^{20}$ variables of the Liouville equation in a molecular liquid to a few equilibrium, thermodynamic averages. This approximation method may be tested using results from molecular dynamics simulations and far infrared spectroscopy.

Taking **A** as a column vector we have the result:

$$\tilde{C}_{\mathbf{A}}(s) = \hat{\mathscr{L}}_a[\langle\mathbf{A}(t)\mathbf{A}^T(0)\rangle\langle\mathbf{A}(0)\mathbf{A}^T(0)\rangle^{-1}]$$

$$= \cfrac{\mathbf{1}}{\mathbf{1}s - i\hat{\Omega}_0 + \cfrac{\mathbf{1}}{\mathbf{1}s - i\hat{\Omega}_1 + \cfrac{\mathbf{1}}{\ddots + \cfrac{\mathbf{1}}{\mathbf{1}s - i\hat{\Omega}_{n-1} + \hat{\phi}_n(s)}\hat{\phi}_{n-1}(0).}\hat{\phi}_1(0)}\hat{\phi}_0(0)}$$

This is (an infinite) continued fraction first derived by Mori. In this equation:

$$i\hat{\Omega}_j = \langle\dot{\mathbf{F}}\mathbf{F}_j^T\rangle\langle\mathbf{F}_j\mathbf{F}_j^T\rangle^{-1}$$

$$\hat{\phi}_j(0) = \langle\mathbf{F}_j\mathbf{F}_j^T\rangle\langle\mathbf{F}_{j-1}\mathbf{F}_{j-1}^T\rangle^{-1}$$

$$\mathbf{F}_j = \left[\hat{1} - \sum_{k=0}^{j-1}\hat{P}_k\right]\hat{\mathscr{L}}\mathbf{F}_{j-1}; \quad j \geq 0; \quad \hat{P}_0 \equiv \hat{P}$$

$$\dot{\mathbf{F}}_j = \left[\hat{1} - \sum_{k=0}^{j-1}\hat{P}_k\right]i\hat{\mathscr{L}}\mathbf{F}_j; \quad j \geq 0,$$

where $\hat{P}_k$ projects into the sub-Hilbert space spanned by $\mathbf{F}_k(0)$. $\hat{\mathscr{L}}_a$ is the Laplace transform. In Appendix 9B we consider spectral consequences of taking **A** as various dynamic quantities.

9.10 Appendix 9B: Applications of the continued fraction*

Consider the rotational Brownian motion of a particle whose orientation is specified by the vector $\mathbf{u}(t)$, the angular velocity $\boldsymbol{\Omega}(t)$, and torque $\mathbf{N}(t)$. Thus using equation (9A.6) for $\boldsymbol{\Omega}(t)$ we see that:

$$\mathbf{I}.\dot{\boldsymbol{\Omega}}(t) = -\int_0^t \hat{\phi}_\Omega(t-\tau)\boldsymbol{\Omega}(\tau)\, d\tau + \mathbf{N}(t)$$

where $\mathbf{I}$ is the molecular moment of inertia tensor and $\hat{\phi}_\Omega$ the memory function. This gives the following equation of motion for the tensor average:

$$\mathbf{I}.\frac{d}{dt}\langle\boldsymbol{\Omega}(t)\boldsymbol{\Omega}(0)^T\rangle = -\int_0^t d\tau\hat{\phi}_\Omega(t-\tau)\langle\boldsymbol{\Omega}(\tau)\boldsymbol{\Omega}(0)^T\rangle \tag{9B.1}$$

so that

$$\mathscr{L}_a\langle\boldsymbol{\Omega}(t)\boldsymbol{\Omega}(0)^T\rangle = [\, i\omega\mathbf{I} + \zeta(\omega)\,]^{-1}.\mathbf{I}.\langle\boldsymbol{\Omega}(0)\boldsymbol{\Omega}^T(0)\rangle$$

* Note, in the appendix, $K_0(0) = \phi_0^{(0)}(0)$; $K_1(0) = \phi_0^{(1)}(0)$; $\gamma = \gamma_a$.

where

$$\langle \boldsymbol{\Omega}(0)\boldsymbol{\Omega}^{T}(0)\rangle = \mathbf{I}^{-1}kT.$$

It is possible to derive a diffusion equation for the orientation vector $\mathbf{u}(t)$, i.e. $f(\mathbf{u}(t); \mathbf{u}(0), t)$ from the stochastic Liouville equation for the movement of $\mathbf{u}$. Before averaging over the ensemble of random fluctuations of angular volocity the Liouville equation is:

$$\begin{aligned}\frac{\partial f}{\partial t} + \dot{\mathbf{u}} \cdot \nabla_u f &= 0 \\ &= -\boldsymbol{\Omega}(t) \times \mathbf{u} \cdot \nabla_u f \\ &= -\boldsymbol{\Omega}(t) \cdot \mathbf{u} \times \nabla_u f. \end{aligned} \tag{9B.2}$$

If the process $\boldsymbol{\Omega}(t)$ is statistically Gaussian then equation (9.B2) may be written:

$$\hat{\mathscr{L}}_a(\partial f/\partial t) = (\mathbf{u} \times \nabla_u) \cdot \hat{\mathscr{L}}_a \langle \boldsymbol{\Omega}(t)\boldsymbol{\Omega}^{T}(0)\rangle \cdot (\mathbf{u} \times \nabla_u) f.$$

This is a Smoluchowski rotational diffusion equation modified to take into account memory effects.

When the Brownian motion is *spherically isotropic* the diffusion equation becomes:

$$\frac{\partial f}{\partial t}(\mathbf{u}; t) = \int_0^t \mathrm{d}s \phi(t-s)(\mathbf{u} \times \mathbf{D}_u)^2 f(\mathbf{u}; s) \tag{9B.3}$$

where

$$D(\omega) = kT/\zeta(\omega) = \int_0^\infty \mathrm{d}t \phi(t) \exp(\mathrm{i}\omega t) = \phi(\omega).$$

Integrating equation (9B.3) by parts over all orientations gives the equation of motion for the average dipole moment ($\boldsymbol{\mu} = |\boldsymbol{\mu}|\,\mathbf{u}$); then:

$$\frac{\partial}{\partial t}\langle \boldsymbol{\mu}; t\rangle = -2\int_0^t \mathrm{d}s D(t-s)\langle \boldsymbol{\mu}; s\rangle.$$

Multiply through by $\boldsymbol{\mu}(0)$ and average over an isotropic distribution of initial orientations, then:

$$\frac{\partial}{\partial t}\langle \boldsymbol{\mu}(t) \cdot \boldsymbol{\mu}(0)\rangle = -2\int_0^t \mathrm{d}s \phi(t-s)\langle \boldsymbol{\mu}(s) \cdot \boldsymbol{\mu}(0)\rangle. \tag{9B.4}$$

This is an *orientational* equation analogous to equation (9B.1) first derived by Nee and Zwanzig (1970). This has been used extensively by Evans and co-workers to describe far infrared data for molecular liquids, rotator phases, and mesophases. Note, however, that it is specifically for isotropic space reorientation and is obviously approximate when the molecules are geometrically anisotropic, as in the extreme case of liquid crystal forming phases.

Equation (9B.4) may be expressed as:

$$\dot{\mathbf{u}}(t) = -\int_0^t \phi_{\mathbf{u}}(t-\tau)\mathbf{u}(\tau)\,\mathrm{d}\tau + \mathbf{f}(t) \tag{9B.5}$$

where $\mathbf{u}$ is the dipole vector, so that:

$$C_{\mathbf{u}}(t) = \langle \mathbf{u}(t) \cdot \mathbf{u}(0)\rangle \equiv P_1(\cos\theta)$$

and

$$\dot{C}_{\mathbf{u}}(t) = -\int_0^t \phi_{\mathbf{u}}(t-\tau)C_{\mathbf{u}}(\tau)\,\mathrm{d}\tau$$

which may be expanded in a Mori continued fraction form:

$$\tilde{C}_{\mathbf{u}}(s) = \frac{C_{\mathbf{u}}(0)}{s + \tilde{\phi}_0(s)} = \frac{C_{\mathbf{u}}(0)}{s + \dfrac{\phi_0(0)}{s + \tilde{\phi}_1(s)}} = \cdots \tag{9B.6}$$

in the space of Laplace transforms. If this is now truncated with $\phi_0(t) = \phi_0(0)\exp(-\gamma_u t)$, an equation is obtained for spherical tops, i.e.:

$$\tilde{C}_{\mathbf{u}}(s) = C_{\mathbf{u}}(0)(s+\gamma_u)/(s^2 + s\gamma_u + \phi_0(0)). \tag{9B.7a}$$

However, if we truncate with $\phi_1(t) = \phi_1(0)\exp(-\gamma t)$, then

$$\tilde{C}_{\mathbf{u}}(s) = (s^2 + \gamma_u s + \phi_1(0))/(s^3 + \gamma_u s^2 + (\phi_0(0) + \phi_1(0))s + \gamma_u \phi_0(0)) \tag{9B.7b}$$

which behaves fairly satisfactorily at far infrared frequencies because $\phi_1(0)$ is related to the mean square torque. This is not defined in any earlier approximant of the series (9B.6). Equation (9B.7b) may be used to describe the most characteristic feature of far infrared spectra in dipolar molecules, the shift of the peak frequency ($\bar{\nu}_{\max}$) of the power absorption coefficient along the gas/liquid coexistence curve for example. This is not possible with an equation such as (9B.7a). Variation of γ_u merely broadens the peak and does *not* shift its position. The physical reason for this is that successive collisions are uncorrelated, as we shall demonstrate in the next section by reference to a model of collision interrupted free rotation, i.e. an inertia-dominated model of molecular dynamics.

Extended diffusion or collision interrupted rotation

Let the assumption leading to equation (9B.7) be modified to:

$$\phi_0(t) = \phi_{0R}(t)\exp(-|t|/\tau)$$

where $\phi_{FR}(t)$ is a memory function defined by

$$\dot{C}_{FR}(t) = -\int_0^t \phi_{FR}(t-\tau)C_{FR}(\tau)\,d\tau.$$

Here $C_{FR}(t)$ is the autocorrelation function describing the 'free rotation' of an ensemble of linear molecules. We are assuming physically that the reorientation of the angular momentum is instantaneous and randomized at each collision according to a Poisson distribution:

$$f_n(t) = \frac{(\omega_0 t)^n}{n!}\exp(-\omega_0 t)$$

where ω_0 is the collision frequency ($=1/\tau$, where τ is the *average* time between collisions).

The memory function $\phi_0(t)$ is related to the correlation function $C(t)$ of the collision interrupted free rotation by the usual integro-differential relation. From this it follows that

$$\begin{aligned}\tilde{C}(s) &= [s+\tilde{\phi}_{FR}(s+1/\tau)]^{-1}\\ &= \tilde{C}_{FR}(s+1/\tau)/[1-\tau^{-1}\tilde{C}_{FR}(s+1/\tau)]\\ &= \sum_{n=0}^{\infty}\frac{1}{\tau^n}\tilde{C}_{FR}^{(n+1)}(s+1/\tau)\end{aligned} \tag{9B.8}$$

using the Taylor theorem. Inverting equation (9B.8) term by term gives:

$$\begin{aligned}C(t) = \langle \mathbf{u}(t)\,.\,\mathbf{u}(0)\rangle = e^{-t/\tau}\Bigg[&C_{FR}(t)\\ &+\frac{1}{\tau}\int_0^t C_{FR}(t-t_1)C_{FR}(t_1)\,dt_1\\ &+\frac{1}{\tau_2}\int_0^t C_{FR}(t-t_1)\,dt_1\int_0^{t_1}C_{FR}(t_1-t_2)C_{FR}(t_2)\,dt_2+\cdots\\ &+\frac{1}{\tau^n}\int_0^t C_{FR}(t-t_1)\,dt_1\int_0^{t_1}C_{FR}(t_1-t_2)\,dt_2\cdots\\ &\times\int_0^{t_{n-1}}C_{FR}(t_{n-1}-t_n)C_{FR}(t_n)\,dt\Bigg].\end{aligned}$$

This is the orientational autocorrelation function of the J-diffusion model for linear molecules where the model assumptions are:

(1) A molecule undergoes free rotational motion until it is interrupted by a hard-core (i.e. adiabatic) collision of zero duration.
(2) Each collision randomizes onto a Poisson distribution the angular momentum in both magnitude and direction.
(3) Successive collisions are uncorrelated, i.e. the instants at which the collisions occur form a purely random process, and the angular momentum changes are uncorrelated.
(4) Collisions change the molecule's rotational velocity but do not change into orientation.

The mean square torque in this model is therefore not defined, and its limitations are clearly revealed in the far infrared, where its behaviour is very similar to that of Figure 9.32.

The planar itinerant librator

This is a special case of the truncated Mori continued fraction applied to the angular velocity vector of an asymmetric top whose reference (dipole) axis is constrained to librate in a plane. The general variable A of Appendix 9A may therefore be designated by ω, the angular velocity, which is the time derivative of θ, the angle between the dipole axis at time t and time zero. The equation of motion is therefore:

$$\ddot{\theta}(t) = -\int_0^t \phi_{\dot\theta}(t-\tau)\dot{\theta}(\tau)\,d\tau + F_{\dot\theta}(t) \tag{9B.9}$$

with (Appendix 9A):

$$\phi_{\dot\theta}^{(0)}(0) = \langle\ddot{\theta}(0)^2\rangle/\langle\dot{\theta}(0)^2\rangle = kT/I_r$$

$$\phi_{\dot\theta}^{(1)}(0) = \frac{\langle\dddot{\theta}(0)^2\rangle}{\langle\ddot{\theta}(0)^2\rangle} - \frac{\langle\ddot{\theta}(0)^2\rangle}{\langle\dot{\theta}(0)^2\rangle}.$$

If equation (9B.9) is truncated with

$$\phi_{\dot\theta}^{(1)}(t) = \phi_{\dot\theta}^{(1)}(0)\exp(-\gamma t)$$

the following expressions are obtained from

$$\begin{aligned}\langle\dot{\theta}(t)\dot{\theta}(0)\rangle = \frac{\langle\dot{\theta}(0)\dot{\theta}(0)\rangle}{(1+\Gamma)}\Bigg[&\left(\cos\beta t + \frac{(\alpha_1+\Gamma\alpha_2)}{\beta}\sin\beta t\right)e^{-\alpha_1 t}\\ &+\Gamma\exp(-\alpha_2 t)/(1+\Gamma)\Bigg]\end{aligned} \tag{9.B.10}$$

where

$$\Gamma = -2\alpha_1(\alpha_1^2+\beta^2)/\alpha_2/(3\alpha_1^2-\beta^2-\alpha_2^2).$$

The root parameters α_1, α_2, and β are related to $\phi_{\dot\theta}^{(0)}(0)$, $\phi_{\dot\theta}^{(1)}(0)$, and γ by:

$$\alpha_1 = (s_1+s_2)+\gamma/3; \qquad \alpha_2 = s_1+s_2+\frac{\gamma}{3}; \qquad \beta = \frac{\sqrt{3}}{2}(s_1-s_2);$$

where

$$s_1^3 = -B/2 + (A^3/27 + B^2/4)^{1/2}$$
$$s_2^3 = -B/2 - (A^3/27 + B^2/4)^{1/2}$$

with

$$A = \phi_\theta^{(0)}(0) + \phi_\theta^{(1)} - \gamma^2/3;$$
$$B = \frac{\gamma}{3}\left(\frac{2\gamma^2}{9} + 2\phi_\theta^{(0)}(0) - \phi_\theta^{(1)}(0)\right).$$

To relate the angular velocity a.c.f. $\langle\dot\theta(t)\dot\theta(0)\rangle$ to the orientational a.c.f. $\langle\cos\theta(t)\cos\theta(0)\rangle$ we use the fact that the angular displacement since $t=0$ is

$$\theta = \int_0^t \dot\theta(t')\,dt',$$

so that:

$$\langle\cos\theta(t)\rangle = \text{Real}\left\langle\exp\left[i\int_0^t \dot\theta(t')\,dt'\right]\right\rangle.$$

This form can be expanded in terms of cumulant averages (Shimizu, 1968):

$$\left\langle\exp\left[i\int_0^t \dot\theta(t')\,dt'\right]\right\rangle = \exp\left[i\langle\dot\theta\rangle t - \int_0^t dt_1\int_0^t dt_2\langle\dot\theta(t_1)\dot\theta(t_2)\rangle + \cdots\right]$$
$$= \exp\left[-\frac{2kT}{I}\int_0^t (t-\tau)C_{\dot\theta}(\tau)\,d\tau\right]$$

where $C_{\dot\theta}(t) = \langle\dot\theta(t)\dot\theta(0)\rangle/\langle\dot\theta(0)\dot\theta(0)\rangle$. On performing the integration:

$$\langle\cos\theta(t)\cos\theta(0)\rangle = \exp\left[-\frac{2kT}{I}\left[A_1(e^{-\alpha_1 t}\cos\beta t - 1)\right.\right.$$
$$\left.\left. - B_1 e^{-\alpha_1 t}\sin\beta t + \frac{\Gamma}{\alpha_2^2}\frac{(e^{-\alpha_2 t}-1)}{1+\Gamma} + C_1 t\right]\right] \quad (9B.11)$$

where:

$$A_1 = \frac{3\alpha_1^2 + 2\alpha_1\alpha_2\Gamma - \beta^2}{(1+\Gamma)(\alpha_1^2+\beta^2)^2}; \qquad B_1 = \frac{2\beta^2\alpha_1 + (\alpha_1 + \Gamma\alpha_2)(\beta^2 - \alpha_1^2)}{\beta(1+\Gamma)(\alpha_1^2+\beta^2)^2}$$
$$C_1 = [2\alpha_1\alpha_2 + \Gamma(\alpha_1^2 + \beta^2 + \alpha_2^2)]/[\alpha_2(1+\Gamma)(\alpha_1^2+\beta_2)].$$

The results of equations (9B.10) and (9B.11) can also be obtained directly from the equations of motion for the itinerant librator, which consists in two dimensions of a central dipolar disk librating within a rigid annulus of respective moments of inertia I and I_1. Libration of the disk occurs with frequency ω_0 and is damped with a friction of coefficient β_2. The overall

motion of the annulus is a Brownian rotation with a friction coefficient β_1 related to the experimental Debye relaxation time. The two equations of motion are:

$$I_2\ddot\theta(t) + I_2\beta_2\dot\theta(t) + I_2\omega_0^2(\theta(t) - \psi(t)) = I_2\dot w(t)$$

for the disk, and:

$$I_1\ddot\psi(t) + I_1\beta_1\dot\psi(t) - I_2\omega_0^2(\theta(t) - \psi(t)) = I_1\dot w(t)$$

for the annulus, where $\dot w(t)$ is the random couple and $I_1\beta_1$ and $I_2\beta_2$ are friction coefficients. In the simple case where $\beta_2 = 0$ these equations may be solved simultaneously in terms of the Laplace transforms of $\theta(t)$ and $\dot\theta(t)$. The resulting correlation functions are identical with the above provided the following identities are made:

$$\beta_1 \equiv \gamma; \qquad \omega_0^2 + \Omega_0^2 \equiv \phi_\theta^{(1)}(0) + \phi_\theta^{(2)}(0);$$
$$\beta_1\omega_0^2 \equiv \gamma\phi_\theta^{(0)}(0), \quad \text{where} \quad \Omega_0^2 = (I_2/I_1)\omega_0^2.$$

From physical considerations of this model, ω_0 may be taken as the far infrared peak frequency, values of I_1 and I_2 may be estimated, and $\beta_1 = kT\tau_D/I_1$. In the more general model β_2 is finite, but this introduces an inconsistency in that the Taylor expansion of the angular velocity a.c.f. now has an unphysical term in t, i.e.

$$\langle\dot\theta(t)\dot\theta(0)\rangle/\langle\dot\theta(0)\dot\theta(0)\rangle = 1 - \beta_2 t + O(t^2).$$

However, this β_2 parameter accounts for the nonharmonicity of the libration, evident in the finite breadth of the far infrared Poley peak and is generally small compared with β_1. For $\beta_2 = 0$:

$$\omega_0^2 = \phi_\theta^{(0)}(0) = \langle\ddot\theta(0)^2\rangle/\langle\dot\theta(0)^2\rangle.$$

Rotation/translation coupling

A direct study of rotation/translation coupling may be attempted by considering the correlation matrix for the vector $\begin{bmatrix}\mathbf{v}\\ \boldsymbol{\omega}\end{bmatrix}$, where $\mathbf{v}$ is the centre of mass translation velocity. If past rotations influence future translations and past translations influence future rotations the matrices $\langle\mathbf{v}(t)\boldsymbol{\omega}^T(0)\rangle$ and $\langle\boldsymbol{\omega}(t)\mathbf{v}^T(0)\rangle$ are not null when $t>0$. Instantaneously (at the same t) the statistical correlation between $\mathbf{v}(t)$ and $\boldsymbol{\omega}(t)$ vanishes. For planar rotation the matrix elements of $\langle\mathbf{v}(t)\boldsymbol{\omega}^T(0)\rangle$ *do not all vanish*, even though the scalar correlation $\langle\mathbf{v}(t)\cdot\boldsymbol{\omega}(0)\rangle$ does. The 'coupling' parameter between rotation and translation also appears in the transforms of $\langle\mathbf{v}(t)\mathbf{v}^T(0)\rangle$ and $\langle\boldsymbol{\omega}(t)\boldsymbol{\omega}^T(0)\rangle$, which emphasizes the inadequacy of a decoupled approximation even when studying autocorrelation functions.

Since the components of $\mathbf{v}$ are mutually statistically uncorrelated, the elements of the correlation matrix of $\begin{bmatrix}\mathbf{v}\\ \boldsymbol{\omega}\end{bmatrix}$ are typified by those of the 2×2 matrix

$$C_{v\omega}(t)=\begin{bmatrix}\dfrac{\langle v(t)v(0)\rangle}{\langle v^2(0)\rangle} & \dfrac{\langle v(t)\omega(0)\rangle}{\langle \omega^2(0)\rangle}\\ \dfrac{\langle \omega(t)v(o)\rangle}{\langle v^2(0)\rangle} & \dfrac{\langle \omega(t)\omega(0)\rangle}{\langle \omega^2(0)\rangle}\end{bmatrix}$$

where v and ω are scalar components. We have

$$\tilde{C}(s)=[s+\tilde{C}_1(s)\phi_1(0)]^{-1}$$

$$=[s+[s+\tilde{C}_2(s)\phi_2(0)]^{-1}\phi_1(0)]^{-1}$$

where $\tilde{\phi}_1(s)=\tilde{C}_1(s)\phi_1(0)$ and $\tilde{\phi}_2(s)=\tilde{C}_2(s)\phi_2(0)$ are the transforms of the first and second memory matrices, and the $\phi_j(0)$ are defined by relations such as those in Appendix 9A, i.e.:

$$\phi_j(0)=\langle \mathbf{f}_j\mathbf{f}_j^T\rangle\langle \mathbf{f}_{j-1}\mathbf{f}_{j-1}^T\rangle^{-1}, \qquad j=1,2,\ldots$$

with

$$f_0=\begin{bmatrix}v(0)\\ \omega(0)\end{bmatrix}, \qquad f_1=\begin{bmatrix}\dot{v}(0)\\ \dot{\omega}(0)\end{bmatrix}$$

and

$$f_2=\begin{bmatrix}\ddot{v}(0)+\langle \dot{v}^2(0)\rangle v(0)/\langle v^2(0)\rangle\\ \ddot{\omega}(0)+\langle \dot{\omega}^2(0)\rangle \omega(0)/\langle \omega^2(0)\rangle\end{bmatrix}.$$

We find that

$$\phi_j^{(0)}=\begin{bmatrix}\phi_{tj} & 0\\ 0 & \phi_{rj}\end{bmatrix}$$

where

$$\phi_{t1}=\langle \dot{v}^2(0)\rangle/\langle v^2(0)\rangle; \qquad \phi_{r1}=\langle \dot{\omega}^2(0)\rangle/\langle \omega^2(0)\rangle$$

and

$$\phi_{t2}=\frac{\langle \ddot{v}^2(0)\rangle}{\langle \dot{v}^2(0)\rangle}-\frac{\langle \dot{v}^2(0)\rangle}{\langle v^2(0)\rangle}; \qquad \phi_{r2}=\frac{\langle \ddot{\omega}^2(0)\rangle}{\langle \dot{\omega}^2(0)\rangle}-\frac{\langle \dot{\omega}^2(0)\rangle}{\langle \omega^2(0)\rangle}.$$

To describe r/t coupling in the context of Mori theory we can proceed phenomenologically to consider successive approximants. The first is defined

by:

$$\tilde{C}_1(s)\phi_1(0)=\begin{bmatrix}\lambda_t & \lambda_{tr}\\ \lambda_{rt} & \lambda_r\end{bmatrix}$$

where the λ's may be interpreted as frictional in origin. It follows that:

$$\tilde{C}(s)=\begin{bmatrix}s+\lambda_t & \lambda_{tr}\\ \lambda_{rt} & s+\lambda_r\end{bmatrix}^{-1}=\frac{1}{\Delta s}\begin{bmatrix}s+\lambda_r & -\lambda_{tr}\\ -\lambda_{rt} & s+\lambda_t\end{bmatrix}$$

where $\Delta(s)=(s+\lambda_t)(s+\lambda_r)-\lambda_{tr}\lambda_{rt}$. Writing $b=2(\lambda_t+\lambda_r)$; $c=\lambda_t\lambda_r-\lambda_{tr}\lambda_{rt}$, we find

$$\begin{aligned}\langle v(t)v(0)\rangle &= \langle v^2(0)\rangle \exp(-bt)[\cos(c-b^2)^{1/2}t\\ &\quad +(\lambda_r-b)/(c-b^2)^{1/2}\sin(c-b^2)^{1/2}t; \qquad c>b^2\\ &= \langle v^2(0)\rangle \exp(-bt)[\cosh(b^2-c)^{1/2}t\\ &\quad +(\lambda_r-b)/(b^2-c)^{1/2}\sinh(b^2-c)^{1/2}t]; \qquad c<b^2\\ \langle \omega(t)v(0)\rangle &= -\frac{\langle \omega^2(0)\rangle}{(c-b^2)^{1/2}}\lambda_{tr}\exp(-bt)\sin(c-b^2)^{1/2}t; \qquad c>b^2\\ &= -\frac{\langle \omega^2(0)\rangle}{(b^2-c)^{1/2}}\lambda_{tr}\exp(-bt)\sinh(b^2-c)^{1/2}t; \qquad c<b^2\end{aligned}$$

with similar expressions for $\langle \omega(t)\omega(0)\rangle$ and $\langle \omega(t)v(0)\rangle$. Since $\langle v(t)\omega(0)\rangle=\langle \omega(t)v(0)\rangle$, it follows that

$$\lambda_{tr}\langle \omega^2(0)\rangle=\lambda_{rt}\langle v^2(0)\rangle$$

and hence only three of the four parameters λ_t, λ_r, λ_{tr}, and λ_{rt} are independent.

The translational a.c.f. involves the rotational λ_r via λ_{tr}. Similarly for the rotational a.c.f. However, even for finite λ_{tr} or λ_{rt} the cross-correlations $\langle v(0)\omega(0)\rangle$ or $\langle \omega(0)v(0)\rangle$ vanish. For roto-translational itinerant oscillation/libration we define the third memory matrix by:

$$\tilde{C}_3(s)\phi_3(0)=\begin{bmatrix}\lambda_t & \lambda_{tr}\\ \lambda_{rt} & \lambda_r\end{bmatrix}$$

and obtain:

$$\tilde{C}(s)=\frac{1}{\Delta_1(s)}\begin{bmatrix}s+\left[s+(s+\lambda_r)\dfrac{\phi_{t2}}{\Lambda(s)}\right]\dfrac{\phi_{t1}}{\Delta_1(s)} & -\dfrac{\lambda_{tr}\phi_{r2}\phi_{r1}}{\Delta(s)\Delta_1(s)}\\ \dfrac{\lambda_{rt}\phi_{t2}\phi_{t1}}{\Delta(s)\Delta_1(s)} & s+\left[s+(s+\lambda_t)\dfrac{\phi_{r2}}{\Lambda(s)}\right]\dfrac{\phi_{r1}}{\Delta_1(s)}\end{bmatrix}$$

where

$$\Delta_1(s) = \left[s + (s+\lambda_t)\frac{\phi_{r2}}{\Delta(s)}\right]\left[s + (s+\lambda_r)\frac{\phi_{t2}}{\Delta(s)}\right] - \frac{\lambda_{tr}\lambda_{rt}\phi_{t2}\phi_{r2}}{\Delta^2(s)}$$

and

$$\Delta_2(s) = \left[s + \left[s + (s+\lambda_t)\frac{\phi_{r2}}{\Delta(s)}\right]\frac{\phi_{t1}}{\Delta_1(s)}\right]\left[s + \left[s + (s+\lambda_r)\frac{\phi_{t2}}{\Delta(s)}\right]\frac{\phi_{r1}}{\Delta_1(s)}\right] - \frac{\lambda_{tr}\lambda_{rt}\phi_{t2}\phi_{t1}\phi_{r2}\phi_{r1}}{\Delta^2(s)\Delta_1^2(s)}$$

with $\lambda_{tr}\phi_{r2}\phi_{r1} = \lambda_{rt}\phi_{t2}\phi_{t1}$. So all correlation functions involve the seven independent phenomenological parameters ϕ_{t1}, ϕ_{t2}, ϕ_{r1}, ϕ_{r2}, λ_t, λ_r, and λ_{tr}.

When the coupling parameter $\lambda_{tr} = 0$ the determinants $\Delta(s)$, $\Delta_1(s)$, and $\Delta_2(s)$ reduce to simple factors, the autocorrelation functions become dependent on only three parameters, as in the rotational case described above.

The seven-parameter theory is too complicated in general for analysis with experimental data over anything but a wide range of conditions (temperature and pressure). The theory should also be adapted for use with more than one experimental technique in an attempt to fix each parameter unambiguously. In the meantime the method developed by Reid in the main body of this chapter can be used with incisive results in some measured cases.

9.11 Acknowledgement

The Science Research Council is acknowledged for financial support to both authors.

9.12 References

Afsar, M. N., Hasted, J. B., and Chamberlain, J. (1976). *Infrared Physics*, **16,** 301.
Berne, B. J., and Pecora, R. (1976). *Dynamic Light Scattering with Applications to Physics, Chemistry, and Biology*, Wiley–Interscience, New York.
Brot, C. (1967). *J. Phys. Radium*, **28,** 789.
Brot, C. (1975). In M. Davies (Ed.), *Dielectric and Related Molecular Processes*, Chem. Soc. Specialist Per. Rep., Vol. 2, p. 1.
Calderwood, J. H., and Coffey, W. T. (1977). *Proc. R. Soc.*, **356,** 269.
Chantry, G. (1971). *Submillimetre Spectroscopy*, Academic Press, New York.
Chenon, M. J., Baron, D., Bader, L., and Compry, C. (1972). *J. Chem. Phys.*, **69,** 1665.
Cole, R. H. (1965). *J. Chem. Phys.*, **42,** 637.
Darmon, L., Gerschel, A., and Brot, C. (1970). *Chem. Phys. Letters*, **7,** 53.
Datta, P., and Barrow, G. M. (1968). *J. Chem. Phys.*, **48,** 4662.

Davies, G. J. (1971). *Ph.D. Thesis*, University of Wales.
Davies, G. J. and Evans, M. W. (1976). *J.C.S. Faraday II*, **72,** 361.
Debye, P. (1929). *Polar Molecules*, Chem. Catalog Co., New York, 1929.
Evans, M. W. (1976). *J. Chem. Soc. Faraday Trans. II*, **72,** 2138.
Evans, M. W. (1977a). In M. Davies (Ed.), *Dielectric and Related Molecular Processes*, Chem. Soc. Specialist Per. Rep., Vol. 3.
Evans, M. W. (1977b). *Adv. Mol. Rel. Int. Proc.*, **10,** 203–271.
Evans, M. W., (1980). *Zeit für Phys., B*, **39,** 75.
Evans, M. W., Grigolini, P., Coffey, W. T., and Evans, G. J. (1982). *Molecular Dynamics*, Wiley–Interscience, New York.
Evans, M. W., Evans, G. J., and Davies, A. R. (1980). *Adv. Chem. Phys.*, **44,** 255–481.
Evans, M. W., Evans, J. G., and Reid, C. J. (1978). *Adv. Mol. Rel. Int. Proc.*, **12,** 301.
Evans, M. W., Grigolini, P., and Ferrario, M. (1980). *Mol. Phys.*, **39,** 1369–1391.
Ewing, G. E. (1969). *Am. Chem. Soc., Accounts of Chem. Research*, **2,** 168.
Fatuzzo, E., and Mason, P. R. (1967). *Proc. Phys. Soc.*, **90,** 741.
Favro, L. (1961). *Phys. Rev.*, **152,** 309.
Ferrario, M., and Grigolini, P. (1979). *J. Math. Phys.*, **20,** 2567.
Garg, S. K., and Smyth, C. P. (1967). *J. Chem. Phys.*, **46,** 373.
Gitarum, S. (1960). *J. Chem. Phys.*, **33,** 639.
Gordon, R. G. (1963). *J. Chem. Phys.*, **38,** 1724.
Gordon, R. G. (1965). *J. Chem. Phys.*, **44,** 1830.
Gordon, R. G. (1965). *J. Chem. Phys.*, **43,** 1307.
Gordon, R. G. (1968). *Adv. Magn. Res.*, **3,** 1.
Grigolini, P., and Ferrario, M. (1979). *Chem. Phys. Letters*, **62,** 100.
Grigolini, P., and Ferrario, M. (1980). *J. Math. Phys.*, **29,** 1315.
Hasted, J. B. (1972). *Dielectric and Related Molecular Processes*, Vol. 1, Chem. Soc., London. p. 121.
Hill, N. (1977). *J. Phys., C.*, **10,** 459.
Johari, G. P. (1973). *J. Chem. Phys.*, **58,** 1766.
Johari, G. P., and Goldstein, M. (1972). *J. Chem. Phys.*, **53,** 2372.
Johari, G. P., and Smyth, C. P. (1972). *J. Chem. Phys.*, **56,** 4411.
Kivelson, D., and Madden, P. (1975). *Mol. Phys.*, **30,** 1749.
Kroon, S. G., and van der Elsken, J. (1967). *Chem. Phys. Letters*, **1,** 285.
Kubo, R. (1965). *Statistical Mechanics of Equilibrium and Non-Equilibrium*, North-Holland, Amsterdam.
Kushick, J., and Berne, B. J. (1973). *J. Chem. Phys.*, **59,** 3732.
Larkin, I. W., (1973). *J.C.S. Faraday Trans. II*, **69,** 1278.
Larkin, I. W., and Evans, M. W. (1974). *J.C.S. Faraday Trans. II*, **70,** 477.
Leroy, Y., Constant, E., Abbar, C., and Desplanques, P. (1967). *Adv. Mol. Rel. Int. Proc.*, **1,** 273.
Levesque, D., Ouentrec, B., and Barojas, J. (1973). *Phys. Rev.*, **7A,** 1092.
Lobo, R., Robinson, J. E., and Rodriguez, M. (1973). *J. Chem. Phys.*, **59,** 5992.
Mandel, M., and Mazur, P. (1958). *Physica*, **24,** 116.
Molitor, A. (1972). *J. Mol. Struct.*, **13,** 261.
Mori, H. (1965). *Prog. Theoretical Phys.*, **33,** 423.
Muller, K. D., and Rothschild, W. G. (1971). *Far Infrared Spectroscopy*, Wiley–Interscience, New York.
Nee, T. W., and Zwanzig, R. (1970). *J. Chem. Phys.* **52,** 6353.
Nelson, E. (1967). *Dynamical Theory of the Brownian Motion*, Princeton University Press, Princeton.

Onsager, L. (1936). *J. Am. Chem. Soc.*, **58,** 1186.
Paolo, T. D., and Sandorfy, C. (1974). *Can. J. Chem.*, **52,** 3612.
Pardoe, G. W. F. (1969). *Ph.D. Thesis,* University of Wales.
Pardoe, G. W. F. (1970). *Trans. Faraday Soc.*, **66,** 2699.
Pardoe, G. W. F., and Gebbie, H. A. (1970). *Symposium on Submillimetre Waves, Polytech. Inst., Brooklyn,* 1970, p. 643.
Poley, J. Ph. (1955). *J. Appl. Sci., B,* **4,** 337.
Quentrec, P., and Bezot, P. (1974). *Mol. Phys.*, **27,** 879.
Reid, C. J. (1979a). *Ph.D. Thesis,* University of Wales.
Reid, C. J. (1979b). *Chem. Phys. Letters,* **66,** 517.
Reid, C. J. (1980). *Chem. Phys. Letters,* submitted 1982.
Reid, C. J., and Evans, M. W. (1979). *J.C.S. Faraday II,* **75,** 1213; *Adv. Mol. Rel. Int. Proc.*, **15,** 281.
Reid, C. J., and Evans, M. W. (1980). *J.C.S. Faraday II,* **76,** 286.
Rowlinson, J. S., and Evans, M. W. (1975). *Chem. Soc. Ann. Report,* **72,** 5.
Shimizu, H. (1968). *J. Chem. Phys.* **48,** 2494.
Singer, K., and Renaud, J., (1979). Private communication.
Steele, W. A. (1976). *Adv. Chem. Phys.*, **34,** 1.
Tituluer, U. M., and Deutch, J. M., *J. Chem. Phys.*, **60,** 1502.
Van der Elsken, J. H., and Wegdam, G. H. (1972). *J. Chem. Phys.*, **57,** 2691.
Wax, N. (Ed.) (1954). *Selected Papers on Noise and Stochastic Processes,* Dover, New York.
Williams, G., Beevers, M., Crossley, J., and Carrington, D. (1977). *J.C.S. Faraday Trans. II,* **73,** 485.
Williams, G., and Hains, P. J. (1971). *Chem. Phys., Letters,* **10,** 585.
Wyllie, G. (1971). *J. Phys.*, C., **4,** 564.